Posiva SKB Report 07
May 2018

Exploring conditioned simulations of discrete fracture networks in support of hydraulic acceptance of deposition holes

Application to the ONKALO demonstration area

Steven Baxter
Pete Appleyard
Lee Hartley
Jaap Hoek
Thomas Williams

POSIVA OY

Olkiluoto
FI-27160 Eurajoki, Finland
Phone +358 2 8372 31
posiva.fi

SVENSK KÄRNBRÄNSLEHANTERING AB

SWEDISH NUCLEAR FUEL
AND WASTE MANAGEMENT CO

Box 3091, SE-169 03 Solna
Phone +46 8 459 84 00
skb.se

ISSN 2489-2742
Posiva SKB Report 07
SKB ID 1673758
Posiva ID RDOC-104887
May 2018
Updated 2018-07

Exploring conditioned simulations of discrete fracture networks in support of hydraulic acceptance of deposition holes

Application to the ONKALO demonstration area

Steven Baxter, Pete Appleyard, Lee Hartley, Jaap Hoek, Thomas Williams

Amec Foster Wheeler

Keywords: Fracture characterisation, Discrete fracture network (DFN), Hydrogeology, Acceptance criteria, Numerical modelling.

Update notice

The original report, dated May 2018, was found to contain editorial errors which have been corrected in this updated version.

Preface

The current report summarises modelling work related to the development of hydraulic acceptance criteria for deposition holes. The work has been performed within a Posiva-SKB collaboration project where experimental Posiva results from Demonstration Tunnel 2 in ONKALO are used in combination with a conditioning methodology for discrete fracture network models developed in an earlier SKB project.

The work has been coordinated by Outi Vanhanarkaus and Lasse Koskinen from Posiva, Jan-Olof Selroos from SKB, and Anders Winberg from Conterra AB (on behalf of SKB).

The report has been reviewed by Aimo Hautojärvi and Pirjo Hellä from Saanio & Riekkola Oy.

Abstract

Discrete fracture network (DFN) modelling provides the framework for an integrated conceptualisation of geological, structural, hydrogeological, rock mechanics and solute transport characteristics for a situation where flow is predominately through a series of connected discrete fractures. Such rock conditions occur at Posiva's Olkiluoto site for geological disposal of spent nuclear fuel, and DFN modelling is expected to fulfil a similar role for SKB's purposes at Forsmark.

The motivation for this study comes from the Posiva/SKB cooperation related to harmonisation of the requirements on the repository including the requirements on the repository host rock and Posiva's RSC (Rock Suitability Classification) protocol. The current study comprises a series of modelling tasks aimed toward improving the Posiva-SKB capability of defining verifiable hydraulic acceptance criteria for deposition hole positions.

The establishment of six experimental deposition holes with preceding pilot holes in Demonstration Tunnel 2 (DT2) in the ONKALO underground research facility provides a means to develop and test a DFN-based modelling strategy aimed at providing additional support to the definition of hydraulic acceptance criteria for deposition holes. Conditioning of each DFN realisation on local observations of individual fracture geometries and in situ flow measurements in DT2 and in the pilot holes / experimental deposition holes drilled beneath it, provides a reduction in uncertainty of predicted post-closure flow and transport properties for individual deposition holes at specific locations. Typically, this amounts to reducing the spread of predicted flow and transport properties at individual deposition holes, thereby increasing the reliability of location specific model predictions.

Sammanfattning

Diskret spricknätverksmodellering (DFN modellering) erbjuder en plattform för integrerad konceptualisering av bergförhållanden där flödet företrädesvis sker genom en serie av konnekterade, diskreta sprickor. Den integrerade konceptualiseringen inkluderar geologiska, strukturgeologiska, hydrogeologiska och bergmekaniska egenskaper samt egenskaper för transport av lösta ämnen. Sådana bergförhållanden råder vid Olkiluoto, Posivas plats för geologisk förvaring av använt kärnbränsle. DFN modellering förväntas inta en motsvarande roll för SKB:s behov på platsen Forsmark.

Motivet för denna studie är Posivas och SKB:s samarbete kring harmoniserade krav på förvaret inkluderande de krav som ställs på förvarsberget, av Posiva hanterad i deras system för klassificering (RSC, Rock Suitability Classification) . Föreliggande studie består av en serie modelleringsövningar syftande till att förbättra Posivas och SKB:s förmåga att definiera verifierbara hydrauliska acceptanskriterier för deponeringshålspositioner.

Etableringen av sex experimentella deponeringshål med föregående pilothål i Demonstrationstunnel 2 (DT2) i det underjordiska forskningslaboratoriet ONKALO erbjuder en möjlighet att utveckla och testa en DFN-baserad modelleringsstrategi. Denna modelleringsstrategi syftar till att ge ytterligare stöd för att definiera hydrauliska acceptanskriterier för deponeringshål. Betingning (konditionering) av varje DFN-realisering på lokala observationer av enskilda sprickors geometrier och inflöden i DT2 tunneln samt i pilothålen/deponeringshålen resulterar i en reduktion av osäkerheten i predikterade flödes- och transportegenskaper för enskilda deponeringshål i specifika lägen efter förslutning. Typiskt resulterar detta i en minskning av spridningen i predikterade resultat av flödes- och transportegenskaper för enskilda deponeringshål, och därmed en ökad tilltro till lägesspecifika modellprediktioner.

Tiivistelmä

Rakoverkkomallinnuksen (Discrete fracture network, DFN) avulla voidaan muodostaa integroitu käsitys kallion geologisista, rakenteellisista, hydrogeologisista, kalliomekaanisista ja aineen kulkeutumiseen vaikuttavista tekijöistä, missä veden virtaus tapahtuu pääasiassa rakojen kytkeytymisen kautta. Tällaiset kallio-olosuhteet ovat Posivan käytetyn ydinpolttoaineen geologisella loppusijoituspaikalla Olkiluodossa, minkä lisäksi rakoverkkomallinnusta tullaan käyttämään samanlaiseen tarkoitukseen SKB:n toimesta Forsmarkissa, Ruotsissa.

Tämä työ on osa Posiva-SKB-yhteistyötä, jossa loppusijoitukseen liittyviä kalliolle asetettuja vaatimuksia ja Posivan kalliosoveltuvuusluokittelua (Rock Suitability Classification, RSC) yhtenäistetään. Tämä työ koostuu useista mallinnustehtävistä, joiden tavoitteena on parantaa Posivan ja SKB:n kykyä määrittää verifioitavat hydrauliset hyväksymiskriteerit loppusijoitusreikien paikoille.

ONKALO-tutkimustilan demonstraatioalueen tunneliin 2 (DT2) tehdyt kuusi koe-loppusijoitusreikää ja niitä edeltäneet pilottireiät antavat mahdollisuuden kehittää ja testata DFN-pohjaista mallinnusstrategiaa, jota voitaisiin hyödyntää loppusijoitusreikien hydraulisten hyväksymiskriteerien määrittämisessä. Kunkin DFN-realisaation ehdollistaminen rakojen geometria- ja vuotohavainnoilla DT2-tunnelissa sekä pilottirei'issä ja niitä seuranneissa koeloppusijoitusrei'issä vähentää ennustetun virtaus- ja kulkeutumisominaisuuksien epävarmuuksia tietyn paikan yksittäisessä loppusijoitusreiässä. Tyypillisesti tämä merkitsee ennustettujen virtaus- ja kulkeutumisominaisuuksien hajonnan pienentymistä yksittäisissä loppusijoitusrei'issä, ja toisaalta lisää mallin ennustusten uskottavuutta.

Contents

1 Introduction

1.1 Background

Discrete fracture network (DFN) modelling provides the framework for an integrated conceptualisation of geological, structural, hydrogeological, rock mechanics and solute transport characteristics for rock conditions where flow is predominately through a series of connected discrete fractures. Such rock conditions occur at Posiva's Olkiluoto site for geological disposal of spent nuclear fuel, and DFN modelling is expected to fulfil a similar role for SKB's purposes at Forsmark. It also provides the basis for quantitative assessment of important structural, flow and transport factors affecting safety assessment, repository engineering and the rock suitability criteria (RSC) system.

The motivation for the study reported here comes from the Posiva/SKB cooperation related to requirements on the repository host rock (VAHA/KUPP) and Posiva's RSC (Rock Suitability Classification) criteria (McEwen et al. 2012) with the common ambition to harmonise the Posiva design basis (Posiva 2012) and corresponding SKB design criteria. Two existing flow based criteria for deposition holes exist based on

- inflows to open deposition holes for use as a predictor of proper installation of the buffer, and
- the post-closure flow and transport conditions around deposition holes.

However, at the time when decision on the location of the deposition holes are made, it will not be possible to measure these directly, and so criteria based on proxy measurements have to be considered such as the specific capacity (flow rate to/from a fracture divided by driving groundwater head change) of the fractures intersecting the pilot hole for the deposition hole. The specific capacity then provides a means to estimate both of the above flow criteria prior to reaming the deposition hole. Subsequent measurements of inflows to the deposition holes could still be a further criterion to ensure a proper installation of the buffer. The establishment of six experimental deposition holes in Demonstration Tunnel 2 (DT2) in the ONKALO provide a test bed for the development and testing of a DFN-based modelling strategy aimed at providing additional support for definition of these acceptance criteria for deposition holes.

A second objective of the current study is to use the measurements acquired from the deposition holes below DT2 for validation of the fracture conceptual model that has been developed for the Demonstration Area (Hartley et al. 2017) as a prototype for the updated Olkiluoto DFN v3 in support of Site Description Model (SDM) 2018. New data on the specific capacity of fractures within the pilot holes for deposition holes, as well as intensity of fractures and inflows in each experimental deposition hole are new data that can be used in prediction-outcome exercises. These exercises provide an illustration of the reliability of the DFN model to make local-scale predictions of geometric and hydraulic properties of the fracture system.

Earlier numerical modelling investigations of correlations between fracture hydraulic properties that could be measured and post-closure flow and transport properties include properties derived from hydraulic injection tests in pilot holes for deposition holes, inflows to pilot holes for deposition holes, and inflows to deposition holes for DFN models of Forsmark (Joyce et al. 2013); a similar study of correlations between inflows to deposition holes and post-closure flows was also performed for an earlier DFN model of Olkiluoto (Hartley et al. 2013c).

The current study comprises a series of modelling tasks toward improving the Posiva-SKB capability of defining verifiable hydraulic acceptance criteria for deposition hole positions. The characterisation of the fracture system and associated numerical DFN model describing the statistical distributions of fracture properties local to the Demonstration Area and technical facilities of ONKALO have been derived by Hartley et al. (2017), and denoted the DADFN model. Interpretation of fracture occurrence and properties in this rock volume yielded several site-specific spatial relationships between fracture properties and other 3D geological models (such as the lithology, brittle and ductile deformation models), correlations between fracture properties (such as aperture and size), as well statistical distributions to describe variability in fracture properties. The DFN model therefore implements a number of spatial constraints and inferred property trends, but still retains probabilistic assignments of individual fracture attributes and properties such as location, size, orientation and aperture. Many equally likely

realisations of the model can be generated to quantify stochastic uncertainty. In their simplest form DFN realisations only reproduce the inferred spatial patterns, correlations and property statistics as measured in the data without honouring specific observations of fracture locations and properties. Such realisations are here described as "unconditioned" since they are not conditioned to reproduce each observed fracture as seen in a tunnel or drillhole. An ensemble of unconditioned realisations is adequate to quantify the expected statistical distribution of fracture properties some distance away from measured fracture data, e.g. at locations of tunnels yet to be excavated.

Where individual fractures have been characterised in drillholes or tunnel walls, the realisations can be modified to match local measurement data of fracture properties. In continuum modelling, conditioning involves changing the values of continuous properties or variables to match the observation made at points. In discrete modelling, conditioning involves swapping or modifying objects (i.e. fractures) and their properties to match the observed characteristics where they intersect a drillhole or tunnel. The matched properties of the conditioned objects as they manifest themselves on the surface of the drillhole/tunnel are therefore deterministic, but their geometry and properties beyond the rock surface may be uncertain and therefore remain the subject of stochastic simulation. Methods for conditioning DFN models have been developed and verified in the DFN-R Posiva/SKB collaboration project (Appleyard et al. 2018, Bym and Hermanson 2018). The benefits of conditioning DFN models are that they reduce uncertainty in predictions made on conditions close to investigation drillholes and tunnels, on the scale of the size of fractures. In a repository operational sense, this means that conditioning DFN realisations on structural and hydraulic characterisation of deposition tunnels and pilot holes offers reduced uncertainty when making predictions of flow and transport properties at nearby deposition hole positions.

The conceptual model for the fracture system around the Demonstration Area, its derivation, and its numerical implementation and calibration on hydraulic data are described in Hartley et al. (2017). Illustrative results from conditioned DFN simulations using structural mapping to predict fracture occurrence near the Demonstration Tunnels are also presented in that report. Hence, the current report should be read in conjunction with that characterisation report.

The current study explores how the methods developed for conditioned DFN modelling can be applied to the structural and hydraulic characterisation so far performed in the Demonstration Area to provide predictions of post-closure flow at six experimental deposition holes beneath Demonstration Tunnel 2. The conditioned realisations honour the locations, orientations and trace lengths of fractures mapped on the surfaces of the nearby ONKALO tunnels and pilot drillholes. Other data used as constraints include measurements from hydraulic injection tests performed in pilot holes drilled prior to the experimental deposition holes (Hjerne et al. 2016), and inflows to the subsequent deposition holes (where the results of the experimental deposition hole leakage measurements have been uploaded to Posiva's POTTI investigation database).

In addition, new data from beneath the floor of DT2 subsequent to the interpretation of the DADFN model offers a validation of the model ability to make predictions of injection tests in pilot holes and inflows to open deposition holes using unconditioned and various types of conditioned DFN realisations. It also demonstrates the successive reduction in uncertainty when making predictions of post-closure flow conditions around a deposition hole by constraining DFN models using different sorts of characterisation data (geometric, injection tests, inflows). Finally, it is noted that despite post-closure flows being critical for the acceptance criteria of deposition holes, it cannot be measured during repository construction. As such two possible criteria are considered for the acceptance of deposition holes related to the measured specific capacity of the pilot holes drilled for deposition holes (i.e. the injection tests); or the inflows under open deposition hole conditions. To evaluate these criteria, this study also considers the correlation of the predicted initial flow rate per unit width, calculated at the start of flow pathways in fractures adjoining the deposition holes (i.e. the post-closure performance measure) with both the corresponding injection test and inflow metrics.

Outcomes from this modelling study will be used in support of the development of procedures for defining hydraulic acceptance criteria for deposition holes and for further refinement of practical modelling procedures and *in situ* hydraulic testing strategies and measurement techniques that eventually will be employed in the screening of potential deposition hole locations to ensure acceptable host rock conditions and performance.

1.2 Conditioning DFN models

The geometric and hydraulic understanding of the fractured rock at Olkiluoto has been integrated to define the numerical DADFN model (Hartley et al. 2017, Chapter 6) for the ONKALO Demonstration Area and technical facilities. Despite including spatial constraints on fracture properties (e.g. proximity to Brittle Fault Zone (BFZ), lithology and ductile domain), the model is inherently stochastic in nature, with realisations of the DFN model only honouring observations from underground engineered features such as tunnels and pilot holes at a statistical level. Conditioning provides a mechanism for further constraining these stochastic DFN realisations to ensure that they each honour individual fracture properties as observed underground. Typical data available for conditioning DFN models consist of fracture traces mapped on the surfaces of tunnels and deposition holes, fractures logged in drillholes, inflows and hydraulic test results. Constraining realisations to match such information makes fracture properties deterministic in the immediate vicinity of the drillhole/tunnel wall, while remaining stochastic for those properties not measured and for fractures away from data controls.

In ConnectFlow the starting point for conditioning simulations is the *a priori* DFN model that is assumed to represent the statistical distributions of fracture properties of the volume being modelled. Different statistical models can apply to different sub-volumes, e.g. for different fracture domains or inside/outside brittle deformation zones. Multiple unconditional realisations are generated to provide a library of possible fractures, including both their properties (traces, flows) as simulated in drillholes and tunnels as well as their other properties not measured (extent, transmissivity). New unconditioned realisations are generated, the fractures intersecting the drillholes and tunnels are removed (since by pure chance they will not be consistent in terms of precise traces and flows with the measurements) and they are replaced with candidates from the library that have comparable traces and flows. A list of potential candidate fractures is identified, similar according to various measures and the final choice is probabilistically weighted by the same measures of similarity. In this way both the background fracturing beyond the drillhole and tunnel mapping as well the conditioned fractures intersecting the drillholes and tunnels are stochastically drawn from statistics of the same *a priori* DFN model. Figure 1-1 summarises the workflow for conditioned simulation of DFN models using ConnectFlow (Appleyard et al. 2018).

The resulting conditioned simulations can be screened against further measurements or tighter acceptance criteria prior to simulations of predictions of flow and transport properties. The library generation can be purely geometric (see Sections 6.1 or 7.1) or include additional flow calculations (see Sections 6.2 or 7.2) so as to select fractures that give rise to similar flows as well as geometries as those observed.

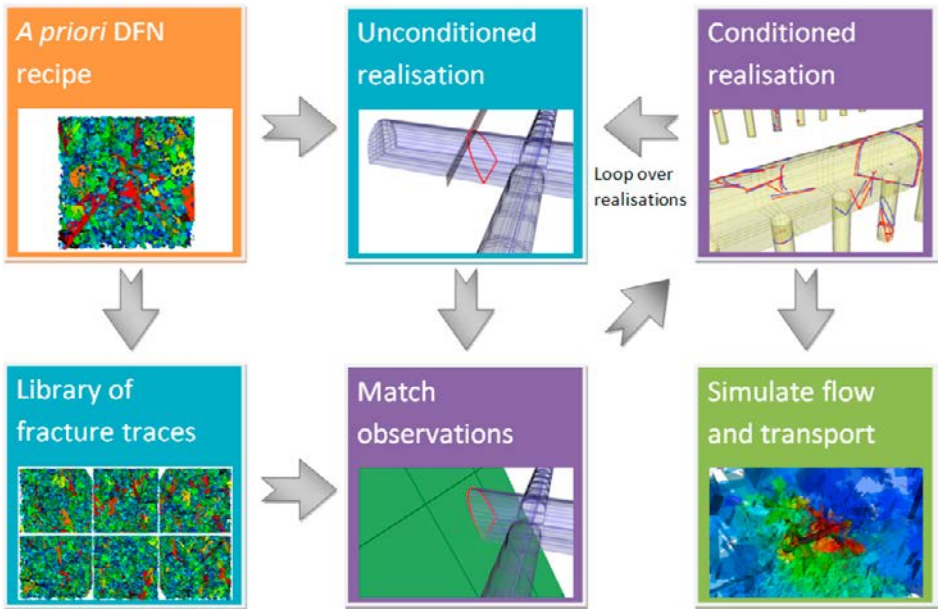

Figure 1-1. *Workflow for conditioned simulations of DFN models using ConnectFlow. This figure is reproduced from Appleyard et al. (2018).*

1.3 Scope of project

In order to assess whether uncertainties in predictions of post-closure flow conditions around a deposition hole can be reduced by the use of different types of subsurface data the following stages in the *in situ* characterisation of the volume around the Demonstration Area are considered in constructing and conditioning DFN models:

0. Structural mapping and hydraulic tests in surface drillholes passing near the Demonstration Area; structural mapping and hydraulic tests in ONKALO pilot holes of the access tunnel, Demonstration Area and technical facilities; structural mapping in the access tunnel, Demonstration Area and technical facilities tunnels.
1. As Stage 0, but with additional structural mapping in pilot holes for deposition holes.
2. As Stage 1, but with additional hydraulic injection tests in pilot holes for deposition holes.
3. As Stage 0, but with additional structural mapping in deposition holes.
4. As Stage 3, but with additional inflow measurements in deposition holes.

A review of available data local to the ONKALO Demonstration Area in support of these simulations is given in Section 1.3.1 with further details in Chapter 3.

Stage 0 provided the data that was used to interpret and calibrate the DADFN model, which forms the basis for unconditioned realisations (denoted as UC simulations).

Stages 1 and 2 provide some additional data from the characterisation of pilot holes for deposition holes drilled beneath Demonstration Tunnels 1 and 2 (see Chapter 3 for diagrams of the layout). The mapping data from ONKALO, some pilot holes for unexcavated sections of the DT1 and DT2, and the pilot holes for deposition holes are used here to condition DFN realisations. A model conditioned on geometric data only at Stage 1 is used to create conditioned models denoted as PHGC (Pilot Hole Geometric Conditioned) simulations, while the additional hydraulic test data from the pilot holes for deposition holes is used as additional constraints in creating conditioned simulations denoted PHHC (Pilot Hole Hydraulic Conditioned).

Stages 3 and 4 replace the data from the pilot holes beneath Demonstration Tunnel 2 with mapping and inflow measurements, respectively, from the experimental deposition holes themselves. Realisations conditioned on the geometric mapping only are denoted DHGC (Deposition Hole Geometric Conditioned), while those also constrained on inflow measurements are denoted DHHC (Deposition Hole Hydraulic Conditioned). It should be noted that these models are conditioned on data from the deposition hole measurements instead of the pilot hole measurements, rather than constraining models on the sequence of both sorts of measurements. It is possible that enforcing both constraints on a model might reduce uncertainty more than individual datasets, especially combining both hydraulic tests in pilot holes and inflows to the subsequent deposition holes.

Overall, five suites of DFN realisations are generated (10 realisations per suite), one without local conditioning, and four forms of DFNs conditioned on local data. Each suite would be expected to yield the same statistical distribution of simulated fracture properties and flows over the whole model domain (see diagrams in Section 1.2), but distributions will differ in predictions of fracture geometry and flow statistics around the deposition holes.

In order to quantify the effects of these fracture geometry and flow statistics, three hydraulic situations are considered for each suite of models:

1. simulate steady-state conditions where the ONKALO tunnels are open and hydraulic injection tests are performed sequentially in each of the packed-off pilot holes, denoted -pi (pilot hole injection), calculating the total outflows, $Q_{outflow}$, from the hole tested into the fractures intersecting the pilot hole;
2. simulate conditions where the ONKALO tunnels and all deposition holes are open, denoted -do (deposition open hole inflows), calculating inflows, Q_{inflow}, from each fracture to the deposition holes; and
3. simulate post-closure conditions where ONKALO and the experimental deposition holes are backfilled with a low hydraulic conductivity buffer of 10^{-10} m/s and 10^{-12} m/s respectively, denoted -pc (post closure flow and transport), calculating the flows (i.e. the average tangential

flow rate per unit width around a deposition hole, U) in fractures adjacent to the deposition holes and flow-related transport resistance between the deposition holes and the boundaries of the domain, as shown in Section 4.3.3.

The scope therefore requires a matrix of five by three sets of DFN flow simulations (see Table 1-1) be performed that enable various comparisons to address several questions toward defining effective procedures for deposition hole acceptance:

- To what certainty do the probabilistic unconditioned realisations predict the measured distributions of injection rates in pilot holes and inflows to deposition holes?
- How reliable are predictions of the measurements constrained by local conditioning of different types of structural and hydraulic information?
- By how much are predictions of the post-closure flows and transport resistance constrained by local conditioning of different types of structural and hydraulic information?
- To what degree are different types of flow measurements (injection test vs. inflows) correlated with simulated future post-closure flows and flow-related transport resistance, and how are these correlations affected by conditioning?

The first two questions relate to quantifying the reliability of model predictions as input to determining appropriate suitability criteria and possibly applying them. The situations corresponding to these validation aspects are highlighted in green in Table 1-1.

Table 1-1. Summary of purpose for each set of DFN simulations – five types of model by three hydraulic situations. The scenarios corresponding to validation aspects based on the predictive capability of models against new data are highlighted green.

	Tunnels open, injection tests in pilot holes for deposition holes, calculating injection rates (-pi)	**Tunnels and deposition holes open, calculating inflows to deposition holes (-do)**	**Tunnels and deposition holes backfilled and saturated , calculating post-closure flow and transport (-pc)**
Unconditioned (UC)	UC-pi – baseline validation that prediction of injection rates are correct order of magnitude, and expected spatial variability	UC-do – baseline validation that prediction of inflow rates are correct order of magnitude, and expected spatial variability	UC-pc – basis for examining correlations between different measured and post-closure flow properties.
Pilot hole geometric conditioned (PHGC)	PHGC-pi – validation that uncertainty in predictions of injection rates can be reduced by conditioning on fracture traces	PHGC-do – validation that uncertainty in predictions of inflows can be reduced by conditioning on fracture traces	PHGC-pc – quantifies the reduction in uncertainty in predictions of post-closure conditions following geometric conditioning & correlations between measured and post-closure flows
Pilot hole hydraulic conditioned (PHHC)	PHHC-pi – quantifies how well local conditioning to the injection tests constrains uncertainty when simulating these tests	PHHC-do – validation that uncertainty in predictions of inflows can be reduced by conditioning on traces and injection tests	PHHC-pc – quantifies the reduction in uncertainty in predictions of post-closure conditions following injection test conditioning and in the correlations between measured and post-closure flows
Deposition hole geometric conditioned (DHGC)	DHGC-pi – simulating injection to preceding pilot holes not of practical relevance once deposition holes are reamed	DHGC-do – validation that uncertainty in predictions of inflows can be reduced by conditioning on fracture traces	DHGC-pc – quantifies the reduction in uncertainty in predictions of post-closure conditions following geometric conditioning and correlations between measured and post-closure flows
Deposition hole hydraulic conditioned (DHHC)	DHHC-pi – simulating injection to preceding pilot holes not of practical relevance once deposition holes are reamed	DHHC-do – quantifies how well local conditioning to inflow measurements constrains uncertainty when simulating this open hole condition.	DHHC-pc – quantifies the reduction in uncertainty in predictions of post-closure conditions following inflow conditioning and correlations between measured and post-closure flows

Other objectives are to test the methodology for DFN conditioning and ensure it is robust relative to the use of different types and combinations of real characterisation data.

1.3.1 Data review

Further constraining the stochastic, unconditioned realisations of the DFN model such that individual fracture properties as observed underground are honoured, allows conditioned simulations of the ONKALO Demonstration Area to be constructed. Typically, the data available for conditioning DFN models consist of fracture traces mapped on the surfaces of tunnels and deposition holes, as well as fractures logged in drillholes (see Chapter 3). The data could be limited to geometrical information, but might also include geological mapping (including fracture morphology and mineralogy, for example), as well as measurements of inflows and/or hydraulic tests.

Fracture mapping in Demonstration Tunnel 2 (DT2), Demonstration Tunnel 1 (DT1) and other surrounding access tunnels is available from the underground investigations (see Section 3.2). In addition, fractures logged within the six pilot holes (0.078 m diameter) drilled in the floor of DT2 are available (see Figure 3-5). These pilot holes were subsequently reamed (1.78 m diameter) to deposition holes (for demonstration purposes only) and geological mappings are also available of the surfaces of these holes (as shown in Figure 3-7). To date a joint Posiva-SKB programme of transient hydraulic injection tests in the pilot boreholes drilled ahead of deposition holes beneath DT2 (Hjerne et al. 2016) has been performed to provide information relating to injection flows within the whole pilot hole (excluding the top 0.5 m which has been packed off) as well as short (c. 0.5 m) packed-off intervals along the hole. Inflows to the six experimental deposition holes have also been recorded. A list of available data is given in Table 1-2, and illustrated in Figure 1-2.

In order for conditioning to be performed effectively using this data it is important that:

1. geometries of recorded traces are linked to the same fracture both along contiguous tunnel walls and separate tunnels or drillholes as far as possible (i.e. expressions of the same fracture are linked by a geologist) ;
2. flow measurements are localised to individual fractures to the extent possible.

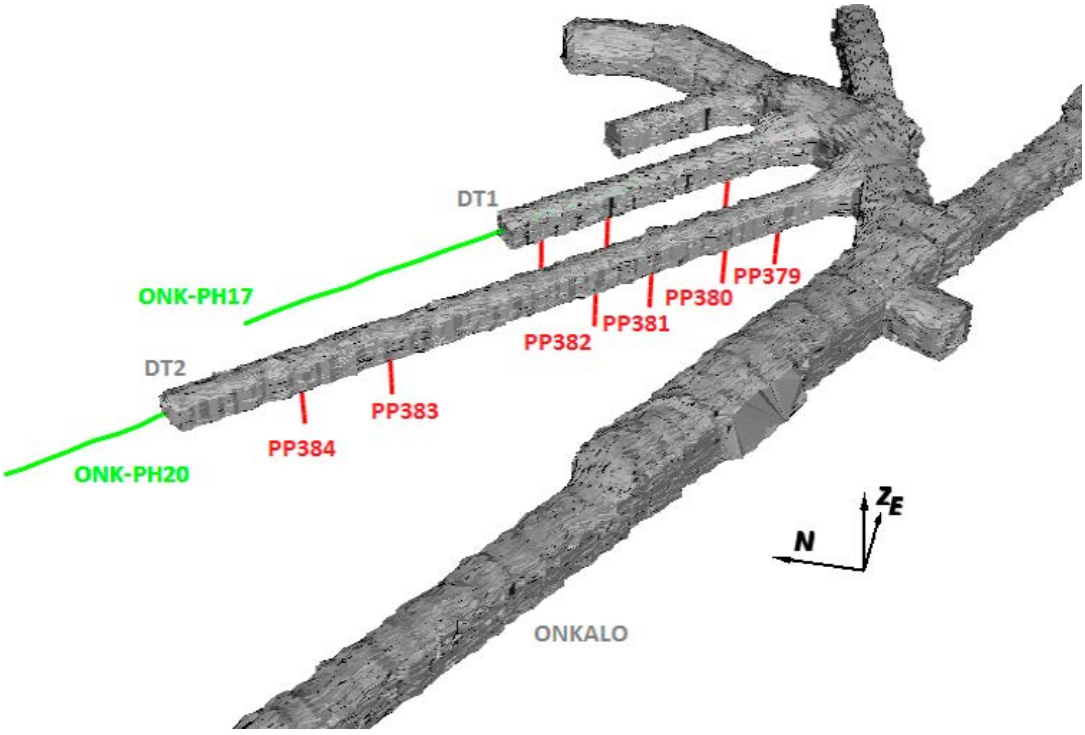

Figure 1-2. *Demonstration and access tunnels local to the Demonstration Area considered in this study, colour coded to indicate the tunnels (grey), pilot holes for deposition holes (red) and pilot holes extending beyond DT1 and DT2 (green).*

In addition, the actual fracture traces recorded on the complex and uneven tunnel surfaces are projected to their equivalent traces on simplified idealised representations of tunnel surfaces as suitable for modelling purposes (to ensure like-for-like comparisons can be made between observed and modelled traces).

Fracture specific capacities have been measured in the pilot holes, ONK-PP holes, both by means of injection testing between packers and by the PFL flow difference method. Hjerne et al. (2016) conclude, *"By and large the section-wise injection test results compared well with the PFL results although the magnitudes of the flow anomaly and resulting evaluated transmissivity was systematically lower for the PFL. The finding was mainly attributed to longer duration of the PFL tests resulting in sampling of larger rock volumes."* Accordingly, the PFL and injection test results are considered to be inter-changeable. In the current study, the transmissivities inferred from the injection tests are utilised as representing the properties of the immediate fractures being conditioned.

Table 1-2. Data available from drillholes and tunnels for conditioning DFN models within the Demonstration Area block domain. Each data source is shown in Figure 1-2.

Source	Data
ONKALO, DT1, and DT2 tunnels	Excavated tunnel surfaces have been digitised for the underground openings of the ONKALO Demonstration Area, including geological mappings of fracture traces. See Figure 3-4.
ONK-PH pilot holes extending from tunnels	ONK-PH20 extends 19.5 m beyond the end of DT2. ONK-PH17 extends 37.5 m beyond the end of DT1 (See Figure 3-3). Data for both pilot holes include fractures interpreted from image logs.
ONK-PP pilot holes drilled from tunnel floors	Three pilot holes for experimental deposition holes drilled from the floor of DT1 (ONK-PP315 - ONK-PP317), and six drilled from the floor of DT2 (ONK-PP379 - ONK-PP384). See Figure 3-5. Transient injection tests have been performed jointly by Pöyry & Geosigma (Hjerne et al. 2016) for the pilot holes in DT2 providing information relating to injection flows within the whole pilot hole (excluding the top 0.5 m which has been packed off) as well as short (c. 0.5 m) packed-off intervals along the hole. It is noted that additional Posiva Flow Log (PFL) measurements are available within the ONK-PP pilot holes for experimental deposition holes in DT2, providing additional measurements of fracture specific capacity.
ONK-EH experimental deposition holes in DT2	Digitised profiles of the DT2 experimental deposition holes (ONK-EH10 – ONK-EH13, ONK-EH15, and ONK-EH16) are available, including fracture trace mappings (see Figure 3-7). Total inflow measurements for the six experimental deposition holes of DT2 are also available.

1.4 Report structure

The remainder of this report is structured as follows:

- The DADFN model, derived in Hartley et al. (2017), is summarised in Chapter 2; and forms the underlying prescription for all subsequent DFN realisations, as well as library generation (for conditioning).
- Chapter 3 details a review of the data available for geometric and hydraulic conditioning of DFN models in the vicinity of the Demonstration Area of the ONKALO. Information includes tunnel and pilot hole geometries; fracture traces mapped within tunnels and experimental deposition holes, as well as those logged in pilot holes from image and core measurements; injection tests performed in the pilot holes; and inflow measurements to open deposition holes.
- A review of the key calibration targets and performance measures for understanding the success of conditioning the respective DFN models are defined in Chapter 4. These include calibration targets of the fracture trace length per unit surface area, fracture locations, injection test flow rates and deposition hole inflows; and performance measures based on post-closure flows.
- Simulation results for post-closure flow and transport in an unconditioned DFN model are presented in Chapter 5. Equivalent results for conditioned DFN simulations of ONKALO Demonstration Area are detailed in Chapters 6 and 7 based on pilot hole and deposition hole data, respectively.
- Chapter 8 presents the main conclusions and outcomes from the current study.

1.5 Acronyms used in this report

BFZ	Brittle fault zone
CTU	Central tectonic unit
DADFN	Demonstration area discrete fracture network
DFN	Discrete fracture network
DFNdb	DFN modelling database
DGN	Diatexitic gneiss
-do	Inflows to deposition holes
DHGC	Deposition hole geometric conditioned
DHHC	Deposition hole hydraulic conditioned
DT	Demonstration tunnel
EH	Experimental deposition hole
EW	East-West fracture set
EW_h	East-West horizontal fracture set
F	Flow related transport resistance
FP	Foliation parallel fracture set
FDZ	Flutanperä deformation zone
HTU	Hydraulic testing unit
Ja	Joint alteration
Jr	Joint roughness
KR	Cored drillhole
M	Closeness-of-fit measure
MD	Measured depth
MFGN	Mafic gneiss
MGN	Mica gneiss
NE	Northeast fracture set
NS	North-South fracture set
NW	Northwest fracture set
OL-	Olkiluoto surfaced based investigation locations, including drillholes
ONK-	ONKALO based investigation locations
PFL	Posiva flow log
PGR	Granitic pegmatoid
PHGC	Pilot hole geometric conditioned
PHHC	Pilot hole hydraulic conditioned
PH	Pilot hole
-pc	Post-closure flow and transport
-pi	Pilot hole injection
PP	Short pilot holes
RSC	Rock suitability classification
SDZ	Selkänummi deformation zone
TGG	Tonalitic-granodioritic-granitic gneiss
U	Average flow rate per unit width tangential to the repository structures
UC	Unconditioned
VGN	Veined gneiss

2 DFN model description

An underlying stochastic DFN model description for generating unconditioned realisations was defined by Hartley et al. (2017), representing the statistical distributions of fracture properties local to the ONKALO Demonstration Area and technical facilities, the so called DADFN model. In contrast to the Olkiluoto DFN v2 models where separate formulations were made for geometric (Fox et al. 2012) and hydraulic (Hartley et al. 2013a) modelling, DADFN prototypes a methodology for integrating the description of fracture geometries (occurrence and orientation) with other 3D geological models (lithology, ductile and brittle deformation) and hydraulics with fracture geophysical, morphological, mineralogical and rock stress data. It is intended that this more comprehensive synthesis of concepts and data will be adopted in the upcoming DFN v3 toward SDM 2018.

In this chapter, a summary of the DADFN model is presented, describing the concepts and numerical implementation of the model. The DADFN model was conceptualised and calibrated over a block extending laterally about 550 m to encompass the Demonstration Area as well as technical facilities. However, for the purposes of this conditioning study, only a sub volume of the DADFN domain is considered, extending approximately 200 m laterally to cover just the Demonstration Area.

2.1 Fracture orientations

Six global fracture sets were defined, related to a number of brittle tectonic episodes with associated palaeostress states that have been identified at Olkiluoto and surrounding areas (Mattila and Viola 2014). Of these

- two are gently dipping sets; one considered to be parallel to foliation and dipping southeast; and one horizontal or having a general east-west strike, and
- four are sub-vertical sets; one striking East-West (EW), one Northeast (NE), one North-South (NS) and one Northwest (NW).

Analysis identified spatial variations in both the mean orientations within a set and the relative intensity between sets. Variations in mean pole are described by a spatial interpolation between measurements; while variations in relative intensity on the scale of the model are considered to be adequately described relative to the different ductile domains.

Additional fault-related fractures were identified, represented numerically by clustering extra fractures around deterministically modelled Brittle Fault Zone (BFZ) planes and with orientations sub-parallel to the BFZ. The extra fractures being created using a parent-daughter type method, and once created the “parent” BFZ centre plane is removed. Three of the BFZ structures (BFZ020B, BFZ045 and BFZ297) were interpreted to have a distinctly higher hydraulic aperture (factor 2) than the remaining BFZs.

The calibrated DFN model parameters for each of the background sets and for fault related fractures are summarised in Table 2-2.

2.2 Fracture intensity

Drivers for fracture intensity were interpreted as being:

- **Ductile domain:** higher intensity in Selkänummi Deformation Zone (around the access and Demonstration tunnels to the north) than in Central Tectonic Unit 1 (around the technical facilities to the south). A small portion of the Flutanperä Deformation Zone (FDZ) overlaps the southern tip of the modelling domain, with intensities equated to those in SDZ as a proxy. A map of the ductile domain is shown in Figure 2-1 for a horizontal slice through the DADFN modelling domain (z = –420 m).

- **Lithology:** higher intensity in lithologies with more variable mechanical properties – higher in diatexitic gneiss than veined gneiss. A map of the lithological units is shown in Figure 2-2 for a horizontal slice through the DADFN modelling domain (z = –420 m), and
- **proximity to faults:** much higher intensity inside brittle deformation zones, or BFZ, and to a lesser extent in the surrounding rock, cf. Figure 2-4.

The 3D geological models for ductile domain and lithology are therefore used as drivers to produce a geocellular model of spatial variations in fracture intensity; a 5 m cell size is used to represent variations in lithologies, see Figure 2-2. Fracture intensity for each of the six global orientation sets, by ductile domain and lithology, are detailed in Table 2-3. In addition, specific clusters of enhanced fracturing in and around each BFZ are included. The thicknesses of BFZ vary significantly, and so the thickness of the clusters of additional fractures is made proportional to the thickness of the deformation zone (see Table 2-1).

Table 2-1. List of modelled BFZs from the combined regional and detailed scale BFZ model with their thicknesses used for each BFZ (here, assumed uniform along the plane) calculated by averaging the interpreted damage zone thicknesses at each drillhole intersection with the BFZ.

BFZ	Average Thickness [m]	BFZ	Average Thickness [m]
OL-BFZ005	3.47	OL-BFZ201	1.47
OL-BFZ020a	2.62	OL-BFZ202	3.77
OL-BFZ020b	3.93	OL-BFZ203	1.07
OL-BFZ025	7.71	OL-BFZ204	0.62
OL-BFZ028	10.80	OL-BFZ205	2.13
OL-BFZ039	14.55	OL-BFZ206	7.90
OL-BFZ043	0.71	OL-BFZ207	5.42
OL-BFZ045	5.01	OL-BFZ216	3.75
OL-BFZ046	1.13	OL-BFZ222	0.46
OL-BFZ063	0.73	OL-BFZ237	1.57
OL-BFZ084	1.92	OL-BFZ238	1.12
OL-BFZ122	1.56	OL-BFZ265	1.27
OL-BFZ123	3.87	OL-BFZ297	1.30
OL-BFZ129	1.45	OL-BFZ300	3.76
OL-BFZ130b	3.97	OL-BFZ346a	0.93
OL-BFZ170	1.81	DSM-BFZ002	0.02
OL-BFZ173	1.62	DSM-BFZ004	0.45
OL-BFZ174	0.66		

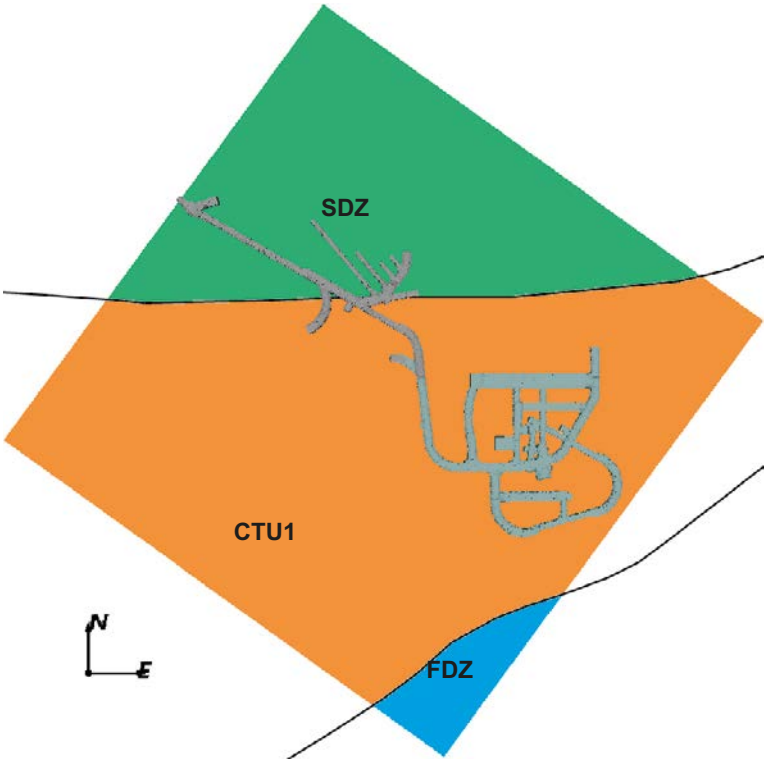

Figure 2-1. *A slice taken through the ductile region model at –420 m; division of detailed-scale domain into SDZ (green), CTU1 (orange) and FDZ (blue) shown. This figure is reproduced from Hartley et al. (2017). This domain is 550m square.*

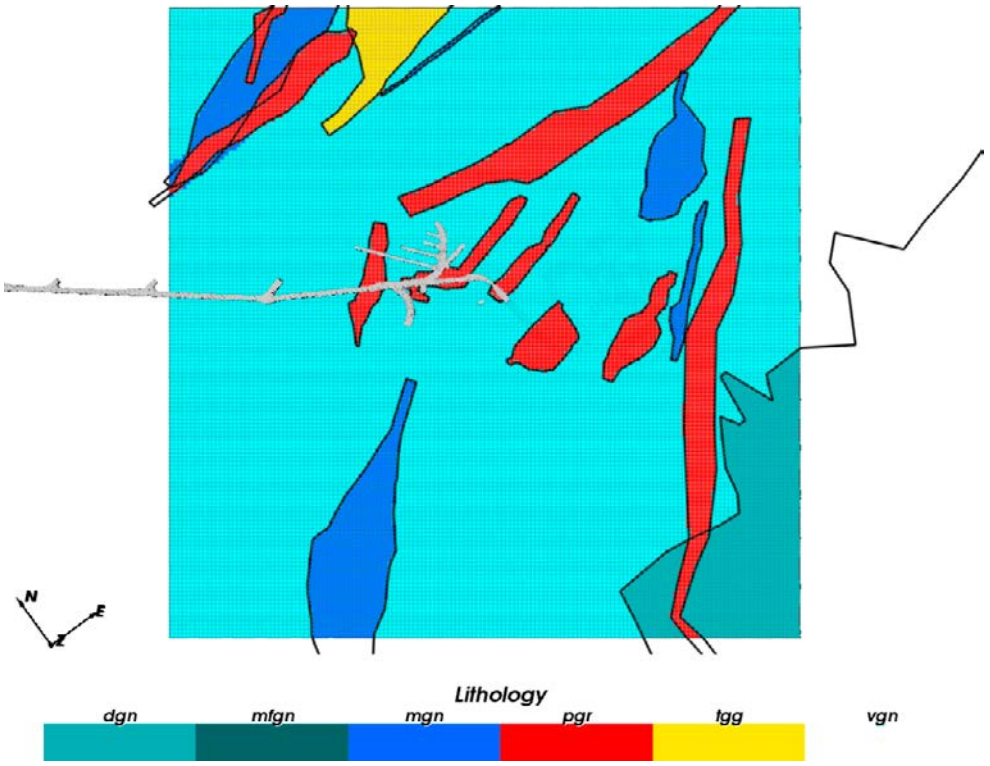

Figure 2-2. *A slice through the geocellular lithology model at –420 m. This figure is reproduced from Hartley et al. (2017). This domain is 550m square, and here rotated.*

2.3 Fracture size and shape

On the basis of data collated across a contiguous range of scales from drillhole scale fracturing, fracture trace mapping in the tunnels, the correlation of structures between drillholes and tunnels, localised seismic reflectors, and up to BFZ structural modelling, the overall intensity-size scaling was found to be well described by a power-law scaling model between intensity and size. The set specific parameterisation of fracture size is summarised in Table 2-2. Little evidence was identified (e.g. from fractures traces mapped between intersecting tunnels, or seismic) during the study to contradict the assumption that shape of fractures at Olkiluoto are equant, i.e. aspect ratios of around unity.

2.4 Fracture openings

The key characteristic determining the spatial distribution, continuity and channelisation of flow through the fracture system is the proportion of fracture surface area containing openings/voids, denoted as ω. A secondary parameter, the typical size or continuity of individual fracture openings, is denoted as a length scale L_h. The proportion of open fracture surface area has been estimated using a combination of geological classifications of fractures and measurement of high resolution single point resistivity recorded as part of the Posiva Flow Logging (PFL) campaign. The potentially open fractures were estimated from fractures identified as electrically conductive; found to be between 30–50 % outside BFZs. A similar analysis for those fractures located within the BFZ identified around 50–70 % as electrically conductive. As such, the DFN models assume the proportion is a function of size, $\omega(r)$, 30–40 % for smaller fractures (radius of decimetres to tens of metres), while 50–70 % is valid for small to large fault zones (radius of few tens of metres to kilometres). These estimates for the proportion of open fractures were fine-tuned through calibration of $\omega(r)$ using DFN simulations of flow to/from pumping drillholes against measurements from PFL tests in pilot holes and surface drillholes, as well as additional information from double packer (HTU) tests in some surface drillholes. The observed scarcity of water conducting fractures required the portion of open fracture area be reduced to about 20 % for fractures with a side length of 1 m, and 40 % for large fractures, side length 100s metres, so as to reduce connectivity of the hydraulically active parts of fractures.

The method for distributing fracture openings over the surface of each fracture was first developed in DFN v2 (Hartley et al. 2013a). Fractures of side length greater than L_h are subdivided into sub-fractures of this size, and deleted or retained probabilistically according to a uniform random deviate relative to the proportion of open fractures; while fractures of side less than L_h are simply deleted or retained using the same method. This reduces the intensity of small scale fractures and turns larger fractures in to a random chequerboard of open and closed sub-fractures, as shown in Figure 2-3. The calibration of flow simulations is far less sensitive to the choice of L_h than ω, although it does have significant effect on the continuity of individual flow and transport pathways. A value of 20 m is chosen for L_h, consistent with the denoted Case C in DFN v2 (Hartley et al. 2013b), while much large values would invoke models behaving similar to the models that have greater hydraulic continuity over single structures, denoted Case A in DFN v2.

A slice through one realisation of the unconditioned DFN model local to the ONKALO Demonstration Area is shown in Figure 2-4; the open portion of each fracture is coloured blue, and the closed proportion grey. This figure also clearly shows the enhanced fracturing around BFZ features within the modelled volume.

It should be emphasised that the current study makes use of the single model interpreted and calibrated in DADFN. However, the model is non-unique, and it is certainly possible that alternative models could be calibrated by varying ω and L_h, or more substantial variants considering uncertainties in fracture intensity and size. The results presented here should therefore be considered as illustrative, and the robustness of conclusions drawn may need to be subjected to alternative viable DFN models as well as additional realisations.

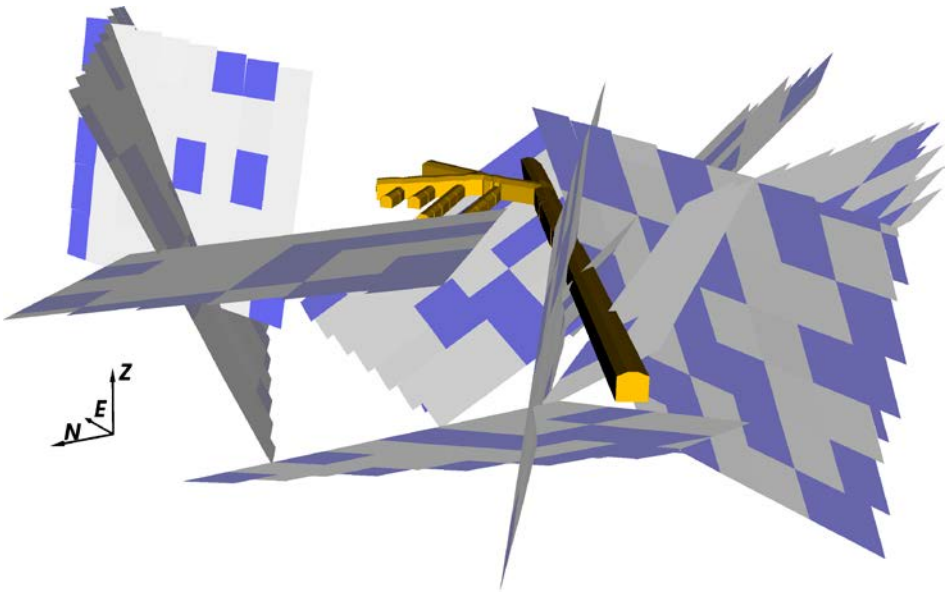

Figure 2-3. *The open (blue) and sealed (grey) areas of a large fracture intersecting the Demonstration Area of the ONKALO. The open fracture area is sampled probabilistically according to a uniform random deviate relative to the proportion of open fractures estimated from geological and resistivity data.*

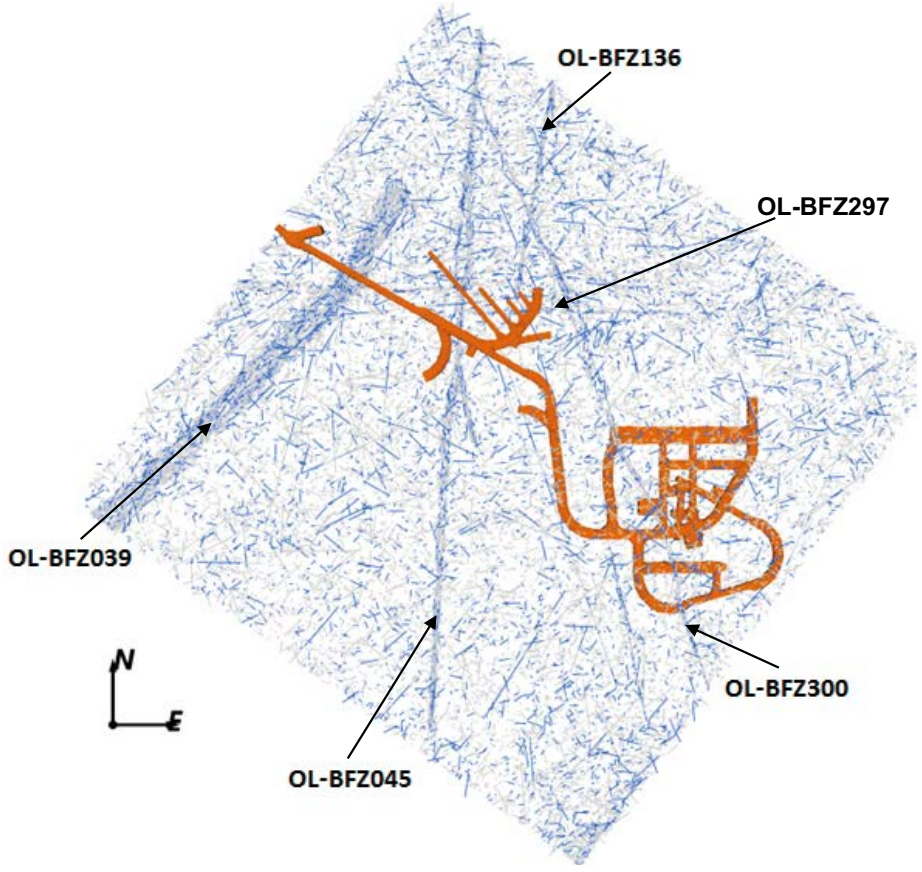

Figure 2-4. *Horizontal slice through all fractures (BFZ related and background) at –420m based on the DADFN modelling domain, which extends c. 500 m laterally to cover the Demonstration Area and technical facilities. Fractures are coloured by hydraulic openness at the length scale L_h = 20m: blue = open, grey = closed. Tunnels are shown in orange. Reproduced from Hartley et al. (2017).*

2.5 Fracture hydraulics

For DADFN, fracture hydraulics are formulated in terms of the spatial and statistical distributions of hydraulic apertures. The hydraulic aperture is assigned according to a function of size and incident rock stress (defined as a function of depth), but also includes probabilistic elements which in turn are a function of geological models. The first part of the formulation is based on the interpretation of a broad power law correlation between fracture aperture, e[m], and length, L[m]:

$$e = aL^b \,. \tag{2-1}$$

Through calibration of flow magnitudes for WCF, Hartley et al. (2017) estimate a coefficient of 1.12×10^{-5} m; with an exponent of 0.3 inferred from correlations between geological aperture and mapped fractures within the ONKALO. In addition, hydromechanical effects are considered as an important mechanism for understanding the occurrence of relatively high transmissivities through normal dilation. An initial unstressed aperture is calculated using the parameters given in Table 2-2, which is then reduced according to a hyperbolic function of effective normal stress on the fracture; see Section 6.3.2 of Hartley et al. (2017) and Section 2.3 of Hartley et al. (2016).

However, a subset of relatively transmissive fractures for this depth has also been identified, forming a very broad distribution of specific flow capacities as measured in hydraulic tests. By linking their occurrence to geological criteria, a semi-stochastic numerical approach is applied to all fractures in the model; probabilistically selecting a subset of fractures falling into at least one of the following three groups:

- **Alteration (using proximity to BFZ and size):** Fractures with high alteration (quantified by the Q-System parameter of Joint Alteration, Ja) correlate with an increased likelihood of water conductance. Spatially, high alteration occurs local to BFZ and in larger fractures, presumably related to increased likelihood of forming pathways for fluids and solutes. Rare fractures with high alteration, Ja≥3, have an increased likelihood of having significant transmissivity:
  - Stochastically select 27 % of fractures within 5m of a BFZ.
  - Stochastically select 17 % of fractures greater than 5m from a BFZ.
  - Double the probability of enhancing the aperture (i.e. 54 % or 34 %) if the fractures are large ($r \geq 5.6$ m).

All percentages used in the above aperture enhancement process are derived from detailed-scale domain data analysis in Hartley et al. (2017, Section 6.3.2).

- **Hydromechanical effects (using orientation):** Reactivation of fractures during the period of high shear to normal stress ratios generated during ice sheet retreat at the end of the last glaciation (edge passing) inducing shear dilation of fracture apertures (Barton et al. 1995) as such conditions briefly occur even at depth provides one possible mechanism for relatively high transmissivities:
  - Select all fractures with $\tau/\sigma_n' > 0.5$ when evaluated using the edge passing stress field of Valli et al. (2011).
- **Surface morphology and low normal stress (using orientation):** Many of the anomalously high transmissivity fractures not described by the above characteristics tend to be at low normal stress and with roughness described as slickensided, smooth or semi-rough, possibly correlating with larger fractures. Fracture morphology as characterised on the drillhole scale does not show any clear spatial pattern:
  - Stochastically identify 49 % of fractures with $\sigma_n' \leq 12$ MPa using the present-day stress field.

It may be noted that because principal stress orientations do not rotate greatly between the edge passing and present-day, then at this depth, fractures identified as potentially undergoing reactivation during the last glaciation (the second group above) are also identified as low normal stress fractures under present-day stress conditions (the third group above).

The initial hydraulic apertures (as originally calculated from the parameters stated in Table 2-2) of fractures selected as being in one or more of the above groups are then enhanced, with calibration indicating tripling of the underlying hydraulic aperture is necessary. The resulting distribution of transmissivity is shown on a horizontal slice (Figure 2-5) and vertical slice (Figure 2-6), calculated from the hydraulic aperture through the cubic law:

$$e = \sqrt[3]{\frac{12\mu T}{\rho g}} \qquad (2\text{-}2)$$

The large transmissivities $> 10^{-9}$ m^2/s can be seen to be generally located as segments in large sub-horizontal fractures or near BFZs.

Table 2-2. Summary of calibrated model parameters from Hartley et al. (2017); detailing six background sets, fault-related sets, and sets specific to three BFZ.

Set	Distribution of poles	Fisher conc.	Power-law (k_r, r_0, r_{min}[m], r_{max}[m])	Intensity P_{32} [m^2/m^3], Thickness (δ[m], α)	Fraction of open area *(ω(0.6), ω(560))*	Initial aperture distribution (a, [m] b, σ)
EW	Fisher	19.4	(2.82, 0.25, 0.5, 320)	Table 2-3, –, –	(0.2, 0.4)	(1.115×10^{-5}, 0.3, 0.0)
EW_h	Fisher	26.3	(2.8, 0.3, 0.5, 320)	Table 2-3, –, –	(0.2, 0.4)	(1.115×10^{-5}, 0.3, 0.0)
FP	Fisher	11.6	(2.8, 0.3, 0.5, 320)	Table 2-3, –, –	(0.2, 0.4)	(1.115×10^{-5}, 0.3, 0.0)
NE	Fisher	18.8	(2.82, 0.1, 0.5, 320)	Table 2-3, –, –	(0.2, 0.4)	(1.115×10^{-5}, 0.3, 0.0)
NS	Fisher	17.9	(2.82, 0.1, 0.5, 320)	Table 2-3, –, –	(0.2, 0.4)	(1.115×10^{-5}, 0.3, 0.0)
NW	Fisher	11.4	(2.82, 0.25, 0.5, 320)	Table 2-3, –, –	(0.2, 0.4)	(1.115×10^{-5}, 0.3, 0.0)
BFZ	Fisher	20.0	(2.8, 0.2, 0.5, 50)	Table 2-1, 15.0, 0.16	(0.2, 0.4)	(1.115×10^{-5}, 0.3, 0.0)
BFZ020B BFZ045 BFZ297	Fisher	20.0	(2.8, 0.2, 0.5, 50)	Table 2-1, 15.0, 0.16	(0.2, 0.4)	(2.23×10^{-5}, 0.3, 0.0)

Table 2-3. Fracture intensity P32 (m^2/m^3) for the size range shown in the Power-law column of Table 2-2 by background fracture set in each of two ductile domains and six lithologies.

	EW		EW_h		FP		NE		NS		NW	
	CTU1	SDZ	CTU1	SDZ	CTU1	SDZ	CTU1	SDZ	CTU1	SDZ	CTU1	SDZ
DGN	0.079	0.475	0.306	0.251	0.497	0.699	0.636	0.528	0.496	0.678	0.332	0.151
MFGN	0.067	0.457	0.258	0.241	0.418	0.672	0.535	0.507	0.417	0.651	0.279	0.145
MGN	0.085	0.558	0.327	0.295	0.530	0.821	0.678	0.619	0.529	0.795	0.354	0.177
PGR	0.067	0.457	0.258	0.241	0.418	0.672	0.535	0.507	0.417	0.651	0.279	0.145
TGG	0.067	0.457	0.258	0.241	0.418	0.672	0.535	0.507	0.417	0.651	0.279	0.145
VGN	0.062	0.399	0.241	0.211	0.391	0.587	0.500	0.443	0.390	0.569	0.261	0.127

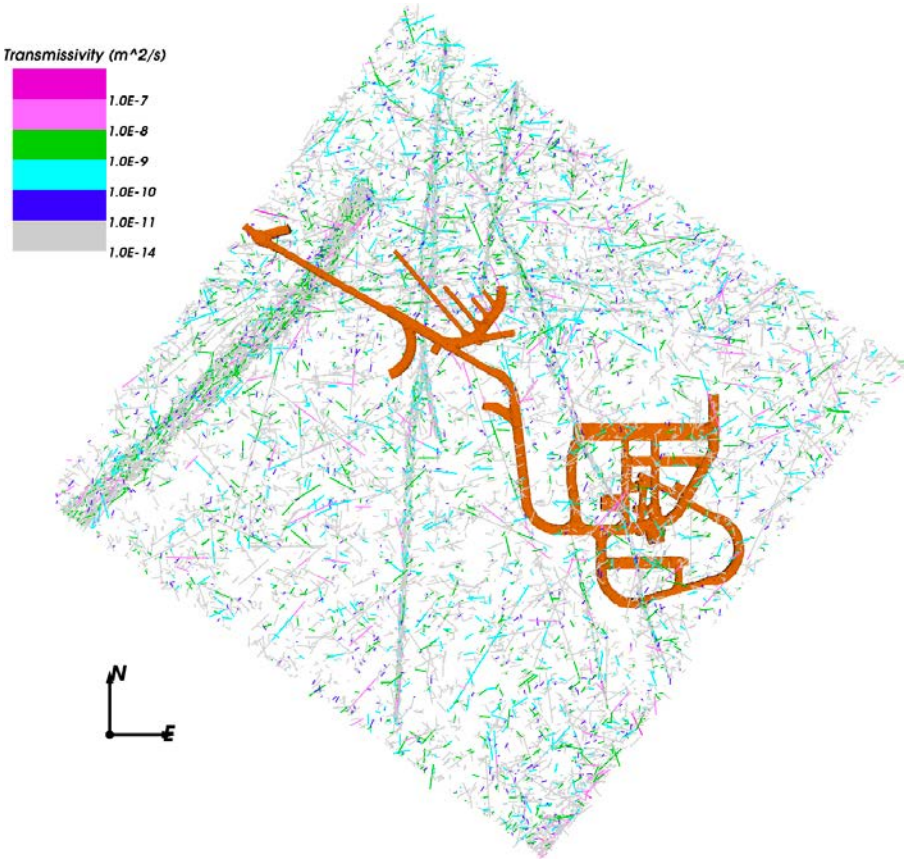

Figure 2-5. *Slice through calibrated model at −420m with fractures coloured by transmissivity or grey if closed. Tunnels are shown in orange.*

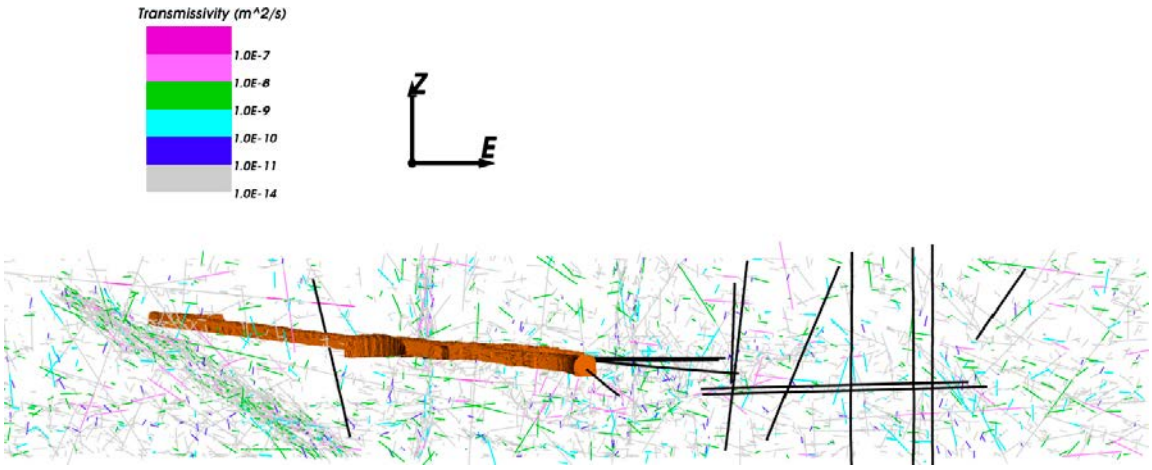

Figure 2-6. *E–W slice through technical facilities and main shaft of calibrated model, view from south looking north with fractures coloured by transmissivity or grey if closed. Tunnels are shown in orange, drillholes in black.*

3 Data collation and review

In this chapter, a review of the data available for geometric and hydraulic conditioning of DFN models in the vicinity of the ONKALO Demonstration Area is detailed. Information includes: the modelling domain; tunnel and pilot hole geometries; fracture traces mapped within tunnels and experimental deposition holes, as well as those logged in pilot holes; injection tests performed in the pilot holes; and inflow measurements to open deposition holes.

3.1 Demonstration block model

For the conditioned simulation of DFN models, a modelling domain is defined local to the Demonstration Area of the ONKALO. The modelling domain used in this study is shown in Figure 3-1, it forms a block extending 325 × 300 m laterally and 120 m deep centred on the Demonstration Area. The block is slightly smaller than that considered for conceptual analysis and model calibration in Hartley et al. (2017), which extended laterally about 550 m to also encompass the technical facilities. The block is restricted in extent since the geometries of the tunnels are modelled explicitly, and it is significantly easier to grid only the Demonstration Area and access tunnels without having to grid the technical facilities and shafts also.

Having said that, the representation of the access tunnels and demonstration tunnels are still idealised, and some details neglected. A comparison between the raw tunnel surfaces and their idealised representations is shown in Figure 3-2. The ONKALO access ramp (ONK-VT), Demonstration Area access tunnels (ONK-TT-4399, ONK-TYT-4399-21) and four Demonstration Tunnels (ONK-TDT-4399-69, ONK-TDT-4399-56, ONK-TDT-4399-44, and ONK-TDT-4399-30) are all included in the model. In addition the six experimental deposition holes beneath DT2 are represented, namely ONK-EH10 – ONK-EH13, ONK-EH15 and ONK-EH16. The model domain provides good agreement with the actual physical tunnel surfaces throughout the block, with deviations only apparent towards the top of access ramp. It is noted that a couple of tunnel niches (ONK-TKU-4219, ONK-TT-4366) extending from the ONKALO ramp, as well as experimental deposition holes located in DT1 are not included in the model.

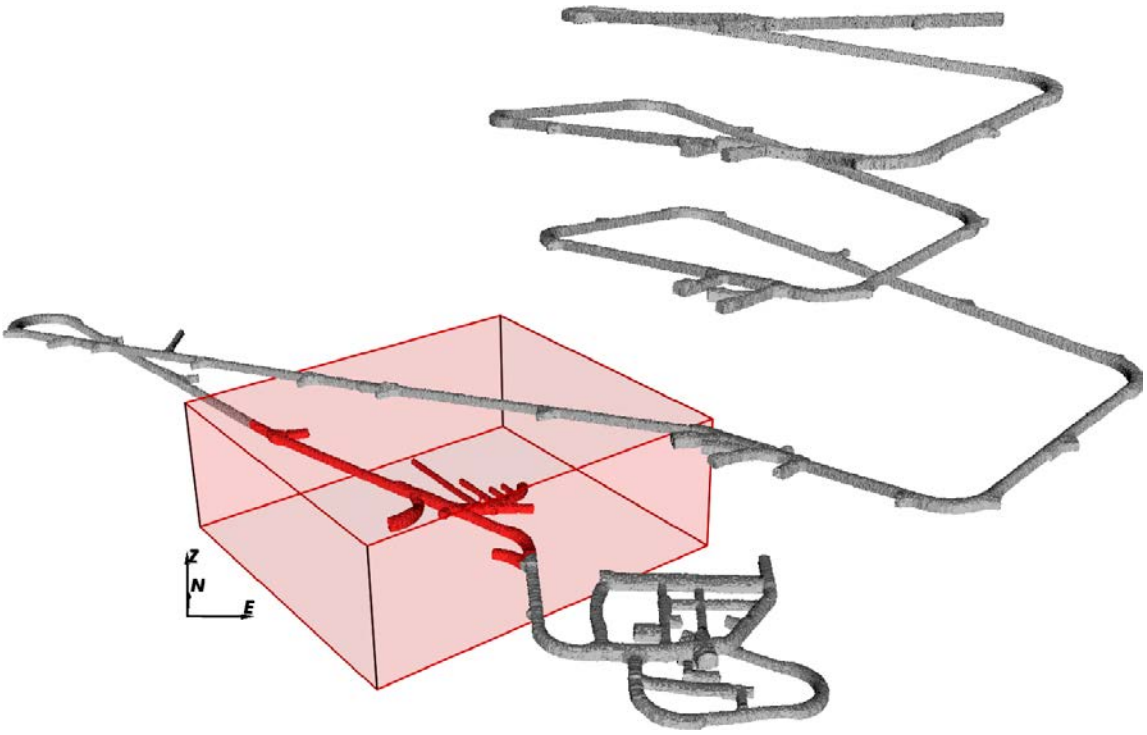

Figure 3-1. *Demonstration Area block model used for all simulations (red).*

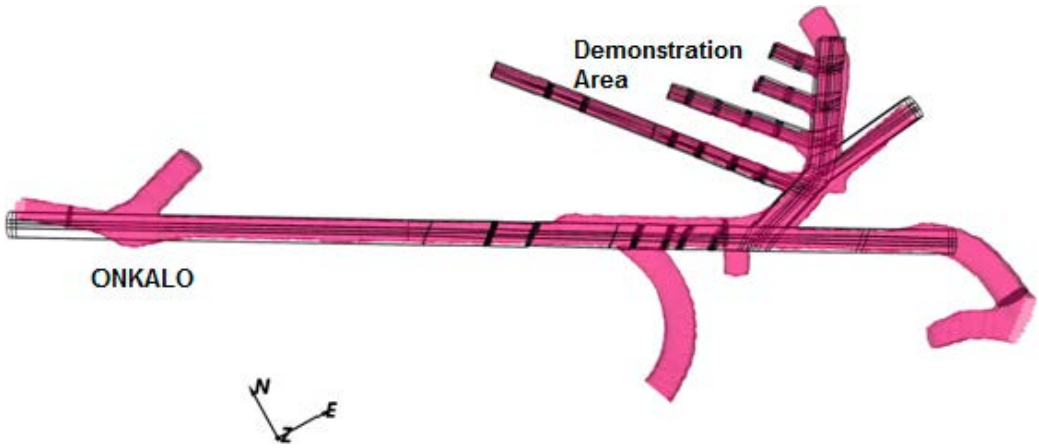

Figure 3-2. *Model representation (black lines) of the access tunnels and Demonstration Area of ONKALO (actual in pink).*

Table 3-1 and Table 3-2 summarise all of the underground openings within the block model for the Demonstration Area, including pilot holes (for tunnels and experimental deposition holes) and tunnels. The availability of geological interpretations of fractures, either from tunnel mapping or drillhole image interpretations is detailed for each underground feature. Cases where pilot holes have been reamed to experimental deposition holes or excavated to tunnels are also recorded.

Table 3-1. Drillholes and tunnels other than those associated with Demonstration Tunnels 1 and 2 that reside within the Demonstration Area block model.

Drillhole		Comment	Tunnel	
Fracture Logs	Name		Name	Fracture Traces
Y	ONK-PH13	ONKALO access ramp	ONK-VT1	Yes
Y	ONK-PH14		ONK-VT1	Yes
No preceding drillhole		Tunnels (without preceding pilot holes) providing access to the demo area: • ONK-TT-4399 leads from the main ONKALO ramp. • ONK-TYT-4399-21 forms a fork from ONK-TT-4399.	ONK-TT-4399	Yes
No preceding drillhole			ONK-TYT-4399-21	Yes
Y	ONK-KR13	Drilled off of ONK-TKU-4219 (located towards top of the ONKALO ramp in model domain). *Note this tunnel is not explicitly included in the model)*	Not excavated to tunnel scale	
Y	ONK-PVA9	Drilled off of ONK-TT-4366 (located off of the ONKALO ramp close to the demo area). *Note this tunnel is not explicitly included in the model*	Not excavated to tunnel scale	
N	ONK-KR16	Drilled off of ONK-TT-4366 (located off of the ONKALO ramp close to the demo area). *Note this tunnel is not explicitly included in the model*	Not excavated to tunnel scale	
Y	ONK-PH23	Pilot hole drilled off of ONK-TYT-4399-21	Not excavated to tunnel scale	
Y	ONK-PH22	Pilot hole drilled off of ONK-TT-4399	Not excavated to tunnel scale	
Y	ONK-PH21	Pilot hole drilled off of ONK-TT-4399	Not excavated to tunnel scale	
Y	ONK-PH27	Short demonstration Tunnel 4	ONK-TDT-4399-69	Yes
Y	ONK-PH26	Short demonstration Tunnel 3	ONK-TDT-4399-56	Yes
Y	ONK-PP416	Drilled between demo 3 and 4	Not excavated to tunnel scale	
Y	ONK-PP417	Drilled between demo 3 and 4	Not excavated to tunnel scale	
Y	ONK-PP418	Drilled between demo 3 and 4	Not excavated to tunnel scale	
Y	ONK-PP419	Drilled between demo 3 and 4	Not excavated to tunnel scale	
Y	ONK-PP420	Drilled between demo 3 and 4	Not excavated to tunnel scale	
Y	ONK-PVA11	Drilled off of ONK-TT-4399	Not excavated to tunnel scale	

Table 3-2. Demonstration Tunnels 1 (DT1) and 2 (DT2) and associated pilot holes and experimental deposition holes.

Drillhole		Comment	Tunnel	
Fracture Logs	Name		Name	Fracture Traces
Y	ONK-PH17	DT1. Note ONK-PH17 extends beyond the end of the tunnel	ONK-TDT-4399-44	Yes
Y	ONK-PP315	First pilot hole / experimental deposition hole drilled in the floor of DT1	ONK-EH6	No
No preceding drillhole		Second experimental deposition hole drilled in the floor of DT1 (bored without a preceding pilot 'PP' hole)	ONK-EH7	Yes
Y	ONK-PP316	Second pilot hole / third experimental deposition hole drilled in the floor of DT1	ONK-EH8	No
Y	ONK-PP317	Third pilot hole / fourth experimental deposition hole drilled in the floor of DT1	ONK-EH9	No
Y	ONK-PH16	DT2 (first section)	ONK-TDT-4399-30	Yes
Y	ONK-PH20	DT2 (second section). Note ONK-PH20 extends beyond the end of the tunnel	ONK-TDT-4399-30	Yes
Y	ONK-PP379	First pilot hole / experimental deposition hole drilled in the floor of DT2	ONK-EH10	Yes
Y	ONK-PP380	Second pilot hole / experimental deposition hole drilled in the floor of DT2	ONK-EH11	Yes (spalling)
Y	ONK-PP381	Third pilot hole / experimental deposition hole drilled in the floor of DT2	ONK-EH12	Yes
Y	ONK-PP382	Fourth pilot hole / experimental deposition hole drilled in the floor of DT2	ONK-EH13	Yes
Y	ONK-PP383	Fifth pilot hole / experimental deposition hole drilled in the floor of DT2	ONK-EH15	Yes
Y	ONK-PP384	Sixth pilot hole / experimental deposition hole drilled in the floor of DT2	ONK-EH16	Yes

3.2 Geological mapping in tunnels

3.2.1 Fracture mappings

Geological mapping data are available for the entire ONKALO, Demonstration Area and technical facilities, with mapped fracture traces available from a tunnel chainage of 3000 m and onwards. ONKALO mapping procedures are described in Engström and Kemppainen (2008) and Norokallio (2015) according to the following three stages (see Baxter et al. (2016) for how the data are used in the DFN database, DFNdb):

- Round Mapping: The first stage of geological mapping is round mapping, and is performed immediately after excavation of the round. Its purpose is to provide geological data; allowing geotechnical assessment of the tunnel rock mass for the continued excavation.
- Systematic Mapping: The second stage of geological mapping is systematic mapping and provides the majority of geological information gathered from the tunnel rounds. The resolution of systematic mapping includes fracture traces with length greater than 0.25 m.
- Supplementary Studies: The third and final mapping stage includes any additional supplementary studies, including: mapping of deformation zone intersections; hydrogeological mapping; Schmidt hammer testing; and petrological, mineralogical and hydrogeochemical sampling.

For conditioned DFN simulations, fracture traces mapped within the tunnel system local to the Demonstration Area are required, including: ONKALO access ramp (ONK-VT1); the access tunnels to the Demonstration Area (ONK-TT-4399 and ONK-TT-4399-21); and the four Demonstration Tunnels (ONK-TDT-4399-69, -56, -44, -30).

Across this tunnel system, 4830 fracture traces have been mapped and are available for conditional simulation. However, these fracture traces do not represent the full distribution of fracture trace lengths intersecting the tunnel; rather they are constrained by a censoring of the mapping procedure adopted. For example, at chainage 4400 m, updated work safety instructions resulted in changes to the working procedures, with subsequent round mappings performed under the shotcreted roof of the previous round. In addition, once this mapping was completed the roof of the newly excavated round was also shotcreted. Therefore, from a chainage of 4400 m, all geological mapping of the roof of the tunnel was performed during the round mapping stage. However, since this mapping phase is mainly for the geotechnical assessment, only fractures that were considered significant and with length greater than 1 m were digitised using the total station. The effects of the reduced intensity of fracture traces mapped on the roof of the tunnels under the working procedures is evident in Figure 3-3; where before a chainage of 4400 m, fracture traces mapped on the roof of ONKALO were interpreted down to a trace length of 0.25 m, whereas post 4400 m chainage, the resolution of geological mapping is 1 m.

Sections of the tunnels not currently mapped also need consideration when building the conditioned DFN simulations. At present, the floors of the ONKALO access ramp and tunnels leading to the Demonstration Area have not been mapped, and therefore no fracture traces are available for conditioning on these tunnel surfaces.

Table 3-3 details the censoring of fracture traces on the floor, walls and roof of each of the seven tunnels considered in the current study. The conditioning algorithm implemented within ConnectFlow conditions all fracture traces above the censoring limit on each of the tunnel surfaces, whilst retaining the stochastically generated fractures which intersect the tunnels with trace length less than the local censoring limitation. By retaining these stochastically generated fractures below the censoring limit, fracture statistics are not unduly distorted as a consequence of limitations of the tunnel mapping procedures.

Table 3-3. Truncation in fracture trace mapping within different tunnels local to the Demonstration Area.

Tunnel	Surfaces	Censoring limit [m]
ONKALO < 4400 m	roof, wall floor	0.25 not mapped
ONKALO > 4400 m	roof wall floor	1.0 0.25 not mapped
ONK-TT-4399	roof wall floor	1.0 0.25 not mapped
ONK-TYT-4399-21	roof, wall floor	0.25 not mapped
ONK-TDT-4399-30 ONK-TDT-4399-44 ONK-TDT-4399-56 ONK-TDT-4399-69	roof, wall, floor roof, wall, floor roof, wall, floor roof, wall, floor	0.25 0.25 0.25 0.25

The mapped fracture traces have also been processed to identify whether the interpreted fractures can be associated with a Brittle Fault Zone (BFZ). Fractures assigned to a BFZ structure are honoured within the conditioning algorithm by selecting potential candidates from the fracture library generated specific to the BFZ related set (see Chapter 2) so as to ensure fractures are selected from a consistent statistical model.

Finally, for DFN conditioning, it is important that any interpretation regarding the continuity of fractures between tunnels and drillholes is utilised. Therefore fracture mappings interpreted in tunnels and drillholes should first be linked before applying the conditioning algorithm which will then adhere to this additional information; constraining the potential fracture sizes that may be selected and retaining the continuity interpreted in the data. If the continuity between fracture traces is not considered, then conditioning will typically bias towards smaller fractures that can still match the observed traces; and the continuity between the tunnels and drillholes will not be enforced. For the data local to the Demonstration Area, geological mapping of fracture traces on tunnel walls typically identifies instances where a single fracture yields two or more disjoint fracture traces. However, fractures identified in drillholes are not linked with other observations, whether interpreted in other drillholes; or interpreted on nearby tunnel surfaces.

3.2.2 Trace projection

A requirement of the conditioning methodology is that the raw digitised fracture traces correspond to planar structures intersecting the modelled tunnel geometry. Figure 3-2 illustrates the tunnel geometries local to the Demonstration Area of ONKALO, representing both the high resolution digitisation as well as the approximated model definition. To successfully condition fracture models using these idealised tunnel geometries, the raw digitisations of the fracture traces require pre-processing, such that they are approximated as the intersection of a planar fracture with the tunnels. The workflow for projecting each fracture trace (or sequence of fracture traces) associated with a single fracture is as follows:

- The orientation of the fracture is calculated from either:
  - Geologist interpretations; or
  - A best fit plane through the digitised fracture trace (where fracture traces are defined by 3 or more non-colinear points).
- An infinite planar fracture is generated using this orientation, and positioned to provide a best fit to the digitised fracture trace. The intersection of this planar fracture with the tunnel geometries (as represented in the mesh) is calculated.
- The intersection of the planar fracture with the tunnel geometry is modified to conform to the extents of the original trace data to form the projected fracture trace.
- The fracture trace can then be exported for conditioning.

Figure 3-4 illustrates the projected fracture traces (red) and the raw digitisations (blue) for tunnels local to Demonstration Area.

The conditioning methodology could also make use of fracture specific (i.e. linked to each geologically mapped trace) inflow data. These data are not readily available currently. Quantitative inflow data for sections within Demonstration Tunnel 2 are being acquired, and it may be possible to attribute this to individual traces either using qualitative inflow mapping from the tunnels, or from hydraulic tests performed in the pilot holes that proceeded the tunnels, since it is sometimes possible to link water conducting fractures seen in the pilot hole to fracture traces later seen on the tunnel wall.

3.3 Pilot hole data in the demonstration tunnels DT1 and DT2

In addition to the fracture traces mapped on tunnels (Section 3.2), pilot holes within the Demonstration Area provide additional data for constraining DFN models through conditioned simulation. This study considers three pilot holes (ONK-PP315 – PP317) of c. 8 m length drilled in the floor of DT1, with an additional six pilot holes (ONK-PP379 – PP384) drilled in the floor of DT2. The location of these pilot holes are illustrated in Figure 3-5. In addition to these nine short vertical pilot holes, the near horizontal ONK-PH17 is drilled beyond the end of DT1, extending 37.5 m; with ONK-PH20 drilled beyond the end of DT2, extending 19.5 m. The locations of ONK-PH17 and ONK-PH20 are shown in Figure 3-3.

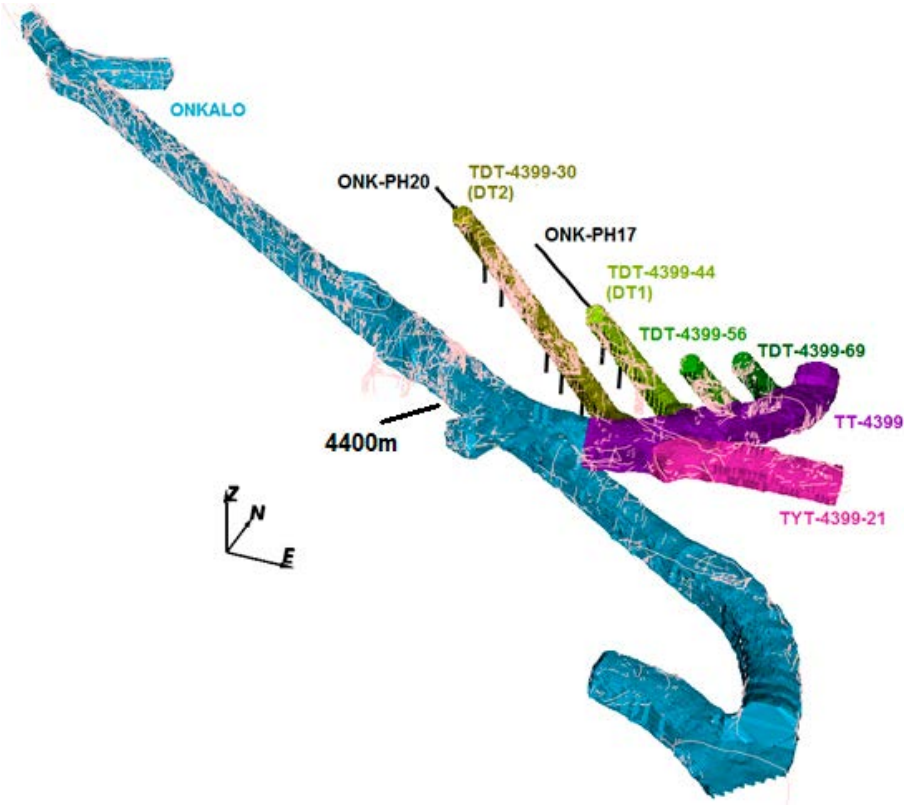

Figure 3-3. *Demonstration and access tunnels local to the Demonstration Area considered in this study, colour coded to indicate the different tunnel regions: blue indicate the main ONKALO ramp; pink/purple access to the Demonstration Area; and green/yellow the demonstration tunnels. Fracture trace geometries are superimposed in pink. The reduced fracture trace occurrence beyond 4 400 m chainage where working procedures were changed is apparent.*

Logged fractures are available for conditioning in all 11 of these pilot holes, with 103 fractures interpreted from core in the ONK-PP holes and an additional 365 interpreted from image in ONK-PH17 and ONK-PH20. In total, orientation data are available for 361 of the 468 interpreted fractures. As for fracture traces, the fractures logged in the pilot holes have been processed and linked to a BFZ where appropriate. Again, fractures assigned to a BFZ structure are honoured within the conditioning algorithm by selecting potential candidates from the fracture library generated within the BFZ related domains (see Chapter 2). The geometric pilot hole data available for conditioning are summarised in Table 3-4. The data in the pilot holes for experimental deposition holes are based on core mapping only, not image interpretation, which means the geometric data are approximate at best.

Table 3-4. Pilot holes that reside within the Demonstration Area block model used for conditioning. Relative numbering of holes is from the tunnel mouth.

Drillhole	Description	Number of fractures	Fractures with orientations
ONK-PH17	ONK-PH17 extends beyond the end of DT1	292	208
ONK-PP315	First pilot hole drilled in the floor of DT1	3	3
ONK-PP316	Second pilot hole drilled in the floor of DT1	10	10
ONK-PP317	Third pilot hole drilled in the floor of DT1	13	0
ONK-PH20	ONK-PH20 extends beyond the end of DT2	73	63
ONK-PP379	First pilot hole drilled in the floor of DT2	2	2
ONK-PP380	Second pilot hole drilled in the floor of DT2	2	2
ONK-PP381	Third pilot hole drilled in the floor of DT2	23	23
ONK-PP382	Fourth pilot hole drilled in the floor of DT2	19	19
ONK-PP383	Fifth pilot hole drilled in the floor of DT2	22	22
ONK-PP384	Sixth pilot hole drilled in the floor of DT2	9	9

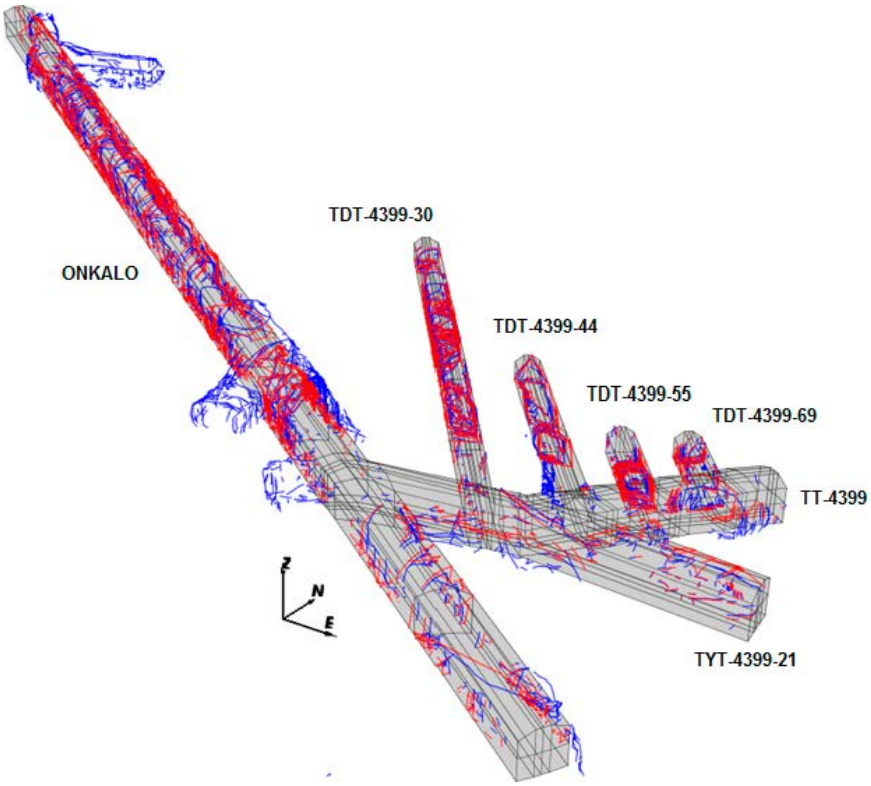

Figure 3-4. *Raw fracture traces (blue) and fracture trace projections (red) onto the idealised tunnel geometries of the Demonstration Area block model.*

3.3.1 Geological context

As detailed in Chapter 2 an underlying stochastic DFN model description for generating unconditioned realisations was defined by Hartley et al. (2017), representing the statistical distributions of fracture properties local to the ONKALO Demonstration Area and technical facilities based on 3D geological models (lithology, ductile and brittle deformation). As such, the DADFN model reflects underlying spatial variation in fracture occurrence based on the local lithological and ductile units as well as proximity to deformation zones. Table 3-5 provides a description of the rock local to each of the six experimental deposition holes in DT2, detailing lithological and ductile mappings as well proximity to BFZ, with the BFZ intersecting the Demonstration Area of the ONKALO also illustrated in Figure 3-6.

Table 3-5. Geological setting of each of the six pilot holes for experimental deposition holes drilled in the floor of DT2.

Drillhole	Deposition hole	Geological setting
ONK-PP379	ONK-EH10	ONK-EH10 lies just inside the Selkänummi Deformation Zone (SDZ), bounding the Central Tectonic Unit 1 (CTU1) at the entrance to DT2. The lithological description of the entire hole is Diatexitic Gneiss (DGN).
ONK-PP380	ONK-EH11	ONK-EH11 lies just inside SDZ, bounding CTU1 at the entrance to DT2. The lithological description of the entire hole is Veined Gneiss (VGN).
ONK-PP381	ONK-EH12	ONK-EH12 lies inside the SDZ. The lithological description is a mixture of DFN, VGN and Granitic Pegmatoid (PGR). The deposition hole is in close proximity to BFZ297.
ONK-PP382	ONK-EH13	ONK-EH13 lies inside the SDZ. The lithological description is a mixture of DGN and VGN. The deposition hole is in close proximity to BFZ297 with BFZ045 also nearby.
ONK-PP383	ONK-EH15	ONK-EH15 lies inside the SDZ. The lithological description is PGR. Two BFZ pass local to the hole, BFZ084 and BFZ346a.
ONK-PP384	ONK-EH16	ONK-EH16 lies inside the SDZ. The lithological description is PGR. The nearest BFZ correspond to those local to ONK-EH15 (namely BFZ084 and BFZ346a).

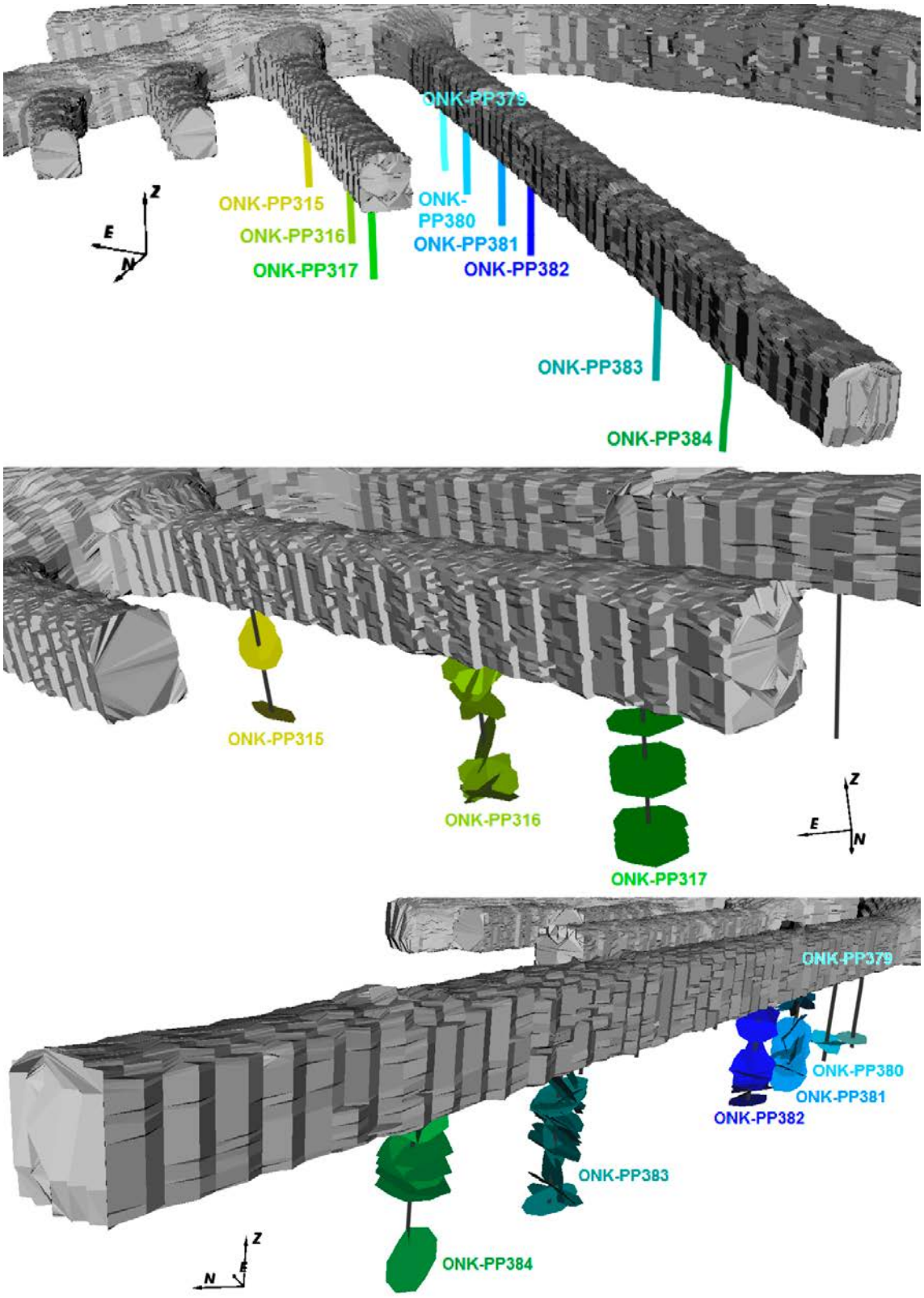

Figure 3-5. *Top: ONK-PP pilot holes as drilled from the floor of the Demonstration Tunnels. Middle: shows the fractures imaged from the pilot holes in DT1; bottom: the fractures from DT2. Note for ONK-PP317 (under DT1), orientation data has not been interpreted for the fractures.*

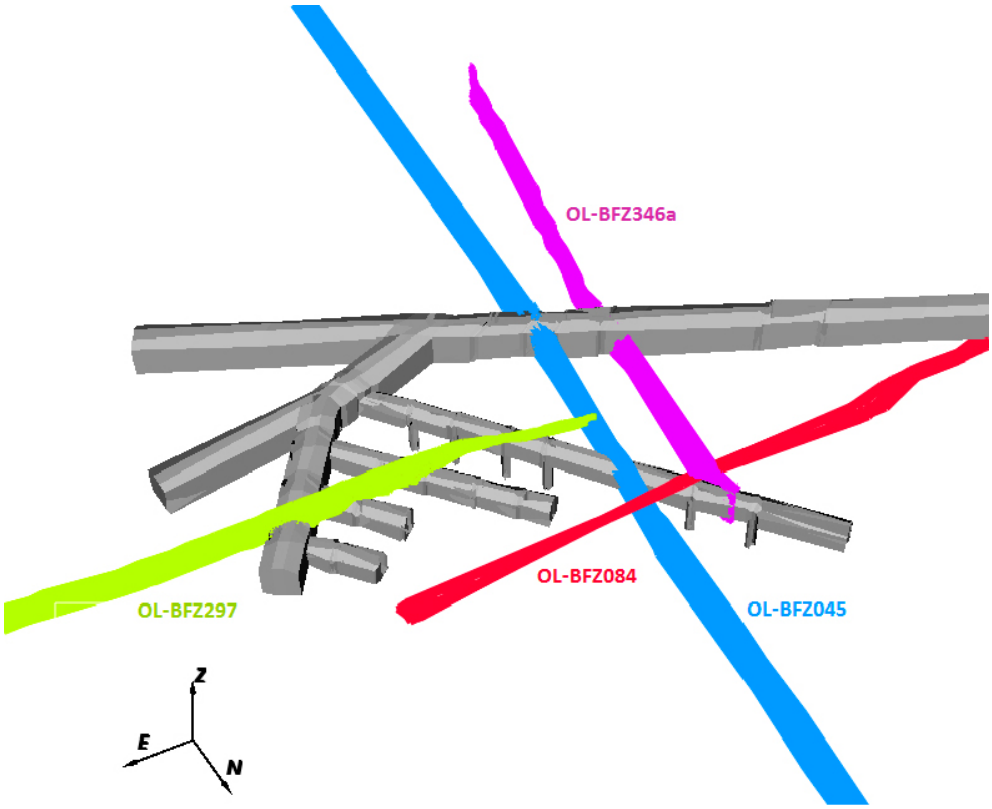

Figure 3-6. *Demonstration and access tunnels local to the Demonstration Area considered in this study. The four BFZ which intersect the Demonstration Tunnel 2 are shown for a slice between −410 m and −420 m elevation.*

3.3.2 Injection test measurements

Transient injection tests for the six pilot holes for experimental deposition holes, drilled in the floor of DT2, have been performed under a joint Posiva-SKB programme by Pöyry and Geosigma (Hjerne et al. 2016). Typically injections were performed for the entire pilot hole (top 0.5 m packed-off) with measurements presented in Table 3-6, corresponding to Geosigma measurements for holes ONK-PP379 and ONK-PP380; and Pöyry measurements for holes ONK-PP381 through ONK-PP384. Selection of these measurements is based on:

- For ONK-PP379 and ONK-PP380, only measurements from Geosigma are available.
- For ONK-PP382 and ONK-PP383, only measurements from Pöyry are available, and
- for ONK-PP381 and ONK-PP384, both teams performed injection tests over the pilot holes, and although Pöyry's results are used in this study, measurements from both teams were consistent.

It is noted that additional Posiva Flow Log (PFL) measurements are available within the ONK-PP pilot holes for experimental deposition holes in DT2, providing additional measurements of fracture specific capacity based on inflows to the holes. These PFL measurements are likely to have higher resolution in identifying locations of individual water conducting fractures intersecting the pilot holes when compared to the injection test measurements, although the injection tests do have higher resolution of flow due to the larger head changes possible. In addition, augmenting these two data sources for flow would potentially provide additional information of local connections to other underground openings. Therefore, combining data for injection tests in pilot holes with inflow to open pilot holes (PFL) could enhance the data available for hydraulic conditioning of the DFN models. However, in this study, these PFL measurements are not considered; with hydraulic conditioning of pilot holes based solely on the injection test measurements detailed above.

Although injection tests for the entire hole can be used as a metric for quantifying the capability of individual DFN models to reproduce measurements, for conditioned DFN simulation, it is necessary to assign the flow to individual fractures intersecting the pilot holes. In addition to the injection tests detailed in Table 3-6, Hjerne et al. (2016) also report additional tests performed at 0.5 m intervals, identifying sections of the pilot holes that are water conducting and those that do not connect to the wider fracture network. Using these 0.5 m interval measurements, the individual fracture contributions to flow in each hole have been estimated based on their proximity to the test (i.e. does it intersect the pilot hole within the tested 0.5m interval); geological mappings for J_r and J_a; and additional mapping information recording whether the fracture is sealed or not. For more information on these geological properties, and their relation to flow, the reader is referred to the conceptual analysis of Hartley et al. (2017, Chapters 4 and 5). A summary of the measured specific capacities for pilot hole sections in ONK-PP381, ONK-PP382 and ONK-PP384 (i.e. those pilot holes with flow measurements above the detection limit) to individual identified fractures is detailed in Table 3-7. It is noted that for ONK-PP381 and ONK-PP384, the sum of the specific capacities for flow in 0.5 m sections of the pilot holes is greater than the total specific capacity measurement for the hole. These differences could be a function of the wider fracture network, or experimental limitations. Hjerne et al. (2016) made some effort to cleanse the specific capacity measurements, although the values used in this study correspond to the raw experimental values detailed in Table 3-6 and Table 3-7.

Table 3-6. Injection tests performed in pilot holes for experimental deposition holes in DT2 over the complete hole (excluding the top 0.5 m which has been packed-off to be considered by a dedicated instrumented test section focused on the perceived EDZ along the tunnel floor).

Name	Source	Duration [min]	Injection head [m]	Q [m^3/s]	Specific Capacity [m^2/s]
ONK-PP379*	Geosigma	9	37.9	$< 1.67 \times 10^{-8}$	$< 4.4 \times 10^{-10}$
ONK-PP380*	Geosigma	6.5	53.2	$< 1.67 \times 10^{-8}$	$< 3.1 \times 10^{-10}$
ONK-PP381	Pöyry	60	59.6	1.50×10^{-7}	2.6×10^{-9}
ONK-PP382	Pöyry	60	23.6	2.33×10^{-8}	1.0×10^{-9}
ONK-PP383*	Pöyry	60	56.5	$< 1.67 \times 10^{-9}$	$< 3.0 \times 10^{-11}$
ONK-PP384	Pöyry	60	71.9	5.00×10^{-8}	7.1×10^{-10}

* indicates flow measurements are below detection limits.

Hydraulic conditioning of fractures on pilot hole hydraulic tests has been limited to only use the measurements from the pilot holes drilled in the floor of DT2 since these measurements provide a direct measurement of fractures that may intersect the experimental deposition holes that follow. It would also be possible to condition the hydraulic properties of fractures intersecting pilot holes ONK-PH17 and ONK-PH20 as well as the pilot holes beneath DT1. Such conditioning is deemed unlikely to directly affect the properties of fractures intersecting the experimental deposition holes below DT2, but could provide additional constraints on the wider fracture network around a possible extension of DT1 and beneath and around a possible extension of DT2, which possibly could have some effect on simulated flows beneath DT2.

Table 3-7. Injection tests performed in pilot holes for experimental deposition holes in DT2. Measurements correspond to injection to 0.5 m intervals of the pilot hole, and for each of the water conducting intervals the number of potential fractures within the interval identified from the DFN database (Baxter et al. 2016). Of these potential matches, an individual fracture is selected from the database based on geological mappings for Jr and Ja; orientation (indicating preferential stress directions); and additional mapping information recording whether the fracture is sealed or not. The selected fracture is then assigned the specific capacity corresponding to the injection interval. For instances where no fracture is identified within the injection test interval, the measured specific capacities cannot be assigned to a fracture mapping and are therefore excluded from the conditioning process.

Name	Depth Interval [m]	Specific Capacity [m^2/s]	Number of Potential Fractures	Selected Fracture / Fracture ID (DFNdb)	Measured Depth (MD) [m]	Dip [°]	Dip direction [°]	Geological Mappings (DFNdb)	
								J_r	J_a
ONK-PP381	3.5–4.0	3.10×10^{-9}	2	77428	3.99	69	320	3	0.75
ONK-PP381	4.0–4.5	3.10×10^{-9}	No fractures in interval						
ONK-PP381	4.5–5.0	6.70×10^{-10}	4	77432	4.82	62	328	3	1
ONK-PP381	5.5–6.0	9.50×10^{-10}	2	77437	5.86	40	110	2	1
ONK-PP381	6.0–7.47	7.10×10^{-11}	4	77440	6.88	23	165	1.5	2
ONK-PP382	1.5–2.0	5.50×10^{-10}	1	77446	1.98	53	300	1.5	1
ONK-PP382	4.5–5.0	6.90×10^{-11}	No fractures in interval						
ONK-PP382	5.0–5.5	6.70×10^{-10}	2	77449	5.17	60	305	1.5	1
ONK-PP382	5.5–6.0	2.60×10^{-10}	4	77452	5.67	5	225	3	1
ONK-PP384	0.5–1.0	6.80×10^{-11}	No fractures in interval						
ONK-PP384	1.5–2.0	8.80×10^{-10}	1	77486	1.85	17	310	3	1
ONK-PP384	2.0–2.5	1.20×10^{-9}	2	77487	2.29	45	240	3	1

3.4 Deposition hole data

Within DT2, the six short pilot holes drilled in the floor of the tunnel were subsequently reamed to experimental deposition holes (ONK-EH10 – ONK-EH13, ONK-EH15, and ONK-EH16) as shown in Figure 3-7. These experimental deposition holes are for demonstration purposes only, and are c. 8 m long, 1.78 m diameter with geological mapping (including digitised fracture traces) performed on the surfaces of the holes. As for fracture trace mapping within the ONKALO tunnels, digitised mappings in the deposition holes require projection on to the idealised surfaces of the model domain (see Section 3.2.2) with the projected traces shown in Figure 3-7. In total, 140 fractures are projected (total trace length 206.9 m), with individual traces post-processed and assigned to a BFZ structure where appropriate. These BFZ related fracture traces are honoured by the conditioning algorithm by selecting potential candidates from the fracture library generated within the BFZ related fracture sets (see Chapter 2). Finally, and as implemented for the demonstration tunnels, the lower confidence limit for truncating observed fracture traces is 0.25 m.

3.4.1 Inflow measurements

Water leakage measurements were performed for all six experimental deposition holes of DT2; evaluating the inflow to the hole under open conditions as 10 minute averages. The experimental procedure includes pre-watering of the walls of the deposition hole; and as such the early time behaviour can over predict flow rates. The inflows to each of the holes are calculated as the average of these measurements; excluding the first hour to avoid pre-watering effects; and are detailed in Table 3-8. Finally, it is noted that for experimental deposition hole ONK-EH15 the estimated inflows are somewhat uncertain, with measurements oscillating between 0 ml/min and 10 ml/min, with much of the data below 1 ml/min – the limit of the measurement tool.

Although the total inflows can be used as a metric for quantifying the performance of individual DFN models to reflect measurements, conditioning DFN simulations requires a flow contribution to be assigned to individual fracture traces observed on the walls of the deposition hole. However as performance measures and potential acceptance criteria for deposition holes are all defined at the scale of the hole, the exact distribution of inflows between the fractures intersecting the deposition hole is not critical. The approach adopted in this study is to assign flow proportionally to the lengths of fracture traces intersecting each hole. Since the injection tests suggested only one or two water conducting fractures per pilot hole, and there are only one or two fractures with long mapped traces, >5m, in the deposition holes, then the inflow was assigned to these larger traces, and shorter ones were assumed not to contribute. The exception being experimental deposition hole ONK-EH16, where the length of all fracture intersections are less than 5 m. Table 3-9 details the assignment of specific inflows to individual fractures intersecting the six experimental deposition holes of DT2 using this methodology.

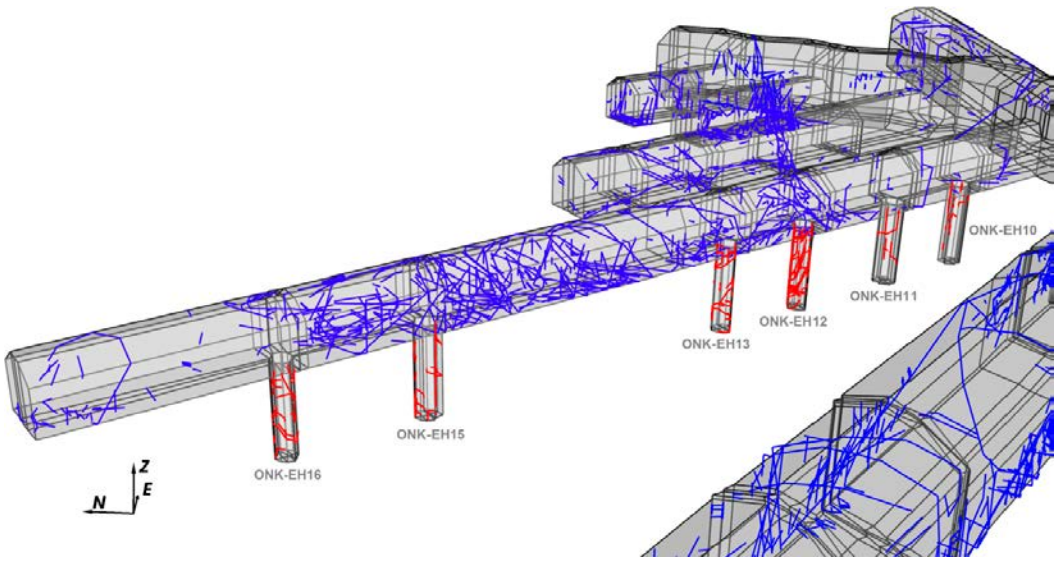

Figure 3-7. *Deposition hole geometries and projected fracture traces within ONK-EH10 – ONK-EH13, ONK-EH15, ONK-EH16 of the DT2 tunnel.*

Table 3-8. Total inflows to each of the six experimental deposition holes of DT2, measured under open hole conditions and taken as the average inflow over 20 hours of measurement (excluding the first hour of the experiment, where pre-watering effects are observed).

Name	Q_{inflow} [ml/min]
ONK-EH10	< 1 ml/min
ONK-EH11	< 1 ml/min
ONK-EH12	5.06
ONK-EH13	2.63
ONK-EH15	0.43
ONK-EH16	1.64

Table 3-9. Inflows to the six experimental deposition holes of DT2, measured under open repository conditions, assigned to individual fracture traces intersecting each of the holes.

Name	Q_{inflow} [ml/min]	Number of Potential Fractures	Selected fracture / Fracture ID (DFNdb)	Length of fracture trace [m]	Flow assigned to fracture [ml/min]
ONK-EH10	< 1	17	–	–	–
ONK-EH11	< 1	6	–	–	–
ONK-EH12	5.06	61	120002	11.13	4.06
			120019	6.12	0.50
			120022	5.62	0.50
ONK-EH13	2.63	26	130010	5.96	2.00
			130018	5.24	0.63
ONK-EH15	0.43	16	140009	7.53	0.43
ONK-EH16	1.64	22	150002	2.40	0.64
			150015	3.32	1.00

3.5 Summary

The available structural mapping from the access tunnels, pilot holes for deposition tunnels, pilot holes for deposition holes and experimental deposition holes were collated for use in generating conditioned DFN models. Hydraulic data used for conditioning were limited to either section specific capacities associated to individual fractures intersecting the injection test section in the pilot holes in the floor of DT2 (see Table 3-7) or inflows to the DT2 experimental deposition holes (see Table 3-9).

The use of data in conditioning could potentially be improved by additional data interpretation and integration:

- Examining if any of the fractures characterised in the pilot holes in the floor of DT2 and/or the experimental deposition holes can be linked to fractures mapped in the DT2 tunnel.
- Assignment of fracture specific inflows to the DT2 tunnel.
- Improved accuracy in the fracture orientations of fractures in pilot holes as inferred from images.

How the data are used in conditioned modelling might also be improved by:

- Conditioning on both constraints from pilot hole injections rates and inflows to subsequent deposition holes, providing fractures can be linked between the two types of holes at a given location,
- conditioning on both deposition hole hydraulics (and/or preceding pilot holes) and inflows to demonstration and access tunnels (needs data as listed above), or
- conditioning on both deposition hole hydraulics (and/or preceding pilot holes) and specific capacities measured in all pilot holes for demonstration and access tunnels.

4 Conditioning, Calibration targets and performance measures

In this chapter, an overview of the conditioning methodology is given, expanding on Section 1.2, summarising the workflows and methodology for verification of the conditioned simulations. A complete description is available in Appleyard et al. (2018). Section 4.1 details the general approach for generating conditioned DFN realisations for the ONKALO Demonstration Area, including a review of the closeness-of-fit measure used in this study to identify suitable fractures for matching individual observed fractures. In addition, **calibration targets** used to confirm conditioned models honour observations are defined in Section 4.2, and **performance measures** related to prediction of flow and transport related properties used in quantitative repository performance assessment are defined in Section 4.3. Some of these also function as quantitative measures of validation of the models, where appropriate this is noted in the definitions.

4.1 The process of conditioned DFN simulation

The workflow for conditioned DFN simulation of the Demonstration Area block model requires the following stages:

1. Idealise geological fracture mapping

Fracture traces from geological mapping of tunnel walls are processed to adhere to the following:

i. the raw digitised fracture traces are projected onto the idealised surfaces used in model simulations rather than the more irregular surfaces of the actual tunnel walls, and

ii. the fracture traces used for conditioning correspond to the intersection of a planar fracture with the modelled tunnel surfaces.

The algorithms used in projection of traces are described in Section 3.2.2.

2. Define the DFN statistical model

The underlying stochastic DFN model description for generating unconditioned realisations is defined providing a means to obtain the statistical distributions of fracture properties local to ONKALO Demonstration Area (see Chapter 2).

3. Library generation

A large set (several thousands) of unconditioned realisations of the DFN are generated to provide a library of possible fracture intersections with drillholes and tunnels. This library, as well as storing the geometry of the associated intersections, also contains all other properties required to define the fracture beyond those that can be measured (e.g. centres, extent and fracture hydraulic aperture), as well as simulated fracture properties (e.g. connectivity and flows). The library generation can be purely geometric or involve flow calculations so as to select fractures that give rise to similar flows as well as geometries of those observed.

4. Conditioning the DFN models

With the library generated, new unconditioned realisations of the same underlying stochastic DFN model are generated, but with the fractures intersecting the drillholes and tunnels with traces longer than the censoring limit (see Table 3-3) removed (since they will not be consistent in terms of precise traces and flows with the measurements by pure chance) and replaced with candidates from the library that provide consistent trace geometries and flows (as required).

An important note with conditioning discrete objects (i.e. fractures) compared to continuous variables is that the observations made are rarely sufficient to fully or uniquely determine the properties of the object. That is why the library contains both the simulated information that is measured as well as the full prescription of each fracture (including information that could not be measured). For example, although measurement may determine the fracture orientation, it does not uniquely specify the extent of the fracture beyond the geological mapping window. Instead, possible candidate fractures for each observation are chosen from a list, compiled from all realisations in the fracture library, with similar properties according to various measures (e.g. orientation and trace length) and the choice is probabilistically weighted by the same measure of similarity. This measure is referred to as the closeness-of-fit. Using this methodology, both the background fracturing beyond the drillhole and tunnel mapping, as well as the conditioned fractures intersecting the drillholes and tunnels are stochastic, and are both drawn from statistics of the same underlying stochastic DFN model.

The overall closeness-of-fit measure *(M)* for fracture traces mapped on tunnel and deposition holes surfaces is defined as

$$M = \sqrt{\left(\sum_{i=1}^{n} a_i^2 M_i^2\right)} \quad , \tag{4-1}$$

the Euclidean norm of a series of individual measures (M_i) and coefficients (a_i) for i different measures of the difference between modelled and measured fracture properties. Appleyard et al. (2018) list a set of up to 10 measures suitable for conditioning on fracture traces on surfaces, and a reduced list of 4 for drillhole data. The ones used in the current study are listed in Table 4-1. The first two are restricted to application to the tunnel mapping, while the last three are relevant to both tunnel mapping and drillhole measurements.

Values for the individual measures and coefficients, as applied to the conditional simulation of the ONKALO Demonstration Area, are detailed in Table 4-1. A maximum difference is specified so as to bound the overall closeness-of-fit, and the weighting is user defined to introduce an appropriate balance between the different metrics. Typically, the weighting coefficients are defined such that when the contribution from an individual component $a_i^2 M_i^2$ is one, that measure provides a reasonable closeness of fit to the observations. For example, for the wall angle, a total discrepancy in the azimuth of the trace start and end when comparing the library fracture trace with the observation would yield an $a_i^2 M_i^2$ of one. Trace length and flow measurements are both given relatively high weights as these are considered important controls on flow predictions. The maximum for individual measures, M_i, are bound by the overall closeness of fit divided by the coefficient for that component, and in the case of wall angle, relative length, flow, and trace angle, these individual maximums are further reduced to constrain the conditioning process. When identifying potential fractures from the library, traces with a closeness-of-fit *(M)* greater than 5, or where any individual component (M_i) is greater than its specified maximum, are excluded. When conditioning a realisation on fracture geometry alone, the measure relating to flow is excluded from the closeness-of-fit. The flow property might be the specific capacity gained from an injection test or might be an inflow under open conditions; the important point is that the flow property in the library is gained from simulations of the flow conditions under which the measurement was made. Different libraries can be used for different flow conditions (e.g. pumping in investigation drillholes, inflows to tunnels, and injection to pilot holes for deposition holes) when conditioning different parts of the subsurface if necessary.

Table 4-1. Parameterisation of the closeness-of-fit measure (Equations (4-1)) for the conditioned simulation of the Demonstration Area of ONKALO. Note that the flow measure is excluded when performing geometrical conditioning only. For further details on these properties, the reader is referred to Appleyard et al. (2018).

Measure	Description	Relevance	Coefficient a_i	Maximum value of M_i
Wall Angle	Sum of the differences in wall angle (i.e. azimuthal angle of the start/end point of the trace on the wall relative to the tunnel centre line).	Tunnel only	0.05	45°
Relative Length	Difference in the lengths of the traces as a proportion of the total length of the traces.	Tunnel only	2	2
Flow	Difference in the log (base 10) of the flows through the fractures.	Tunnel and drillhole	2	2 orders of magnitude
Trace Angle	Dihedral angle between the fractures implied by the traces. If no fracture is implied by the observed traces, the angle between the traces themselves.	Tunnel and drillhole	0.125	15°
Trace Distance	Distance between the centre points of the two traces, or for secondary traces the distance between the points at which the two fractures intersect (or would intersect) the tunnel centre line	Tunnel and drillhole	1	5 m

4.2 Calibration targets

Calibration targets provide a check that conditioned realisations reproduce the data they are supposed to honour. Several quantitative targets are suggested as being appropriate by Appleyard et al. (2018). In this study a combination of visual and numerical tests were applied:

- fracture trace intensity (P_{21}) for fracture traces longer than the censoring limit (Table 3-3) on the mapped tunnel surfaces (see Section 4.2.1), and
- fracture location (see Section 4.2.2).

4.2.1 Fracture trace intensity (P_{21})

The first calibration target is that the model should accurately reflect the observed P_{21} on the conditioned tunnel surfaces; and is defined as the total length of fracture traces per unit area of tunnel wall. Calibration targets are mostly applicable to data sets containing a significant number of fracture traces, and as such the fracture traces on the six experimental deposition holes are excluded from these targets. For the geological mapping, P_{21} is calculated from the traces projected from the raw digitised fracture mapping onto the idealised surfaces used in model simulations; and as such accounts for the variable censoring of the mapping (see Table 3-3). Figure 4-1 shows an example of observed and conditioned traces, whose lengths can be easily determined.

The premise for this calibration target requires that the fractures added to the DFN model through conditioning should accurately reflect the P_{21} from geological mapping. It is noted that whilst accurately reflecting the underlying P_{21} of the mapping is a necessary requirement for successful conditional simulation of the DFN; it is not, on its own, a sufficient condition. That is, a DFN model representing the P_{21} from geological mapping may not reflect the orientation, position or length of individual traces, or the overall number of traces on a tunnel, and if necessary these additional fracture trace properties should be confirmed independently.

The acceptance test for the P_{21} calibration target is that the conditioned fracture intensity should be within 5 % of the equivalent value from mapping, and vary by no more than 20 % of the variation of P_{21} between unconditioned realisations.

Results for checking calibration targets for conditioning on the tunnel traces are presented in Section 6.1. Additional comparisons of P_{21} checks for individual deposition holes are reported in the DADFN report, Hartley et al. (2017).

Predictions of P_{21} in the experimental deposition holes are also use as validation targets, see Figure 6-3.

4.2.2 Fracture location

Whereas the P_{21} calibration target applies to the set of conditioned fracture traces above the censoring limit in the model, it is also important to have a measure that verifies the quality of conditioning for individual observations (i.e. individual fractures are located correctly, with correct length and orientation). The fracture location calibration target considers individual fracture traces, comparing the geological mapping with the modelled fractures sampled from the library. Although quantitative metrics, such as the Euclidean separation of centres or the dihedral angle between mapped and modelled fractures can be calculated, typically a qualitative visual inspection of the model is sufficient for appreciating the success of model conditioning and it is this later approach that has been adopted in this study.

For illustration of conditioned simulations of the Demonstration Area, two locations along the DT2 tunnel are considered: one sparsely fractured, and one densely fractured:

- Densely fractured area: Approximately mid-way along DT2, the tunnel intersects BFZ045 and BFZ084, resulting in a volume of rock with increased fracture intensity due to clustering of fractures around these two deformation zones (see Hartley et al. 2017, Chapters 4–6).
- Sparsely fractured area: The mapping performed at the entrances to both DT1 and DT2 indicates long sections of intact rock with minimal fracturing. Geological mapping were similar to those performed elsewhere in the Demonstration Area, and performed on washed tunnel surfaces, in good lighting, and as such the reduction in fracture intensity is not a consequence of the mapping procedures but rather a reflection of high rock quality in this area.

Figure 4-2 illustrates the idealised geological mappings in DT2 (i.e. projection of the mapped fractures to the idealised surface of the tunnels) for both the densely fractured and sparsely fractured rock volumes. For each of the conditional simulations performed, the geological mappings in these areas are compared with one realisation each of the unconditioned and conditioned DFN model to ensure that the fracture location target is suitably met.

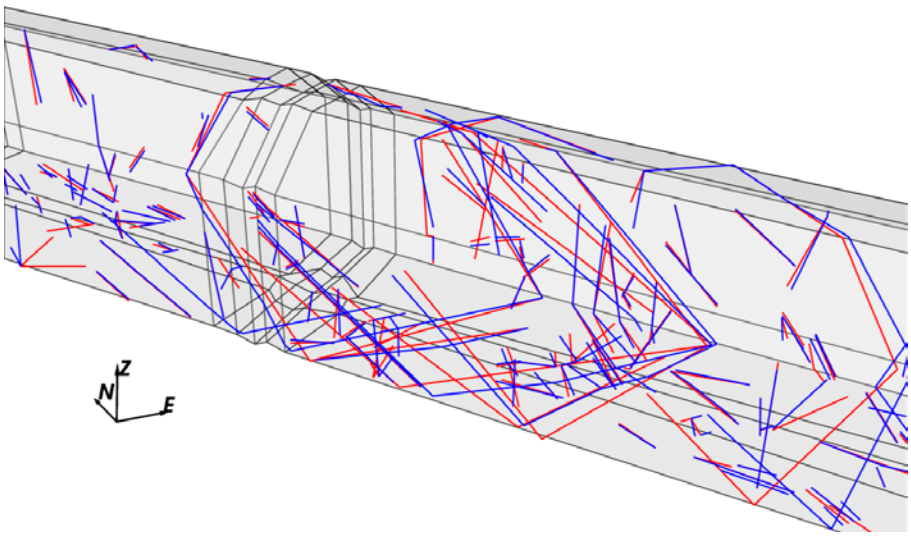

Figure 4-1. *Observed (blue) and conditioned (red) traces on a length of tunnel with deposition holes. The length of each of trace contributes to the P_{21}.*

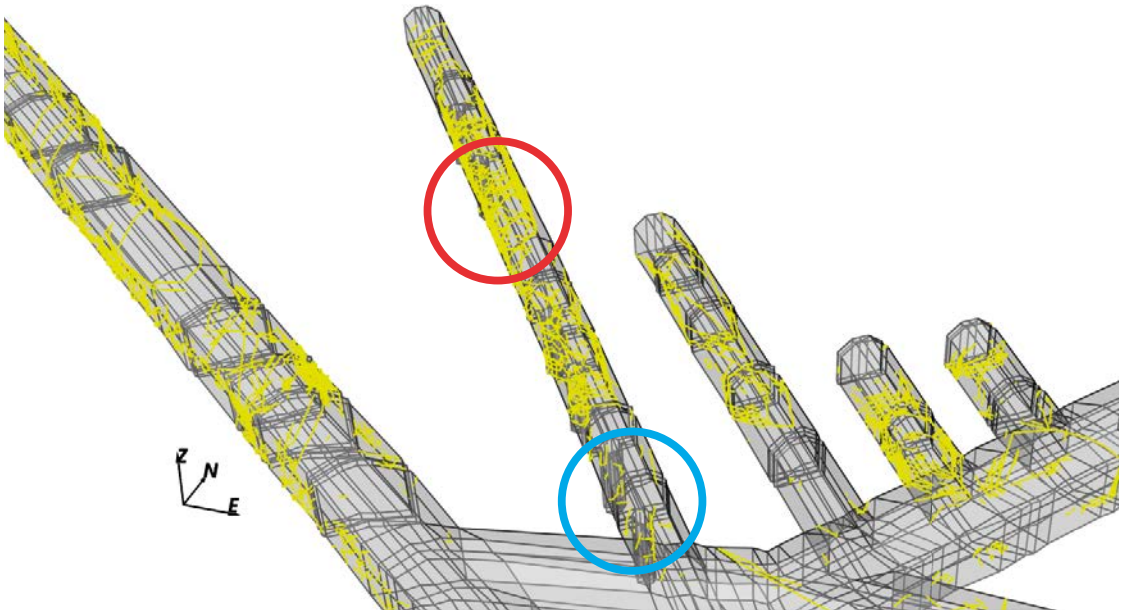

Figure 4-2. *Illustration of the idealised geological mappings in both densely fractured (red) and sparsely fractured (blue) areas of DT2; used for qualitative assessment of the fracture location calibration target. A close up of this image is shown in Figure 6-4 and Figure 6-5.*

4.3 Performance measures

Performance measures are flow quantities derived under different hydraulic conditions. In this study, they can be used to evaluate whether the conditional simulations improve predictions of flow-related metrics, relevant for repository safety. Here, three performance measures are considered, associated to the following flow conditions:

- specific capacity of injection tests performed in the pilot holes for deposition holes,
- inflows to the deposition holes under open repository conditions, and
- post-closure flow around deposition holes.

Strictly the term performance measure is reserved for quantities used as inputs to repository performance assessment. The post-closure flow around the deposition hole is an important input to assessment of buffer erosion and radionuclide release rates; inflows under the operational period affect proper installation, saturation and performance of the buffer; while specific capacity is a physical property of a fracture affecting the above flow properties and transport.

Although understanding post-closure flow conditions is important for the acceptance criteria of deposition holes, it cannot be measured whilst the repository is open during construction. As such two possible criteria are considered for the acceptance of deposition holes related to the measured specific capacity of the pilot holes drilled for deposition holes (i.e. the injection tests); or the inflows at open deposition hole conditions. To evaluate these criteria, this study also considers the correlation of the predicted initial flow rate per unit width (i.e. the post-closure performance measure) as defined in Section 4.3.3 at deposition hole positions with both the corresponding injection test and inflow metrics.

4.3.1 Injection tests in pilot holes (-pi)

The first flow metric is the specific capacity derived from injection tests in pilot holes for deposition holes, which can be measured during operations (see Table 3-6). Each pilot hole is considered in turn; packing-off the top 0.5 m, and performing simulations at injection pressures consistent with the experiment. Note that because proposed hydraulic acceptance criteria are defined for the full hole, simulated injection tests are also performed for the full hole, rather than shorter (c. 0.5 m) sub-lengths of the pilot hole which have also undergone injection tests (see Section 3.3).

The injection test performance measure is calculated for each pilot hole using the unconditioned model (UC) and those conditioned on data from pilot holes for deposition holes (PHGC and PHHC), see Chapter 6. In each case, 10 realisations of the DFN are considered. By conditioning the DFN, model predictions of individual injection tests should improve, and the variability between realisations of the model reduce when compared to the unconditioned model.

Prediction of specific capacities in pilot holes can also be a validation target for simulations versus measurements, see Section 5.1 and Section 6.1.2.

Numerical Approach

ConnectFlow is used to simulate the six injection tests in sequence, corresponding to injection to the whole pilot hole (but excluding the top 0.5 m which is packed-off). The injection pressure within each pilot hole corresponds to an increase in pressure over the packed-off baseline pressure recorded in that hole. As such, simulations of the injection tests require two calculations to be performed, the first simulating the packed-off pressures in the pilot holes; and the second simulating injection to each pilot hole in turn (at the appropriate over-pressure). In all cases, the tunnels would be held at atmospheric conditions and the far-field boundary conditions would be hydrostatic (see Figure 3-1 for further description of the modelling domain).

The requirement to perform two simulations when modelling the injection tests increases the numerical requirements of the conditioning methodology, especially when considering the extensive library generation stage, and may result in the methodology becoming intractable. Therefore, the following assumption is made within the models. Rather than applying a pressure gradient between the tunnels and the far-field boundary, they are instead both set to hydrostatic conditions, and as such, the pressure across the modelling domain prior to injection is hydrostatic. The injection test is then simulated based on the required injection pressure above hydrostatic pressure, removing the requirement to first simulate the pressures within the packed-off pilot holes.

Essentially, this simplification assumes that the contribution to the flow field local to the injected pilot holes from the pressure gradient between the far-field boundary and the open tunnel system can be neglected. In other words, the injection test simulations are dominated by the pressure gradient between the tunnel and the injected hole, and the degree of tortuosity and choking in the fracture system between these two features. This simplification makes the problem significantly more tractable.

Therefore, the injection tests are modelled as steady state simulations based on the above simplification, with hydrostatic conditions applied throughout the domain for the initial conditions.

4.3.2 Inflows to open deposition holes (-do)

The inflow performance measure considers operational conditions for the repository, calculating the inflow to each deposition hole under open repository conditions. Experimental inflow measurements are available for comparison (see Table 3-8). Unlike the injection tests considering injection to each of the pilot holes in sequence; a single flow simulation is performed for all tunnels and deposition holes to simultaneously calculate the inflows to each deposition hole.

Similarly to the injection tests, successful conditioning is identified by both:

- improved model prediction of the inflows to each of the six experimental deposition holes (when compared to an unconditioned model), and
- reduced variability in these inflow predictions between realisations of the conditional simulations (when compared to an unconditioned model).

Numerical Approach

ConnectFlow is used to simulate inflows to the experimental deposition holes under open repository conditions for each realisation of the DFN model. Only one simulation is required, as all deposition holes are opened simultaneously. The model imposes hydrostatic boundary conditions on the far boundary and atmospheric pressure in the deposition holes and tunnels.

The inflows to open deposition holes are modelled as steady state simulations, with hydrostatic pressure used for the initial conditions.

4.3.3 Post-closure flow (-pc)

The post-closure performance measure is derived from simulation of flows in fractures intersecting each deposition hole under post-closure saturated conditions. Here, the hydraulic conductivity of the backfilled tunnels is set at 10^{-10} m/s, and the buffer in the deposition holes has hydraulic conductivity 10^{-12} m/s, respectively; these are sufficiently low so as not to form transport pathways.

Numerical Approach

ConnectFlow is used to simulate post-closure flows using a combined DFN (fractured rock) and CPM (tunnel / deposition hole backfill) model with imposed conservation of flux on the DFN – CPM interface. Across the modelling domain (including far-field boundary conditions) a linear head gradient of 0.005 is assumed (see Figure 3-1), oriented northeast and vertically upwards via the unit vector (−0.69, −0.69, 0.23). The assumption for this head gradient is based on a typical gradient seen under post-closure conditions by Hartley et al. (2013a). Using this model specification, steady-state flow simulations are performed with appropriate output generated for subsequent particle tracking calculations (see below).

Particle Tracking

The resulting fracture flow fields calculated from the above simulations are used as the basis for particle tracking calculations (releasing particles into the fracture network at the mantel surface of the deposition hole). The particle tracking method uses a stochastic network routing method based on the flow field between pairs of intersections (Hartley et al. 2013a, Appendix C). An example of typical particle tracks for one realisation of the DFN is shown in Figure 4-3.

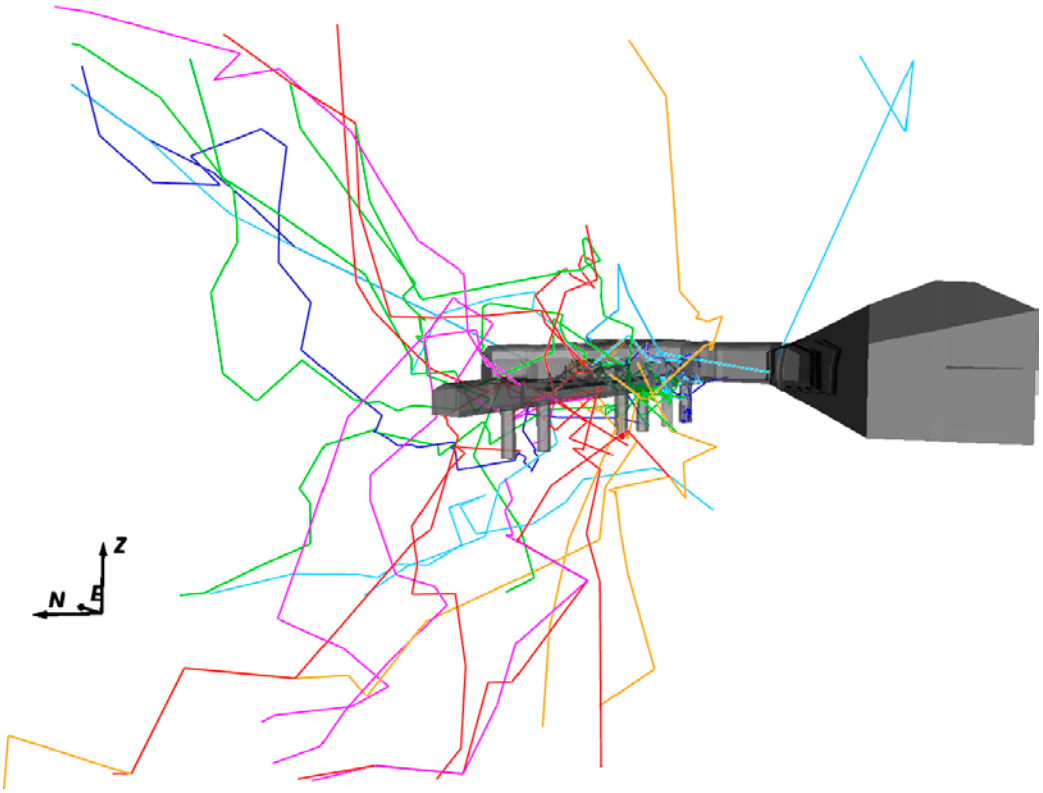

Figure 4-3. *Tracked particles originating at each experimental deposition hole. Coloured by hole of origin: PP379 – dark blue; PP380 – sky blue; PP381 – green; PP382 – orange; PP383 – red; PP384; pink. A linear head gradient of 0.005 is applied; oriented northeast and vertically upwards.*

To obtain the flow metric *(U)*, the average flow rate per unit width tangential to the repository structures needs to be calculated. In ConnectFlow, this is determined using the Cordes-Kinzelbach (CK) mass-conserving method (Cordes and Kinzelbach 1992, Amec Foster Wheeler 2016). As standard in ConnectFlow, each fracture (or discretised sub-fracture) is divided into squares of four finite elements and any intersection is mapped on to the finite element edges (but retains its properties such as its length). The CK method further subdivides each triangular finite element into four CK sub-triangles as shown in Figure 4-4.

To calculate *U*, the vector transport velocity in each sub-triangle that shares a point with the mapped intersection between discretised surface element and sub-fracture (i.e. those with arrows in Figure 4-4) is calculated. These are then combined as follows:

$$U_i = \frac{\hat{\vec{l}_i}}{s} \cdot \sum_s \left(e_{t_s} \vec{v_s} \right) \tag{4-2}$$

$$U_f = \sum_i \left(l_i e_{t_i} U_i \right) \Big/ \sum_i \left(l_i e_{t_i} \right) \tag{4-3}$$

$$U = \sum_f U_f \tag{4-4}$$

where:

- $\vec{v_s}$ is the transport velocity in a CK sub-triangle [m/yr],
- e_{t_s} is the transport aperture of the CK sub-triangle [m],
- s is the number of CK sub-triangles on which flow is defined [–],
- $\hat{\vec{l}_i}$ is a unit vector along the original intersection (between sub-fracture and surface element) [–],
- l_i is the length of the original, physical intersection (as opposed to the intersection mapped to the finite element edge) [m],
- U_i is the flow rate per unit width associated with the original intersection [m^2/yr],
- e_{t_i} is the mean transport aperture of the sub-fracture [m],
- U_f is the weighted average flow rate per unit width associated with the fracture as a whole [m^2/yr],
- U is the average flow rate per unit width associated with the deposition hole as a whole [m^2/yr].

The velocities in the CK sub-triangles adjacent to the mapped intersection (i.e. the blue triangles in Figure 4-4) are averaged, and the component of the average vector tangential to the original intersection (e.g. in the direction of the arrows in Figure 4-4) is calculated (Equation 4-2). To scale up to the intersection between the fracture as a whole and the deposition hole, an average of the sub-fracture/surface element intersections is taken, weighted by the contact area between the fracture and deposition hole, i.e. the product of the length of the intersection and transport aperture (Equation 4-3). Finally, the *U* for the deposition hole is the sum of those for each fracture intersecting the hole (Equation 4-4).

In this work, transport aperture is assumed constant over a sub-fracture (and thus equal to the mean transport aperture e_{t_i} in all CK sub-triangles). As such, Equation 4-2 could in this case be rewritten as:

$$U_i = \frac{e_{t_i} \hat{\vec{l}_i}}{s} \cdot \sum_s \vec{v_s} \tag{4-5}$$

In addition the flow-related transport resistance, F_r [m^{-1} a], along particles tracks with the post-closure flow field is calculated from the start point at the rock surface of the deposition hole interface to the outer model boundary as the sum of twice the advective travel time, t_r, in each fracture divided by the transport aperture, e_t,:

$$F_r = \sum_l \frac{2\mathrm{t}_{rl} \delta l}{\mathrm{e}_{tl}} \quad . \tag{4-6}$$

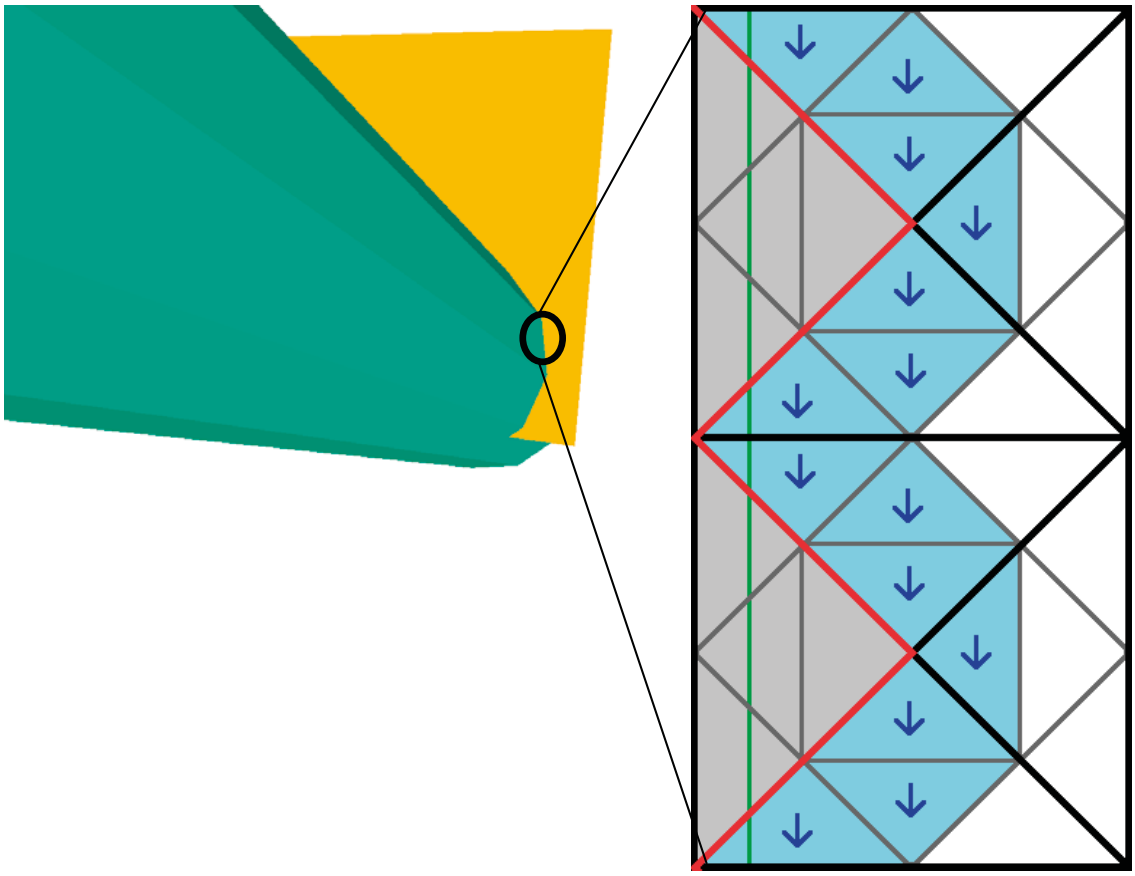

Figure 4-4. *Depiction of the measurement of U based on the flow in a small section of the intersection between a fracture and deposition hole. Left: a fracture (yellow) intersects a deposition hole (green). Right: the fracture is discretised as a regular array of rectangular blocks, each is divided into four triangular finite elements for the flow solve (bounded by black and red lines), and each of them is then subdivided into four sub-triangles for calculating the flow field and particle tracking (bounded by dark grey lines). Two rectangular blocks are depicted here. The green line indicates the physical intersection between the finite elements and the deposition hole, the red line indicates how it is mapped to the finite element edges. Grey areas are areas of the fracture that are ignored because they are within the deposition hole. Blue arrows show the tangential component of the flow vectors used to calculate U (tangential to the original intersection, not to the mapped intersection) in the blue triangles.*

5 Post-closure flow and transport: unconditioned (UC) DFN

Using the underlying stochastic DFN model description as summarised in Chapter 2, ten realisations of the unconditioned DFN are generated local to the Demonstration Area. The unconditioned model (UC) provides baseline validation that prediction of injection rates to pilot holes as well as inflows to open deposition holes are in the correct order of magnitude and with the expected spatial variability. It also forms the basis for examining correlations between different measured and post-closure flow properties (as defined in Section 4.3) to identify improvements in model prediction of possible criterion suitable for deposition hole acceptance. These can then be compared with equivalent results for conditioned DFN simulations. The flow metrics simulated are:

1. the hydraulic injection tests to each pilot hole for a deposition hole (results in Section 5.1),
2. inflows to open deposition holes (results in Section 5.2), and
3. the initial flow rate per unit width at post-closure conditions (results in Section 5.3) at deposition hole positions.

5.1 Injection to pilot holes (UC-pi)

The unconditional simulation of this flow metric for the hydraulic injection in each of the pilot holes for deposition holes (UC-pi) is presented in this section. The full specification of this metric is detailed in Section 4.3.1, with simulations representing open repository conditions and sequential injection to each of the short vertical pilot holes drilled in the floor of DT2.

The simulations quantify the degree of reliability the DADFN model can offer in making hydraulic predictions when not conditioned on local data, only the analysis of and calibration on fracture geometric and hydraulic statistics, noting that significant efforts were made in the model's conceptualisation to recognise correlations between fracture and geological properties.

Figure 5-1 shows the simulated specific capacities in each of the pilot holes for experimental deposition holes for the ten realisations of the unconditioned DFN. Only the 28 (out of 10 realisations × 6 holes) instances where pilot holes are hydraulically connected to the wider network are shown; while each pilot hole is intersected in a subset of realisations due to the sparsity of connected fractures. *In situ* measurements from the injection tests are included for comparison; as reviewed in Section 3.3.2, with ONK-PP379, ONK-PP380 and ONK-PP383 recording no flows above the detection limit of the tool; denoted in the figure by orange vertical lines. For all pilot holes except ONK-PP379, realisations of the unconditioned DFN span the measurements; whereas for ONK-PP379 the detection limit exceeds the maximum predicted. It is interesting to note that even for the unconditioned realisations, fracturing is predicted to be less around ONK-PP379 and ONK-PP380 as these lie further from a Brittle Fault Zone (BFZ) and in the least fractured veined gneiss lithology and within the CTU1 ductile domain, while the closed end of the tunnel intersects a number of BFZ and lies in the more fractured granitic pegmatoid lithology and the SDZ domain (see Figure 2-5, and figures in Section 6.1 of Hartley et al. 2017). This initial part of DT2 is also devoid of deformation zones.

The predicted specific capacities in pilot holes for deposition holes are somewhat uncertain when considering the variability between realisations of the unconditional DFN. Simulations vary by 1–4 orders of magnitude between pilot holes, with a range of about 2 orders of magnitude in individual pilot holes where the majority of realisations are hydraulically active. This uncertainty will be considered further when simulating conditioned models using pilot hole (Chapter 6) and deposition hole (Chapter 7) data.

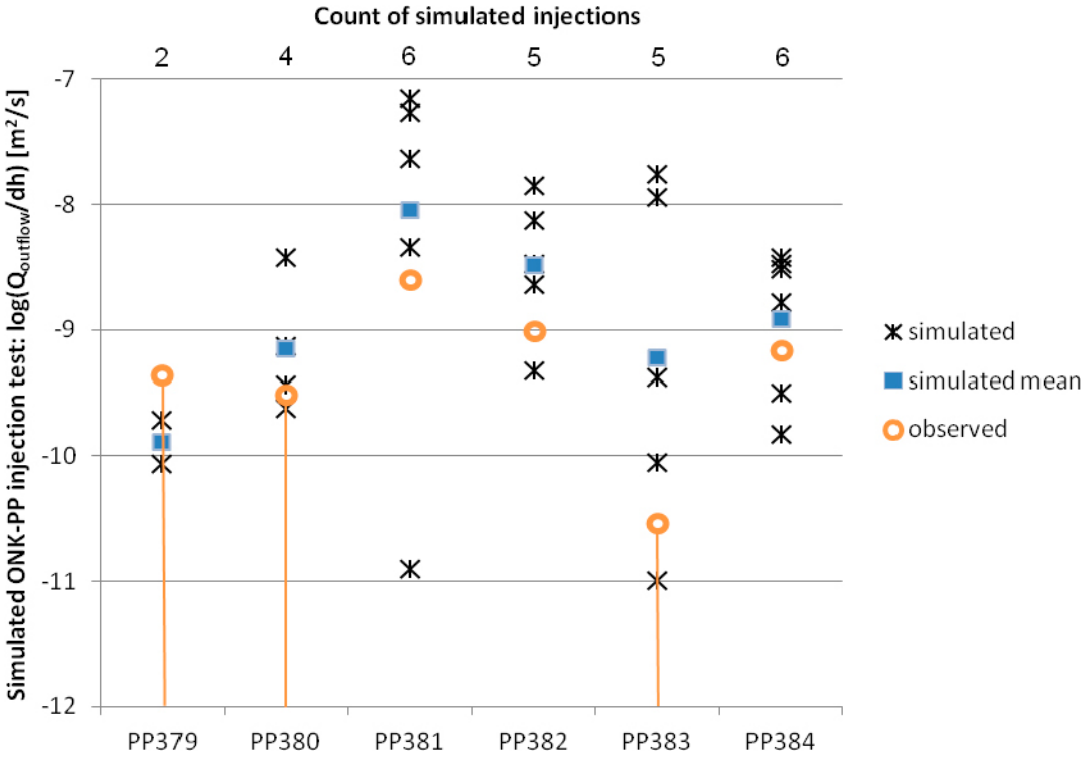

Figure 5-1. *Log specific capacity from simulated injection tests by pilot hole for ten realisations (black markers) of the unconditioned DFN (UC-pi). Geometric mean (blue squares) from simulations together with the injection test measurements (orange circles) are shown. Orange lines indicate measurements not being above the detection limit of the tool. The number of realisations with non-zeros flows is recorded on the top axis.*

5.2 Inflows to deposition holes (UC-do)

The unconditioned simulation of the second flow metric is presented in this section, representing inflows to each of the six experimental deposition holes in DT2 (UC-do). The full specification of this performance measure is detailed in Section 4.3.2, with simulations representing open repository conditions for all tunnels and deposition holes simultaneously. Again, these results measure the degree of reliability the DADFN model can offer in making hydraulic predictions without local conditioning.

Figure 5-2 shows the simulated inflows to each of the deposition holes for ten realisations of the unconditioned DFN. As for pilot holes for deposition holes (see Figure 5-1), only those realisations where the deposition hole is hydraulically connected to the wider fracture network are shown. Measured inflows are included for comparison; as reviewed in Section 3.4.1, with no inflow measurements recorded in either ONK-EH10 or ONK-EH11 above the detection limit of 1 ml/min. Consistent with the injection test simulations, the unconditioned realisations correctly predict the sparsity of connected fractures near the entrance to DT2 as affecting the latter two holes. For all deposition holes, measurements are spanned by the realisations of the DFN model, with variability between realisations in the range of 2–3 orders of magnitude (except for ONK-EH10). This reduced uncertainty compared to the injection to pilot holes (see Section 5.1) could be a consequence of inflows under open-hole conditions being less sensitive to connections to the tunnel than corresponding injection tests within pilot holes for deposition holes. The extent to which the uncertainty in model predictions for inflows is reduced when considering conditioned simulations based on either mapping the deposition holes; or the preceding pilot holes is considered in Chapters 7 and 6, respectively.

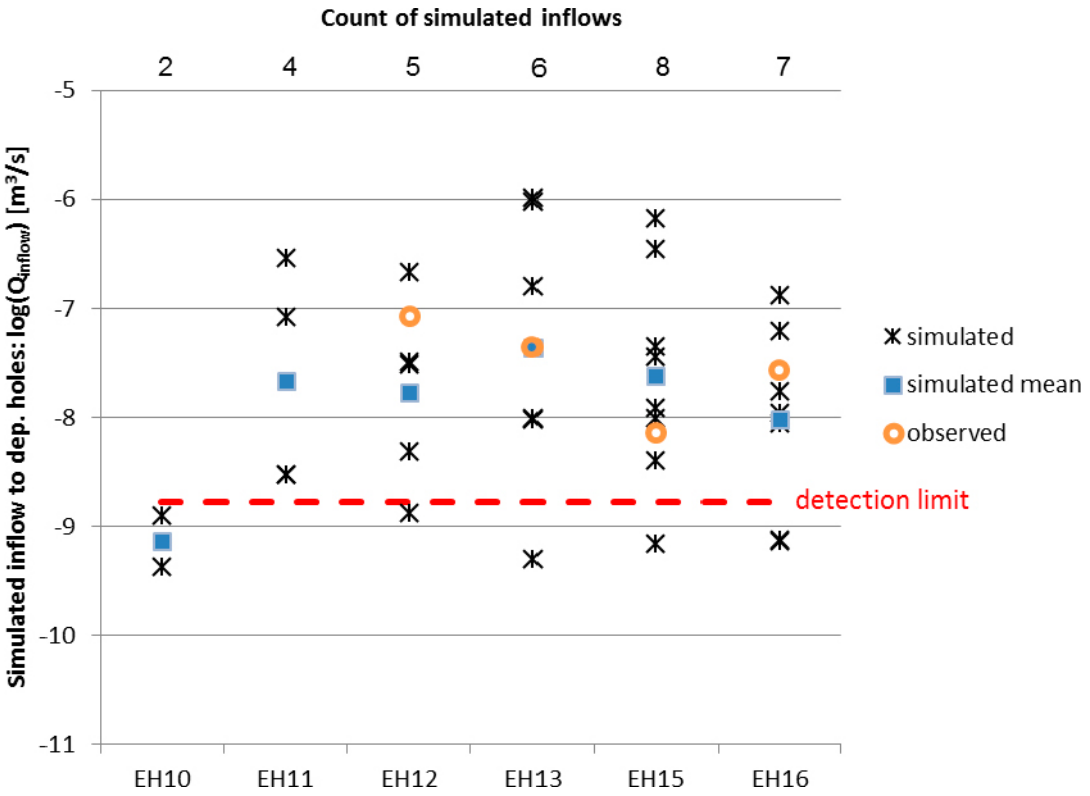

Figure 5-2. *Log inflow simulated for open deposition holes for ten realisations of the unconditioned DFN (UC-do). The geometric mean of the simulations (blue squares) are shown, with measured flows (orange circles). The detection limit is about 0.1 ml/min (1.7×10^{-9} m^3/s). The number of realisations with non-zeros flows is recorded on the top axis.*

The inflows to individual deposition holes, as measured at the time of repository construction, may form part of a possible criterion for their acceptance. However, from a construction standpoint, there is benefit in predicting the inflow characteristics of a deposition hole from the injection tests performed in the preceding pilot holes, since it affects resaturation and the potential for proper installation of the buffer. Inflows are calculated for atmospheric pressure at the walls of the deposition tunnels and holes. The correlation between the specific capacities inferred from injection in each of the pilot holes for deposition holes (Section 5.1) and the values calculated from inflows to deposition holes is shown in Figure 5-3. All ten realisations of the unconditional DFN are considered; with a dashed line indicating the equivalence in specific capacities between models (assuming the same fractures are intersected at the pilot hole and deposition hole scales and accounting for the different radii of pilot holes and deposition holes). Typically, results correspond to instances where the specific capacities calculated from injection to the pilot holes exceed those simulated in open deposition holes; a consequence of the nature of the hydraulic tests performed. The injection tests identify the maximum flow capacity of the fracture network in the vicinity of each pilot hole, considering injection into each pilot hole sequentially (in turn). In contrast, deposition hole inflows correspond to open repository conditions throughout the system, and so water will leak toward the part of the network connected to the open tunnel system with least resistance. The exact relation between the simulated inflow to deposition holes and injection tests in pilot hole for deposition holes is a function of the different ratio of connections from the hole to pressurised parts of the DFN as opposed to open tunnel volumes. As the relative connectivity to the open tunnel increases, the specific capacity calculated from tunnel inflow simulations will be reduced compared to the pilot hole injections.

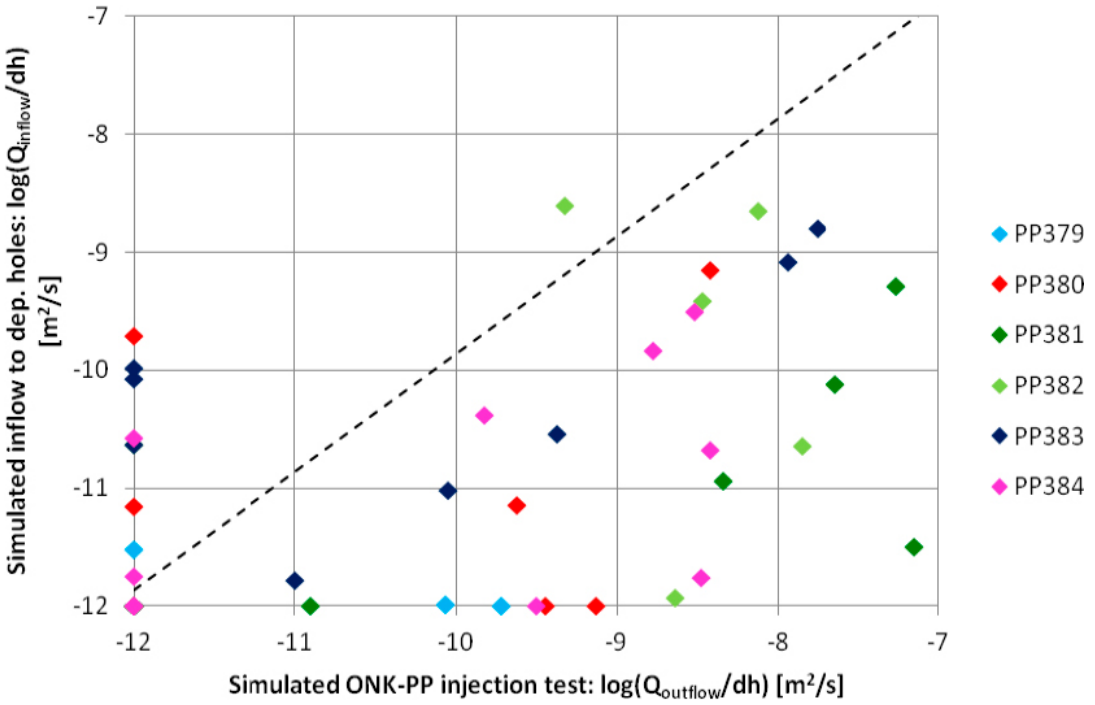

Figure 5-3. *Specific capacity for simulated inflows to open deposition holes, calculated as the inflow divided by hydrostatic pressure at the deposition hole (UC-do) against corresponding specific capacity simulated from hydraulic injections in the whole pilot holes (excluding the top packed-off 0.5 m) for deposition holes (UC-pi). Ten realisations of the unconditioned DFN are shown.*

Although the majority of realisations / pilot holes adhere to this behaviour, three other cases are also observed:

1. **Deposition hole specific capacity > pilot hole specific capacity:** One point, corresponding to ONK-PP382 (realisation 6) occurs where the specific capacity of the deposition hole is greater than for the preceding pilot hole. This can occur in instances where the large diameter deposition hole intersects additional, hydraulically active, fractures that do not intersect the preceding pilot hole; as shown in Figure 5-4.
2. **Deposition holes are hydraulically inactive, but pilot hole injections identify non-zero specific capacity:** Five pilot holes for deposition holes predict non-zero specific capacity under injection conditions; but upon reaming, the open deposition holes predict no inflow. This can be a consequence of the injection into pilot holes utilising groundwater pathways between underground openings with associated head gradients (e.g. between the injection hole and the DT2 tunnel floor), whilst hydraulically isolated from the wider fracture network. When considering the open deposition holes, the head gradient to other underground openings is no longer available to drive this flow path. An example is presented in Figure 5-5, corresponding to pilot holes ONK-PP380 (deposition hole ONK-EH11). The only hydraulic connection out of the pilot hole is to the DT2 tunnel floor.
3. **Pilot holes are hydraulically inactive, but deposition hole specific capacity is non zero:** Under open deposition hole conditions, there are 32 out of 60 (10 realisations × 6 holes) instances of non-zero inflows predicted. Of these, nine simulations did not indicate flow when considering injection into the preceding pilot holes (corresponding to points on the vertical axis shown in Figure 5-3). It is likely this is a consequence that upon reaming the hydraulically isolated pilot holes, the larger deposition holes create hydraulic connections to the fracture network. This case is similar to case 1, and is illustrated by an example shown in Figure 5-4.

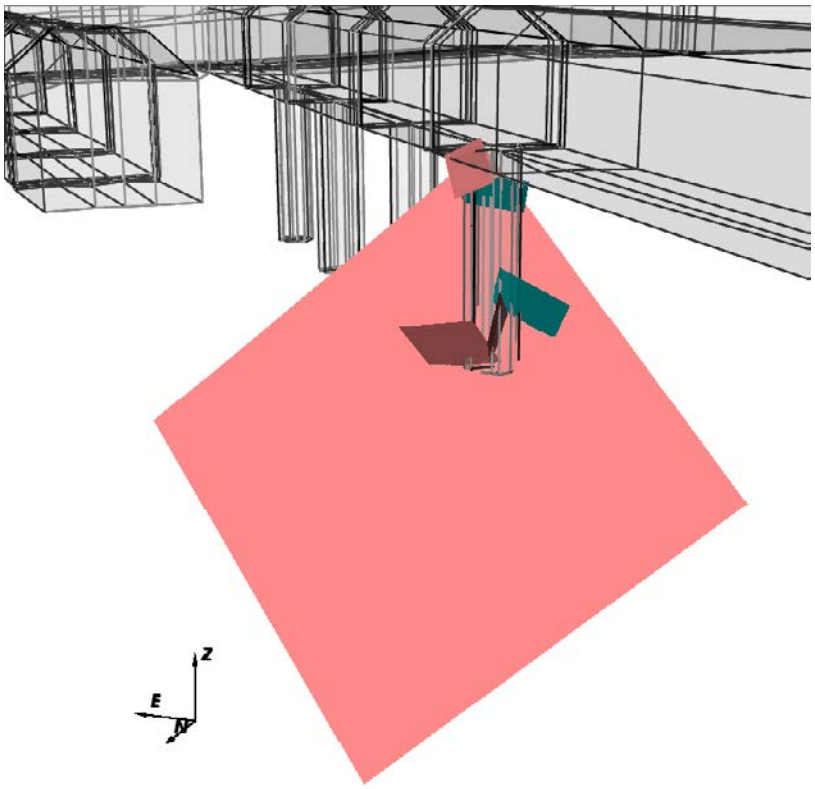

Figure 5-4. *Illustration of the DT2 deposition hole, ONK-EH13 (ONK-PP382), for the sixth realisation of the unconditioned DFN model. Fractures intersecting both pilot hole and deposition hole are shown in blue; with fractures only intersecting the deposition hole shown in pink.*

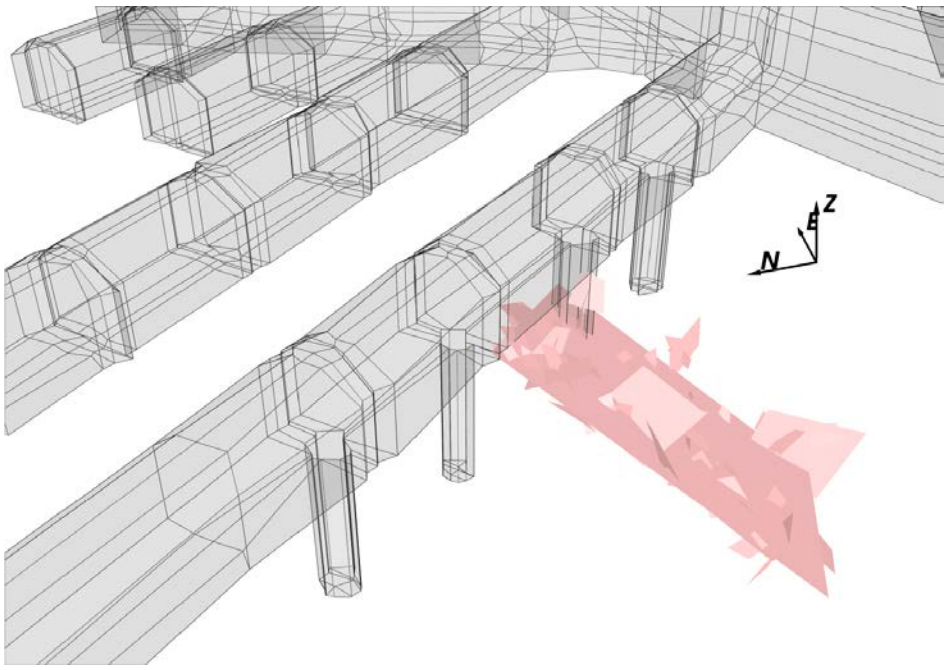

Figure 5-5. *Illustration of the DT2 deposition hole, ONK-EH11 (ONK-PP380), for the first realisation of the unconditioned DFN model. Fractures clustered around the pilot hole are shown, indicating only hydraulic connectivity with the DT2 tunnel.*

5.3 Post-closure flow and transport (UC-pc)

The unconditioned simulation of the third flow metric is presented in this section, predicting initial flow rates per unit width at saturated post-closure conditions (UC-pc). The full specifications of these simulations are detailed in Section 4.3.3; defined to represent saturated conditions in both tunnels and deposition holes backfilled with a low permeability porous medium.

The variability in predicted initial flow rates per unit width for the six experimental deposition holes is shown in Figure 5-6 corresponding to ten realisations of the unconditioned DFN, with the uncertainty between realisations for a given deposition hole ranging from about 3 to 4 orders of magnitude. The extent to which this uncertainty in model predictions is reduced when considering conditional simulations is assessed in Chapters 6 and 7 for conditioned DFN models based on pilot holes for deposition holes, or deposition holes, respectively.

Although post-closure flow is fundamental to the acceptance of deposition holes; it is not measureable during the operational phase. Instead, predictors for low post-closure flow rates are sought, providing indication of post-closure performance based on measurements taken during open repository conditions. Two possible criteria for the acceptance of deposition holes could be to: 1) infer performance measures from the specific capacity of the fractures intersecting the entire pilot holes drilled for deposition holes (i.e. the injection tests, simulated to exclude the top half metre of the pilot hole); or 2) the inflows at open deposition hole conditions. As such, correlations between simulated post-closure flows adjacent to the entire deposition hole for ten realisations of the unconditioned DFN model (UC-pc) are compared to corresponding simulations of injection tests in pilot holes (UC-pi) in Figure 5-7 (as detailed in Section 4.3.1); and inflows to open deposition holes (UC-do) in Figure 5-8 (as detailed in Section 4.3.2). When comparing injections to pilot holes with the post-closure flows, the following is observed (Figure 5-7):

- The majority of pilot holes and realisations of the unconditioned DFN which predict non-zero specific capacities during the injection test simulations also predict post-closure initial flow rates below the equivalence line (deposition hole specific capacity multiplied by post-closure head gradient) shown. It is observed that the predictions for these pilot holes do not particularly cluster, with limited correlation between the injection test specific capacities and post-closure initial flow rates observed.
- Of the 60 injection tests simulated; 32 did not form hydraulic connections from pilot holes to the wider fracture network. In Figure 5-7 points lying on the vertical axis of correspond to instances where reaming the pilot hole to deposition hole scale provides new hydraulic connections to the wider DFN.

When comparing the simulated inflows to open deposition holes with post-closure flows the following is observed (Figure 5-8):

- For the unconditioned DFN, a smeared positive correlation is observed between the simulated inflows to deposition holes and the post-closure initial-flow rates. This can occur because under open tunnel conditions inflows will be drawn towards any part of the network having a low resistance to discharge in the tunnel openings; resulting in under-prediction of the deposition hole specific capacity. In contrast, when both deposition holes and deposition tunnels are successively backfilled and the natural head gradient around the Demonstration Area recovers, this disturbance will no longer occur and flow paths between the deposition holes and other underground (backfilled) openings can occur.
  - A specific case of this effect occurs in a number of deposition holes, where no inflows under open repository conditions are calculated, but subsequent predictions show non-zero initial flows under post-closure conditions (i.e. the vertical axis in Figure 5-8). In this case, zero inflows occur due to the deposition holes connecting solely to neighbouring tunnels / deposition holes (all underground excavations are open with zero head gradient between them). In contrast, under post-closure conditions, the background head gradient of the site can create flows between connected deposition holes or the tunnel system.

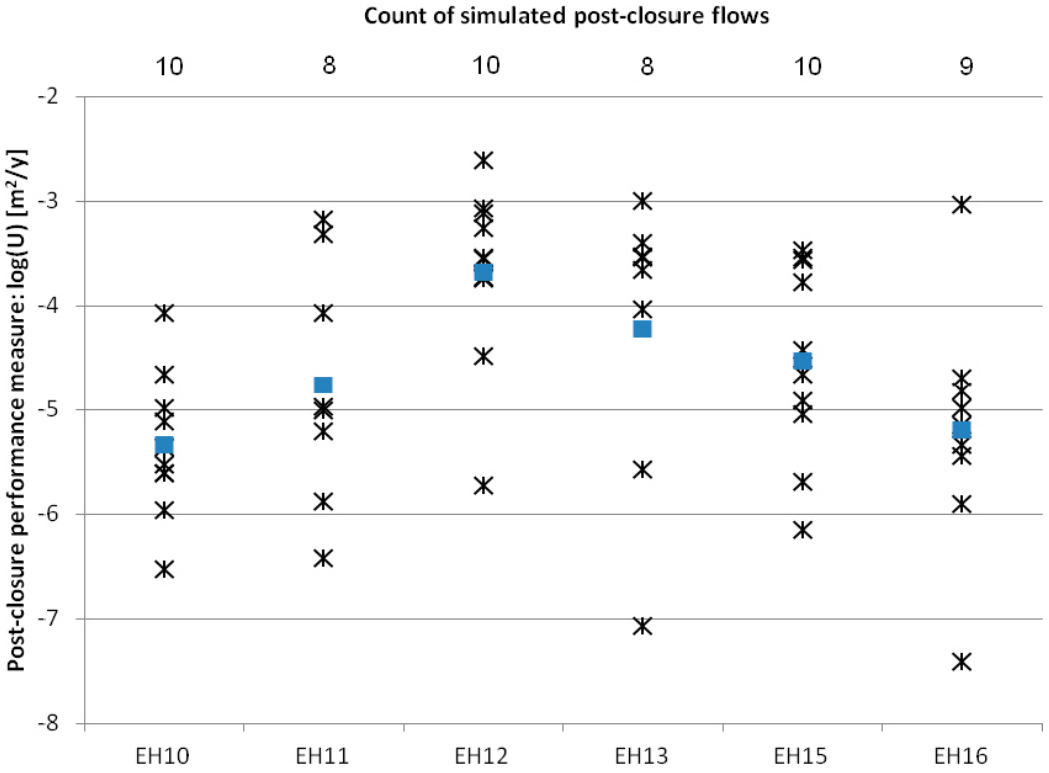

Figure 5-6. *Initial flow rates per unit width (U) simulated for saturated post-closure conditions around each deposition hole from ten realisations of the unconditional DFN (UC-pc). The geometric mean of the simulations (blue squares) are shown.*

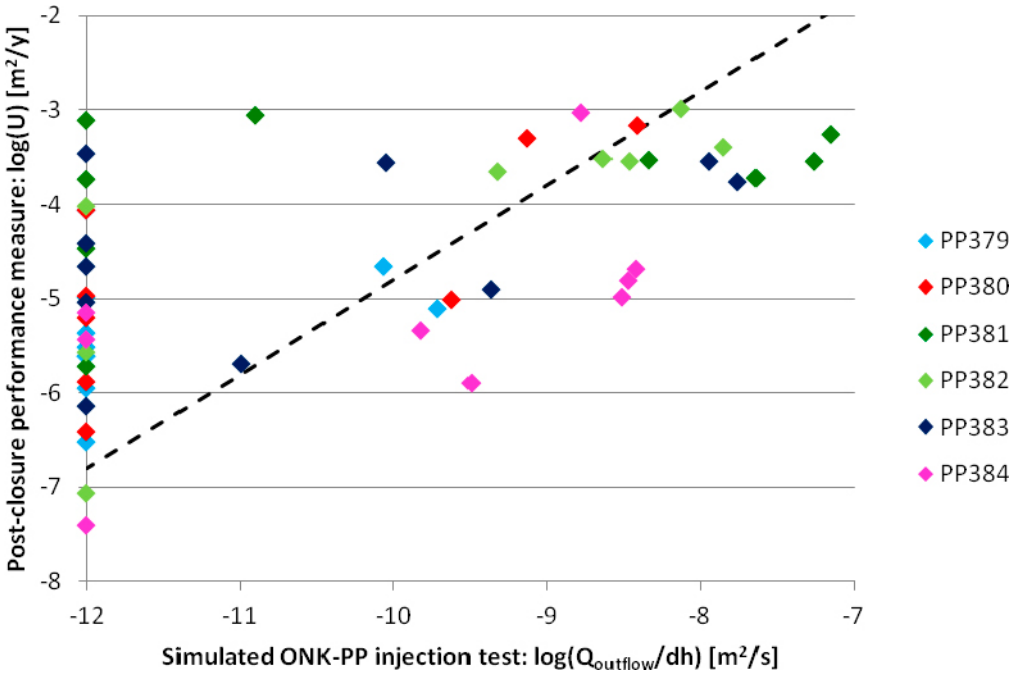

Figure 5-7. *Initial flow rates per unit width (U) for saturated post-closure simulations (UC-pc) compared to specific capacity simulated from hydraulic injection in pilot holes for deposition holes (UC-pi). Ten realisations of the unconditioned DFN are considered with dashed line indicating an equivalence flow rate between the models.*

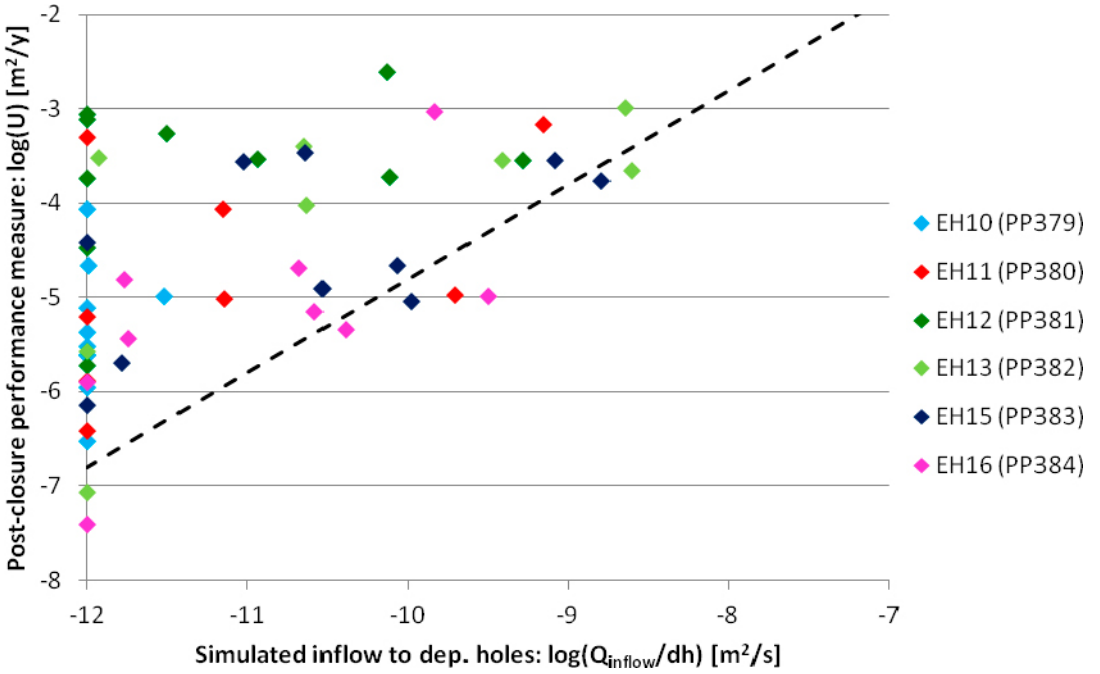

Figure 5-8. *Initial flow rates per unit width (U) for saturated post-closure simulations (UC-pc) compared to specific capacity from simulation of open deposition holes (UC-do). Ten realisations of the unconditioned DFN are considered.*

The simulated flow metrics using the unconditioned DFN typically exhibit large variability between realisations and deposition holes, and weak correlations between the predicted specific capacities and post-closure flows. This variability is likely enhanced by the underlying stochastic DFN description of fracture openings (see Chapter 2); since the conceptualisation of sparsity and heterogeneity within large fractures give rise to channelised groundwater pathways for the simulated flow field through the network and within individual fractures. This study implements the base DFN model for the Demonstration Area and Technical Facilities defined in Hartley et al. (2017), with fracture openings sampled at a 20 m subscale along each fracture, see Figure 2-3. In addition to this model, Hartley et al. (2017) considered a number of variants both increasing and decreasing the scale of fracture openings (Section 6.3 therein). It is anticipated that increasing the size of individual fracture openings would to some extent reduce the heterogeneity of the fracture flow, and consequently reduce the variability in predictions of these flow metrics. The converse would be true if the size of the openings was reduced. Although some of this variability is a consequence of the sparsity of the hydraulic connections in the fracture system, which is an inherent property of the distribution of measured hydraulic material properties at this depth.

The reciprocal of flow-related transport resistance ($1/F$) is shown in Figure 5-9 as a cross-plot with the specific capacity simulated from hydraulic injection in pilot holes for deposition holes. Ten realisations of the unconditioned DFN are considered, and for each realisation, ten particles are released at the point of maximum flux from each of the deposition holes with a non-zero flow, and tracked through the fracture network and tunnels. A dash line provides a simplistic estimate of $1/F$=Specific capacity $\times$ $(dh/dx)/2L$, where dh/dx is the head gradient (assumed to be 0.005), and L is the transport distance (assumed to be 50 m to the model boundary). The flow-related transport resistance shown in Figure 5-9 corresponds to the minimum value over the 10 particle tracks for each realisation and each deposition hole; assumed to best detect the most conductive backbone of the network connected to each deposition hole. This conductive backbone of the network probably has greatest influence on flow measurements like injection and inflows at the hole. However, the distribution of F will be effected by the properties of the immediate fracture system with several different routes and corresponding F to reach these conductive pathways. The presence and properties of this conductive backbone of the network will at best only be hinted at by the minimum of F, but could be completely masked by other aggregate measurements such as the median. Most values of calculated transport resistance are above that predicted by the specific capacity from injection at the pilot hole scale, although it is noted that to truly represent the transport in rock fractures, the specific capacities due to outflows into the tunnel should be removed from these comparisons.

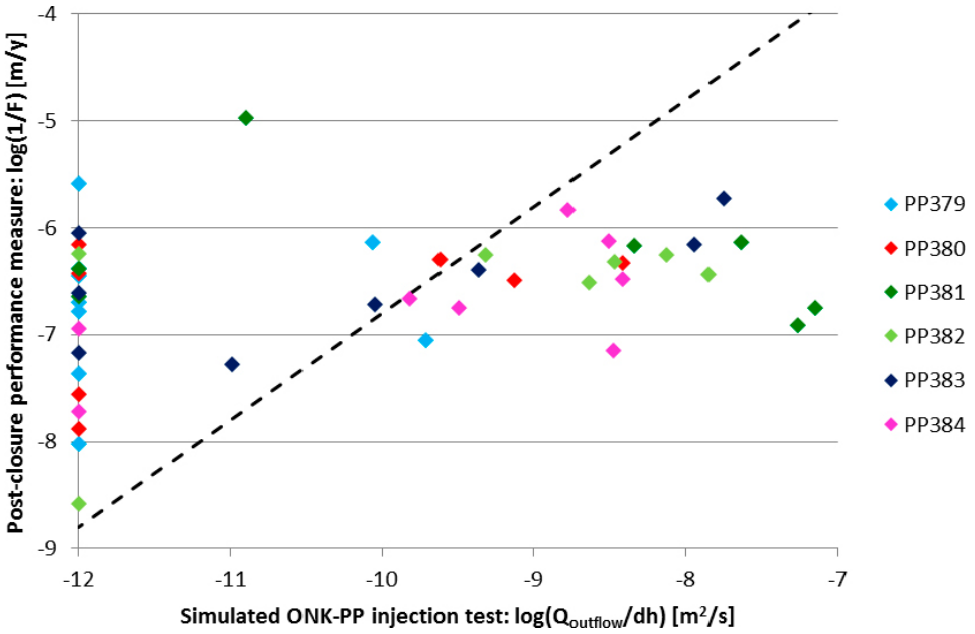

Figure 5-9. *Reciprocal of flow-related transport resistance (1/F) for saturated post-closure simulations (UC-pc) compared to specific capacity simulated from hydraulic injection in pilot holes for deposition holes (UC-pi). Ten realisations of the unconditioned DFN are considered with dashed line indicating an equivalence flow rate between the models. The dashed line is a simple analytical estimate of 1/F.*

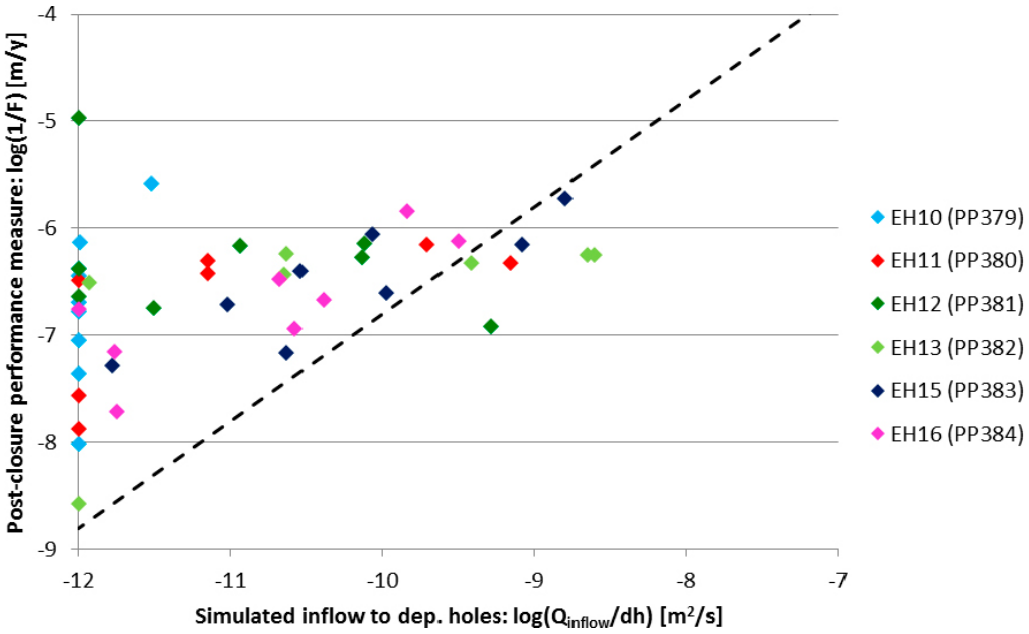

Figure 5-10. *Reciprocal of flow-related transport resistance (1/F) for saturated post-closure simulations (UC-pc) compared to specific capacity from simulation of open deposition holes (UC-do). Ten realisations of the unconditioned DFN are considered. The dashed line is a simple analytical estimate of 1/F.*

An equivalent figure comparing the reciprocal of flow-related transport resistance with inflows to open deposition holes is shown in Figure 5-10. Across the ten realisations of the unconditioned DFN, a weak correlation is observed, and the simulations span the prediction based on the specific capacity from inflows.

6 post-closure flow and transport: conditioned DFN for pilot holes (PH)

In this chapter, the conditional simulation of a DFN local to the ONKALO Demonstration Area is considered; consisting of ten realisations of the DFN model conditioned to:

- fracture traces mapped on the ONKALO ramp and main access tunnels to the Demonstration Area,
- fracture traces mapped in the four demonstration tunnels (including DT2),
- fracture interpretations within the pilot holes extending beyond DT1 (ONK-PH17) and DT2 (ONK-PH20),
- fracture interpretations within the three pilot holes drilled in the floor of DT1, and
- fracture interpretations within the six pilot holes for deposition holes, drilled in the floor of DT2. Optional also the injection tests performed in these holes.

The reader is referred to Chapter 3 for a detailed review of the available data for conditioning DFN models of the Demonstration Area of ONKALO. The conditioning on geometric data only is denoted 'PHGC' (see Section 6.1); quantifying the extent to which the uncertainty in predictions of injection rates for pilot holes, inflows to deposition holes and post-closure flows are reduced by conditioning on fracture traces. In contrast, conditioning using both geometric and hydraulic data is denoted 'PHHC' (see Section 6.2); quantifying the ability of local conditioning on injection rates and to reduce uncertainty in predictions of inflows to deposition holes and post-closure flows. A summary is provided in Figure 6-1 of the conditioning data used in this chapter which includes fracture traces mapped in the ONKALO and Demonstration Area tunnels, as well as fractures interpreted in the pilot holes for deposition holes (ONK-PP) and other pilot holes (ONK-PH).

6.1 Geometric conditioned DFN of pilot holes (PHGC)

The geometric conditioned simulation of the ONKALO Demonstration Area based on data from the pilot holes for deposition holes (PHGC) is detailed in this section. Using the conditioning methodology defined in Chapter 4, a library of 33 000 realisations of the unconditioned DFN model is generated, creating a total of more than 30 million distinct fractures generating over 48 million fracture traces (note each fracture may intersect multiple tunnels generating multiple fracture traces). However, for the library generation to remain computationally tractable not all fracture sizes are generated within each of these realisations; a number of the realisations generate only larger fractures – typically those hardest to match due to multiple tunnel intersections. It is sufficient that small fractures are only created for a subset of the realisations; noting that the power-law size model is biased towards the generation of these small fractures. A breakdown of the library generation by fracture size is detailed in Table 6-1. Using these libraries, ten realisations of the conditioned DFN are generated, and using these conditioned models, three flow metrics (see Chapter 4) are evaluated, considering

- injection tests performed sequentially in each of the six short pilot holes for deposition holes in DT2 (Section 6.1.2),
- inflows to the six experimental deposition holes of DT2 during open repository conditions (Section 6.1.3), and
- the initial flow rate per unit width under saturated post-closure conditions at deposition hole positions (Section 6.1.4).

In each case predictions are compared to the unconditioned model simulations detailed in Chapter 5; identifying any reduction in modelling uncertainty associated with the conditioning process.

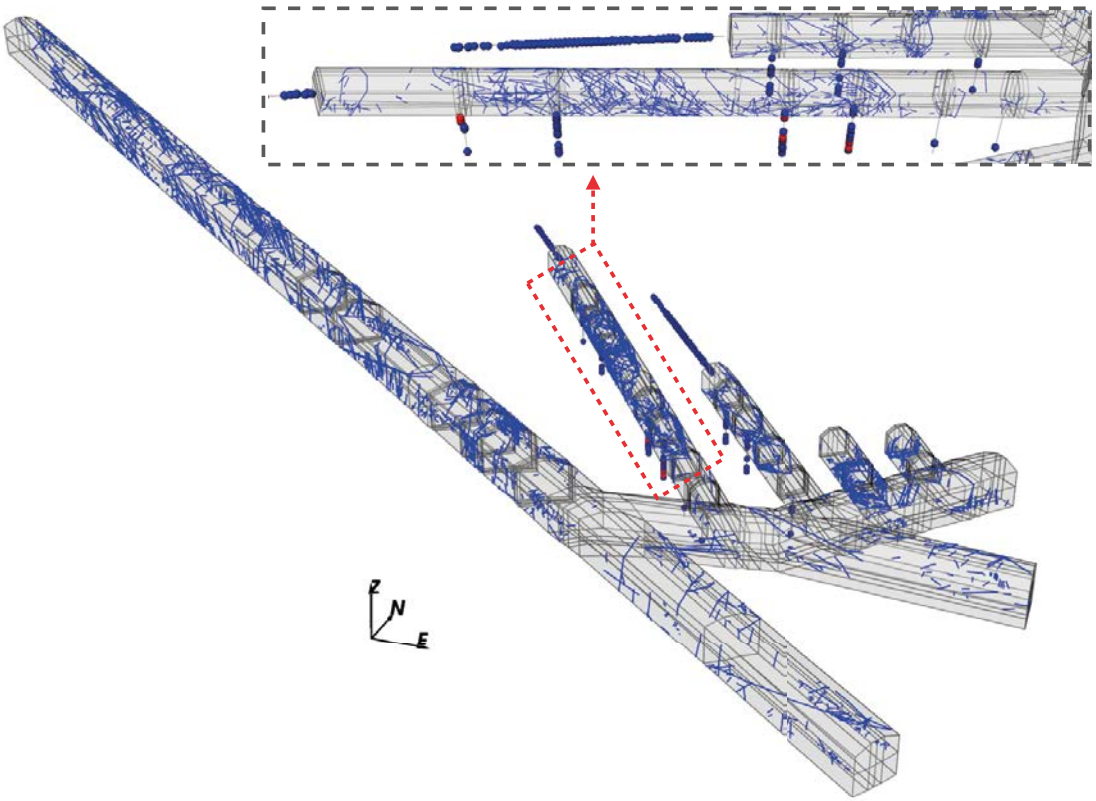

Figure 6-1. *Summary of the data utilised for conditioning of DFN local to the ONKALO Demonstration Area based on pilot holes for deposition holes. The mapping conditioning data corresponds to the blue traces on the modelled tunnel walls, while conditioning data from pilot holes is shown as spheres at the point of intersection. The few red spheres correspond to interpreted fractures assigned flow for conditioning (see Section 6.2).*

Table 6-1. Sizes of fractures and numbers of realisations in each generated library.

Library	Smallest fracture radius (m)	Largest fracture radius (m)	Number of realisations
All-fractures	0.5	320	2000
Small-fractures	1.5	320	5000
Medium-fractures	5.0	320	7000
Large-fractures	25.0	320	19000

6.1.1 Calibration targets

In addition to these flow metrics, two calibration targets (detailed in Section 4.2) are considered to provide checks that the conditional simulations are working effectively. These are:

- comparison of fracture intensity (P_{21}) on the conditioned tunnel surfaces with geological mappings, and
- comparison of individual fracture locations on the conditioned tunnel surfaces.

Fracture intensity (P_{21})

The fracture intensity target requires the conditioned model should accurately reflect the P_{21} of the observed fracture traces mapped on the tunnels of the ONKALO; where for the geological mapping, the intensity is calculated from the idealised fracture traces corresponding to synthetic tunnel surfaces.

Recall that the acceptance test for the P_{21} calibration target is that the conditioned fracture intensity should be within 5 % of the equivalent value from mapping, and vary by no more than 20 % of the variation of P_{21} between unconditioned realisations (Appleyard et al. 2018). These limits are chosen to allow for the inherent statistical uncertainty expected for the conditioned model whilst ensuring the model is sufficiently consistent with measurements. In this case, the P_{21} corresponds explicitly to the conditioned fractures, and as such accounts for the variable censoring of the mappings (see Table 3-3).

Figure 6-2 illustrates the intensity for all ten realisations of the conditioned DFN, calculated from the intersection of fractures above censoring limits with all underground openings in the ONKALO Demonstration Area. Clearly only minimal variation is observed between realisations of the conditioned DFN model, with these models consistently reflecting the mapped P_{21}. As such, they are around 20 % lower than the unconditioned DFN simulations, which consistently over predicted the intensity of fracture trace mappings.

The fracture intensity, P_{21}, calculated for each experimental deposition hole is shown in Figure 6-3 for ten realisations of the conditioned DFN model. This figure quantifies the reliability of simulations made for unconditioned realisation with the DADFN model, and after conditioning on the trace data from the DT2 tunnel above.

Predictions in ONK-EH12 and ONK-EH16 are consistent with mapping and the overall differences between deposition holes is predicted. However, generally, model predictions for P_{21} are too low in ONK-EH10 and ONK-EH11; and too high in ONK-EH13 and ONK-EH15 (although some realisations are significantly closer than others). Note the deposition hole predictions for P_{21} cannot be assessed against the calibration targets as their small volume are not statistically significant.

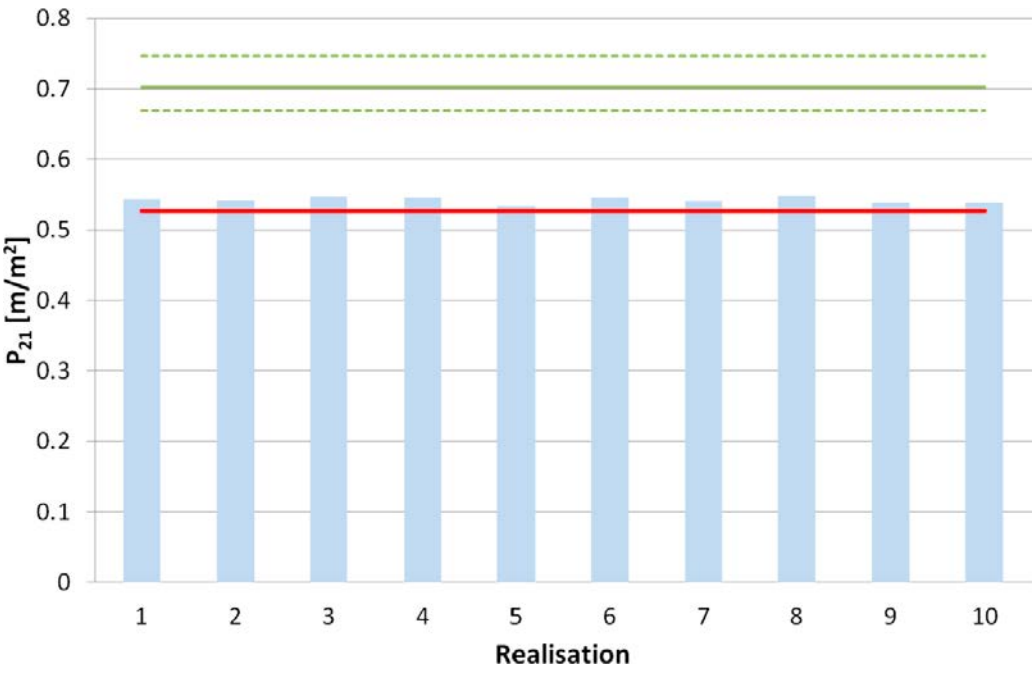

Figure 6-2. *Intensity (P_{21}) for all fracture intersections with underground openings in the ONKALO Demonstration Area. Ten realisations of a conditioned simulation of the tunnels and pilot holes are shown, with the conditioning algorithm only considering geometric properties. Data from the idealised geological mapping are shown in red, with maximum, minimum and mean values from ten realisations of the unconditioned simulations shown in green.*

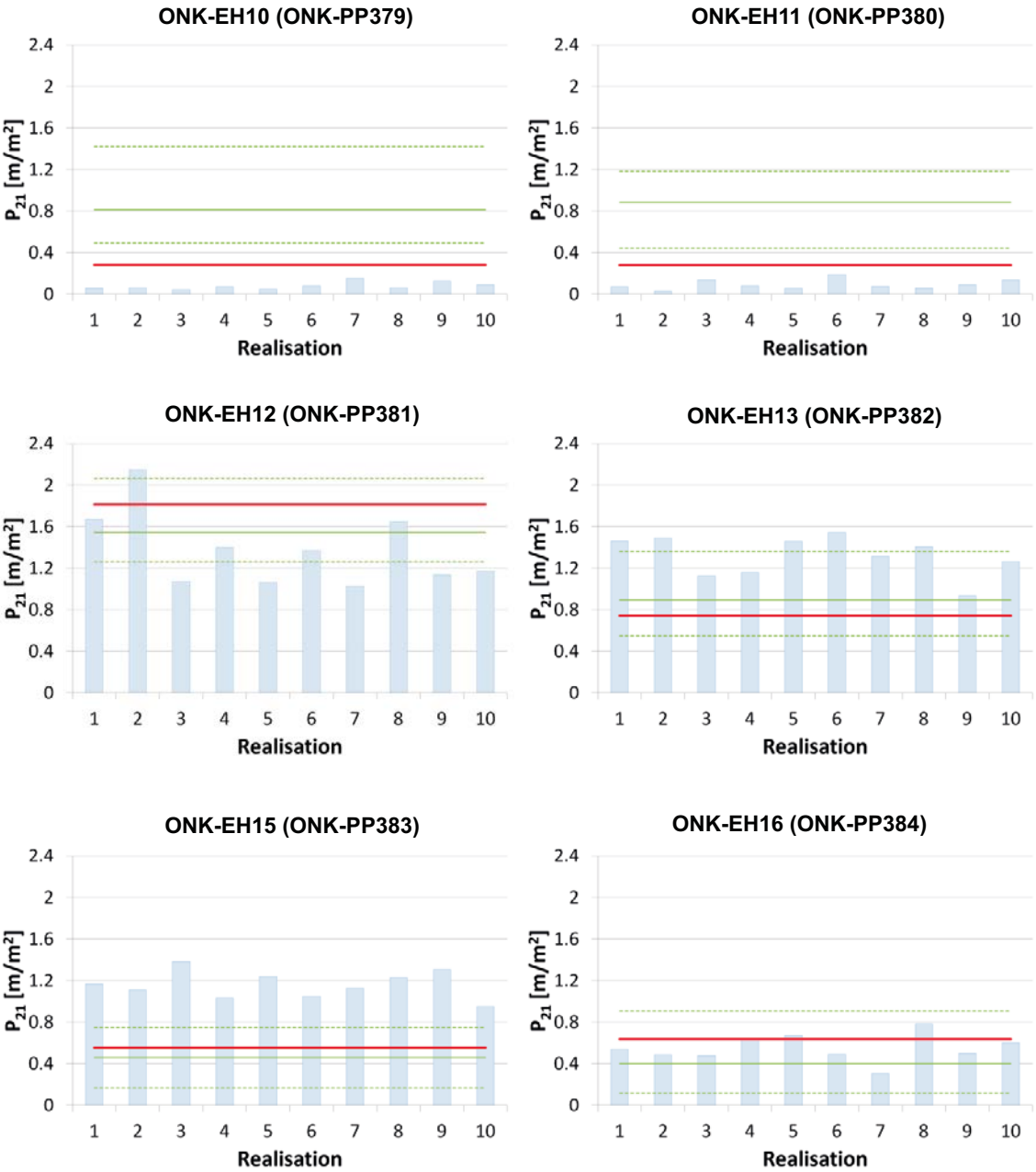

Figure 6-3. *Intensity predictions (P_{21}) for fracture intersections with the six deposition holes of DT2. Ten realisations of a conditioned simulation of the tunnels and pilot holes are shown, with the conditioning algorithm only considering geometric properties. Data from the idealised geological mapping are shown in red, with maximum, minimum and mean values from ten realisations of the unconditioned simulations shown in green.*

For comparison, the intensity of mapped fractures as well as the range of intensities calculated for ten realisations of the unconditioned simulations are shown in Figure 6-2 and Figure 6-3. It is observed that:

- The acceptance test for P_{21} is passed for the conditioned DFN models. The maximum difference between simulations and mapping is 4 %. The variability in P_{21} for the unconditioned DFN models is 0.078 m^{-1}, whereas for the conditioned simulations the variability is only 0.014 m^{-1}; 18 % of that of the unconditioned models.
- The unconditioned models consistently over-predict the measured P_{21}. This is likely a consequence of the censoring limits on the mapping given in Table 3-3 being applied as a hard limit, and as an estimate at that. In reality the likelihood of recording a fracture trace will increase with the length of the trace (for example only a proportion of fracture traces between 0.5 m–1.0 m will

be mapped, even though the censoring limit is estimated at 0.5 m). As such the mapped fracture traces will not provide a complete data set of all fractures mapped as intersecting the tunnel, but rather a subset of those observed.

It may be appropriate to re-assess the fracture size model against recent supplementary mapping studies on cleared sections of floor in ONKALO to quantify uncertainties in the size model and the effects of the censoring limit on the scale of decimetres-metre.

Fracture location

The fracture location calibration target provides a metric to ensure that individual fractures are in the correct location, have correct length and orientation. Details of this calibration test are provided in Section 4.2.2; with two regions of the Demonstration Area block-scale domain considered, one sparsely fractured, the other densely fractured. For illustration, in each region the mapping is visually compared to one realisation of the unconditioned and conditioned DFN model. The following is observed from visualising the realisations of the DFN model:

- **Densely fractured area**
  Figure 6-4 illustrates the fracture traces from mapping in this innermost region of DT2, comparing a single realisation of the unconditioned and conditioned DFN model. Enhanced fracturing local to BFZ is included in the underlying stochastic DFN model prescription, and intensity of fracture traces predicted by the unconditioned model reflects this. The model also orientates fractures sub-parallel to the BFZ structure, so the orientation of fracture traces from the unconditioned model is broadly similar to mapping. However, the unconditioned model does not honour locations, size and orientation of individual mapped races – unlike the conditioned model, which is in good agreement. Agreement is not exact because conditioned fractures are sampled from the library according to the closeness-to-fit function (See Section 4.1) providing similar, but not identical matches.
- **Sparsely fractured area**
  Figure 6-5 illustrates fracture traces at the beginning of DT2, comparing the few mapped structures with those simulated from a single realisation of the unconditioned and conditioned DFN model. The underlying stochastic DFN model does not fully predict the reduced fracture intensity in this region of the Demonstration Area; located on the border of the low intensity VGN and PGR lithologies, as well as being in the low intensity CTU1 ductile domain and far from a BFZ. However, it is readily observed that the conditioned model better fits the observed fracture traces, reducing the overall intensity of fractures simulated to intersect the tunnel in this region. In addition the size and orientation of individual fracture traces simulated in the conditioned models are broadly consistent with measurements.

6.1.2 Injection to pilot holes (PHGC-pi)

The first flow metric, based on the geometrically conditioned DFN models for pilot holes drilled in the floor of DT2 (PHGC-pi) is detailed in this subsection. Simulations consider the injection into the whole of the packed-off six pilot holes for deposition holes (excluding the top 0.5m which is packed-off) sequentially (in turn), with results directly comparable to the unconditioned DFN models in Section 5.1. Again, the simulations make predictions without prior knowledge of the measured outcomes, and hence provide a validation of conditioned simulations.

The specific capacities calculated from the simulated injection tests in each of the pilot holes are shown in Figure 6-6. Only those pilot hole realisations which hydraulically connect to the wider DFN are shown; equating to 34 instances, with connections clearly more prevalent in pilot holes ONK-PP381 through ONK-PP384. These hydraulic connections to the wider DFN provide a flow pathway through the connected fracture network to any of the model boundaries (including open tunnels); providing a pathway for injection. No account is taken for the individual transmissivities of fractures along this connected pathway. In contrast, pilot holes ONK-PP379 and ONK-PP380, are located towards the sparsely fractured entrance to DT2 tunnel, and therefore have reduced connectivity. *In situ* measurement results from the injection tests are included for comparison; with ONK-PP379, ONK-PP380 and ONK-PP383 recording no flows above the detection limit of the tool. Typically simulations span the measurements (with the exception of ONK-PP382 where all simulations slightly over predict the specific capacity).

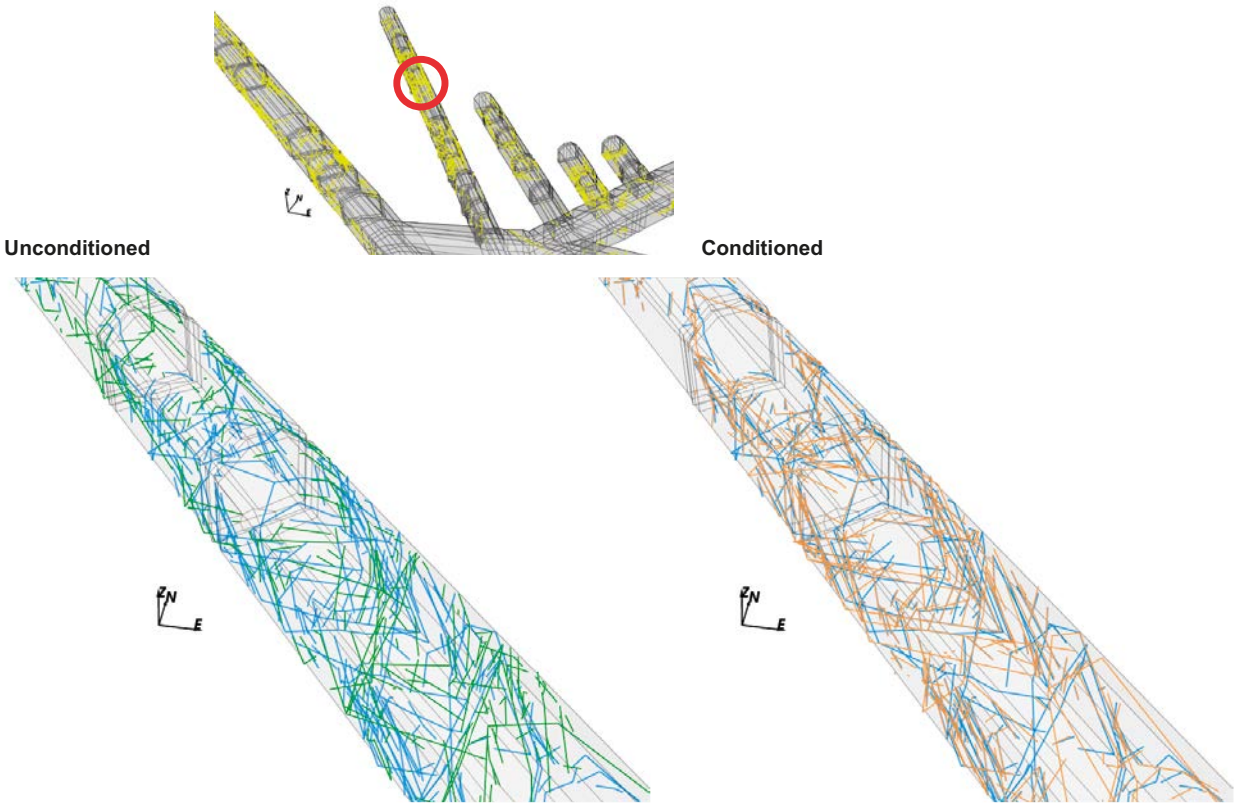

Figure 6-4. *Geological mapping (blue) and predicted fracture traces from an unconditioned DFN model (left, green) and a conditioned DFN model (right, orange). The section shown is mid-way along Demonstration Tunnel 2; two BFZ (BFZ045 and BFZ084) intersect the tunnel here yielding an intensely fractured region of rock.*

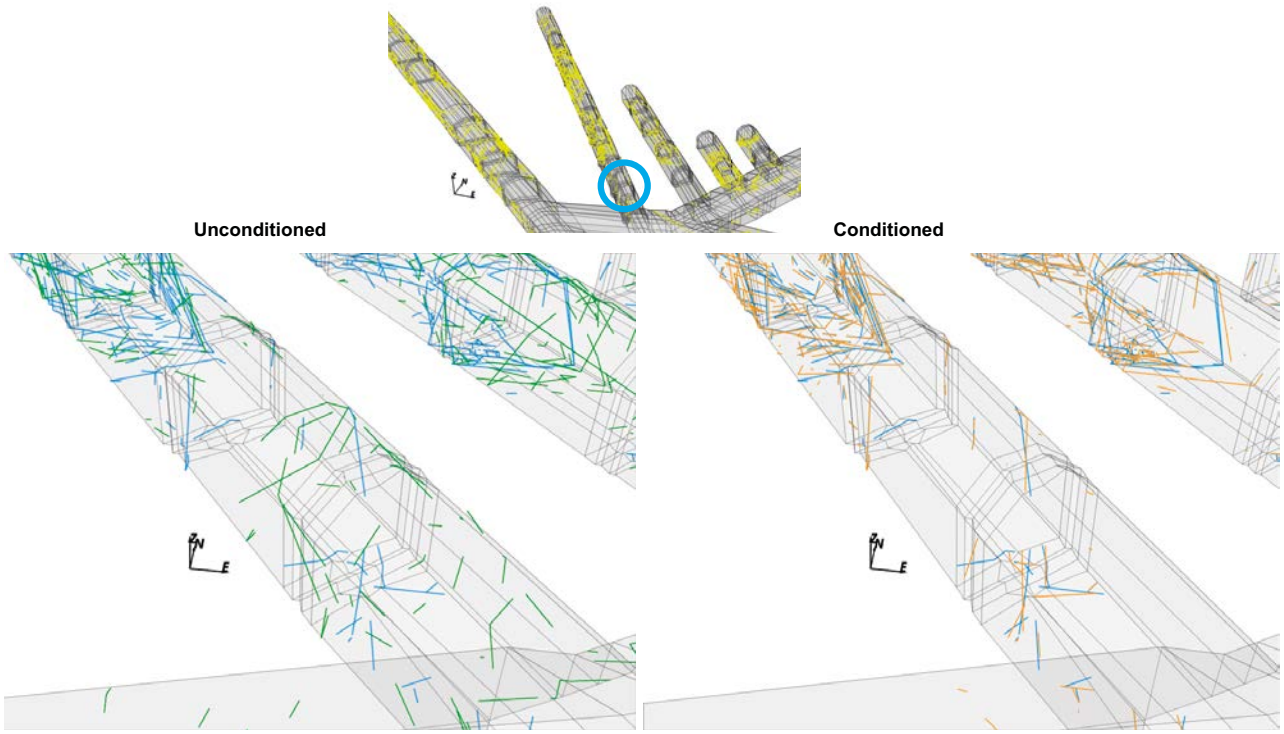

Figure 6-5. *Geological mapping (blue) and predicted fracture traces from an unconditioned DFN model (left, green) and a conditioned DFN model (right, orange). The section is at the beginning of Demonstration Tunnel 2 consisting an extended volume of intact rock with sparse fracturing.*

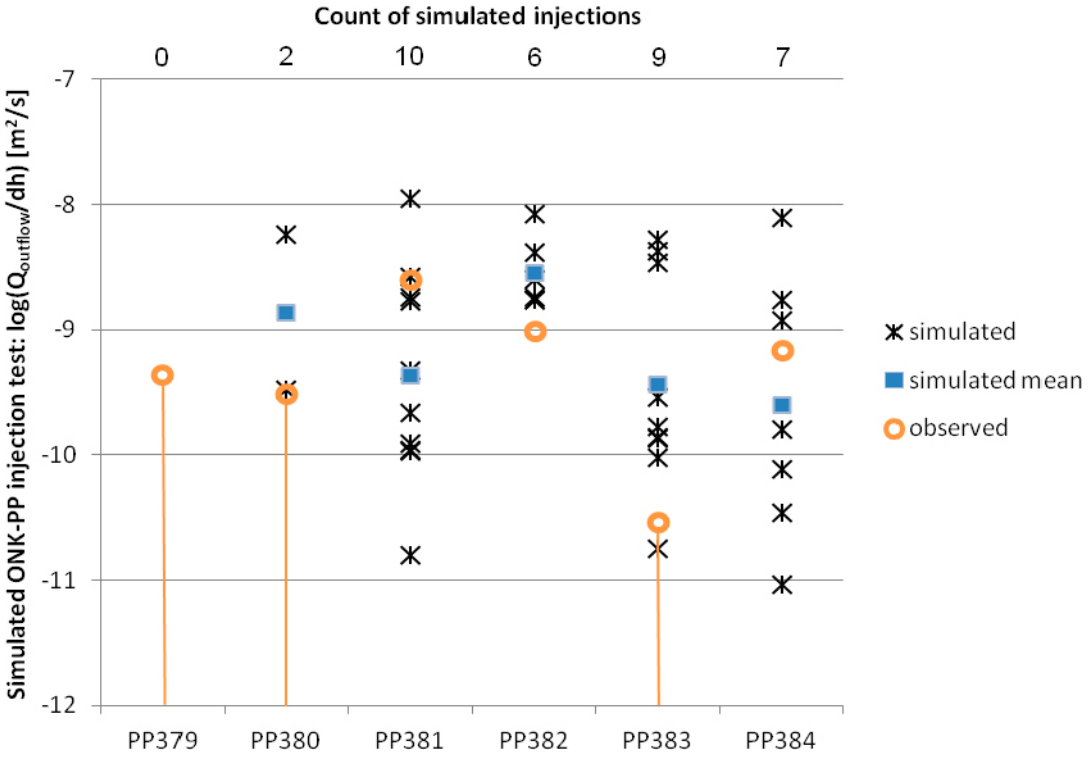

Figure 6-6. *Log specific capacity from simulated injection tests by pilot hole for ten realisations (black markers) of the conditional DFN (PHGC-pi) based on geometric data including data for pilot holes of deposition holes. Geometric mean (blue squares) from simulation and injection test measurements (orange circles) are shown. Orange lines indicate measurements not being above the detection limit of the tool.*

Although still somewhat uncertain, the variability in predicted injection rates in pilot holes for deposition holes is reduced between realisations of the conditional DFN when compared to the unconditioned model. For the unconditioned realisations, simulated specific capacities were shown to vary by up to 4 orders of magnitude; reduced to 3 for the geometric conditioned DFN.

6.1.3 Inflows to deposition holes (PHGC-do)

Simulation of the second flow metric, considering the inflows to the six experimental deposition holes under open repository conditions is detailed in this subsection. Simulations utilise the geometrically conditioned DFN models for pilot holes drilled in the floor of DT2 (PHGC-do), with results directly comparable to the unconditioned DFN models in Section 5.2. Once again, these results provide a prediction-outcome comparison.

Figure 6-7 shows the predicted inflows to each of the deposition holes for ten realisations of the conditional DFN; illustrating only those realisations where the deposition hole is hydraulically connected to the wider fracture network. *In situ* measurements record no inflow above detection limit to either ONK-EH10 or ONK-EH11, located in the intact rock volume at the beginning of the DT2 tunnel; although several model realisations do predict inflows at these locations although a significant number are below the detection limit. In contrast, the inflows measured in each of the four experimental deposition holes located further along DT2 are spanned by the stochastic variability in the model predictions for the ten realisations considered. It is noted that conditioning the DFN based on the geometric data including pilot holes for deposition holes does not substantially reduce the stochastic uncertainty of inflow predictions at the deposition hole scale when compared to the unconditioned model.

Similar to Figure 5-3 for the unconditioned simulations, Figure 6-8 illustrates the correlation between the simulated specific capacities from inflows to open deposition holes (PHGC-do) against corresponding hydraulic injection tests in the pilot holes for deposition holes (PHGC-pi). Typically, results fall into one of three categories as described in Section 5.2, with additional illustrations of a typical fracture network in each case.

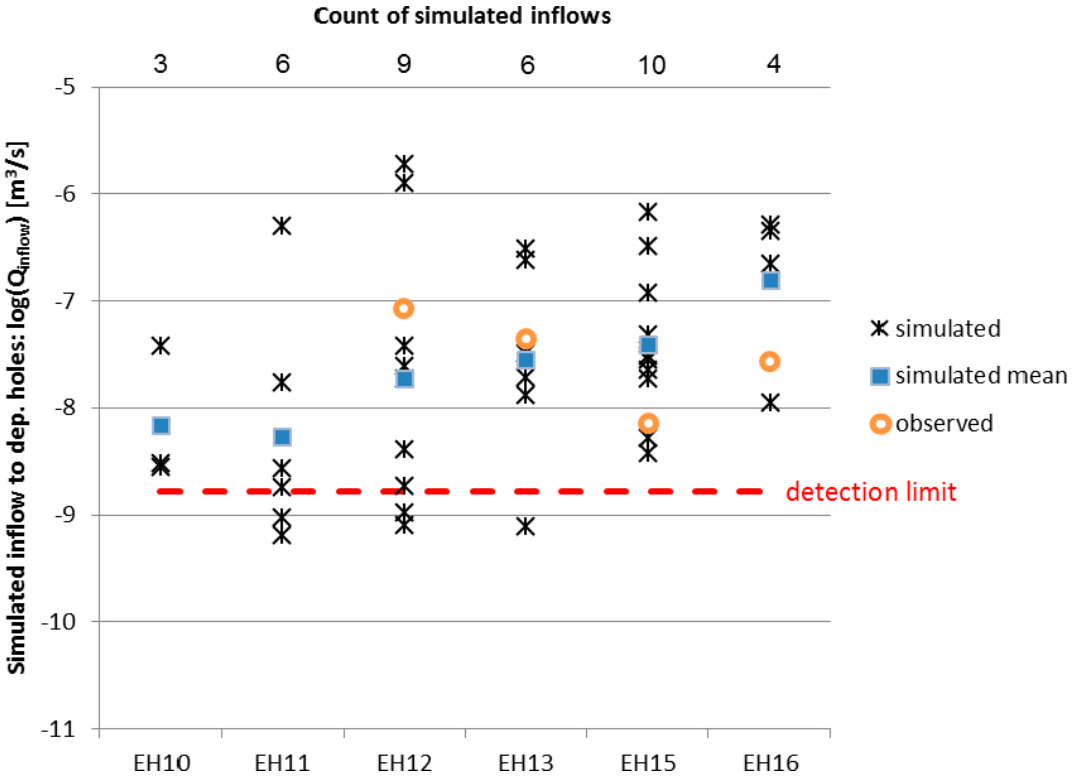

Figure 6-7. *Log inflow simulated for open deposition holes for ten realisations of the conditional DFN (PHGC-do) based on geometric data for pilot holes for deposition holes.*

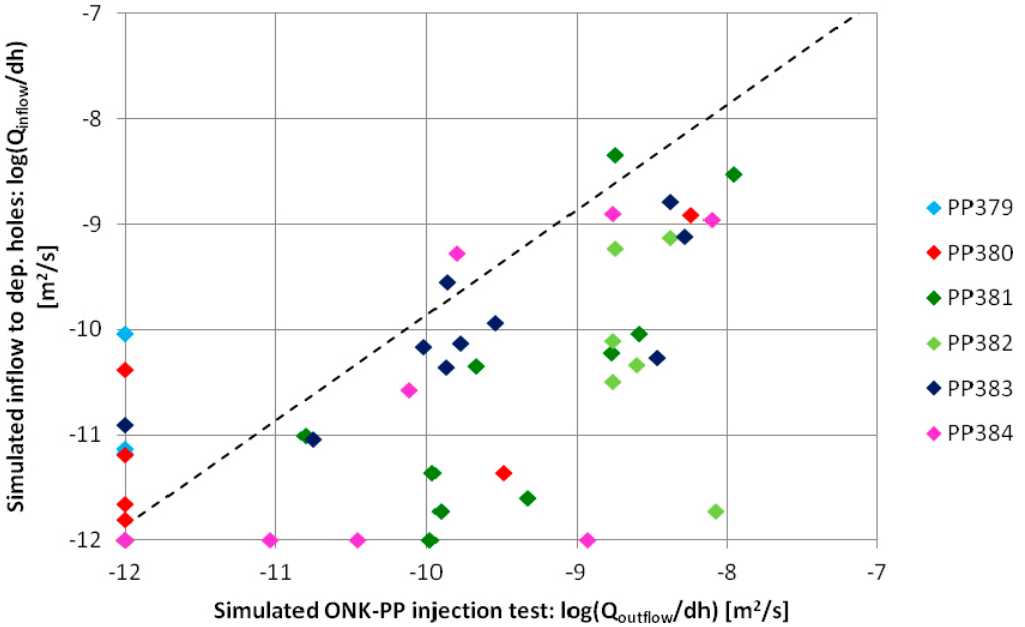

Figure 6-8. *Specific capacity from simulated inflows to open deposition holes (PHGC-do) against corresponding specific capacity simulated from hydraulic injections in the pilot holes for deposition holes (PHGC-pi). Ten realisations of the conditional DFN based on geometries for pilot holes for deposition holes are shown.*

6.1.4 Post-closure flow (PHGC-pc)

Simulation of the post-closure flow metrics, based on the geometrically conditioned DFN models for pilot holes drilled in the floor of DT2 (PHGC-pc) is detailed in this subsection; with results comparable to the unconditioned DFN models in Section 5.3.

The variability in predicted initial flow rates per unit width for the six experimental deposition holes is shown in Figure 6-9 corresponding to ten realisations of the conditioned DFN. The stochastic uncertainty in model predictions is similar to the unconditioned DFN models, with variability between deposition holes in the range of 2 to 4 orders of magnitude.

Two possible criteria are considered for the acceptance of deposition holes as a proxy for the post-closure flow conditions; one infers the performance of the hole from the specific capacity of the pilot holes drilled for deposition holes; the other the inflows at open deposition hole conditions. Similarly to the unconditioned model, cross-plots comparing post-closure flow for ten realisations of the conditional DFN model are considered; comparing with injection tests in pilot holes (PHGC-pi), Figure 6-10; and simulated inflows to open deposition holes (PHGC-do), Figure 6-11. A detailed review of the equivalent charts for unconditioned models is presented Chapter 5; with the following key differences observed when considering conditioned models:

- Of the 60 injection tests simulated (six pilot holes, ten realisations of the DFN); 26 do not form hydraulic connections from pilot holes to the wider fracture network. These points lie on the vertical axis of Figure 6-10 and offer slight improvement over the unconditioned model where 32 such instances were found. This scenario occurs when reaming the pilot hole to deposition hole scale causes hydraulic connection of the hole to the wider DFN.
- A weak positive correlation is observed between the simulated inflows to deposition holes and the post-closure initial-flow rates. However, when comparing to the unconditioned simulations, the number of deposition holes which predict zero inflow (corresponding to the vertical axis in Figure 6-11) is reduced to 22 from 28. These no inflow predictions can occur when the deposition hole does not form connections to the wider fracture network (although localised connections to neighbouring tunnels and deposition holes are viable).
- For both injection tests and inflows to open deposition holes, the stochastic variability between the ten realisations considered is slightly reduced when conditioned models based on geometric data including from pilot holes for deposition holes are compared to the unconditioned simulations. This can be observed by the enhanced clustering of points in Figure 6-10 and Figure 6-11 when compared to Figure 5-7 and Figure 5-8, respectively.

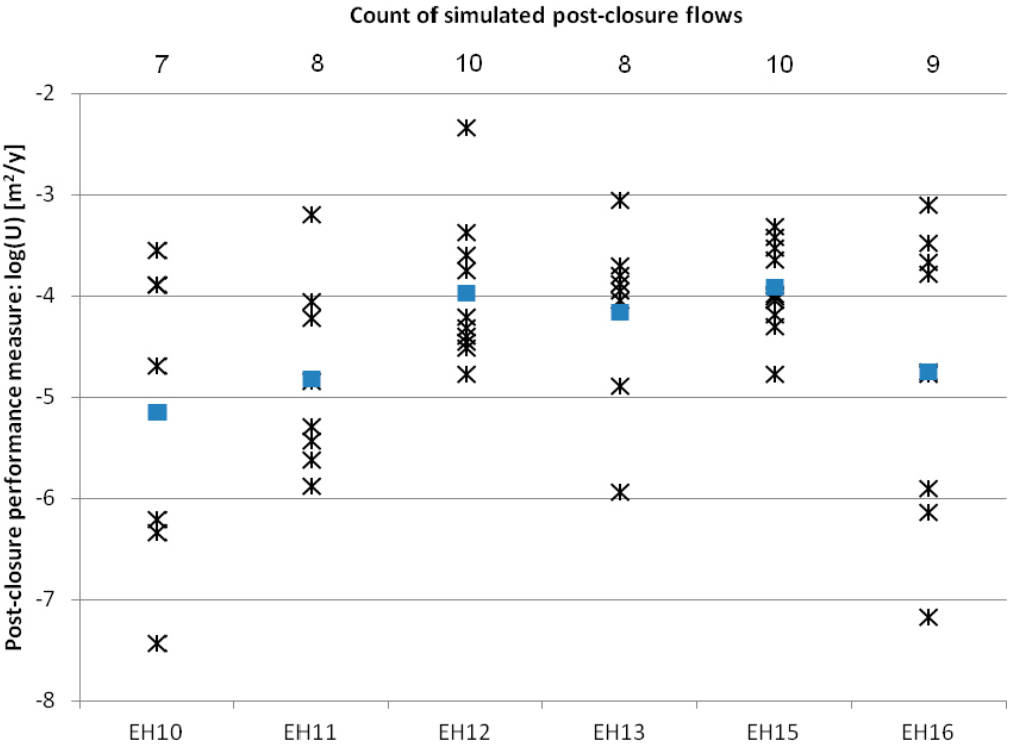

Figure 6-9. *Initial flow rates per unit width (U) simulated for saturated post-closure conditions from ten realisations of the conditional DFN (PHGC-pc). Conditioned DFN models are based on geometry data including data for pilot holes of deposition holes.*

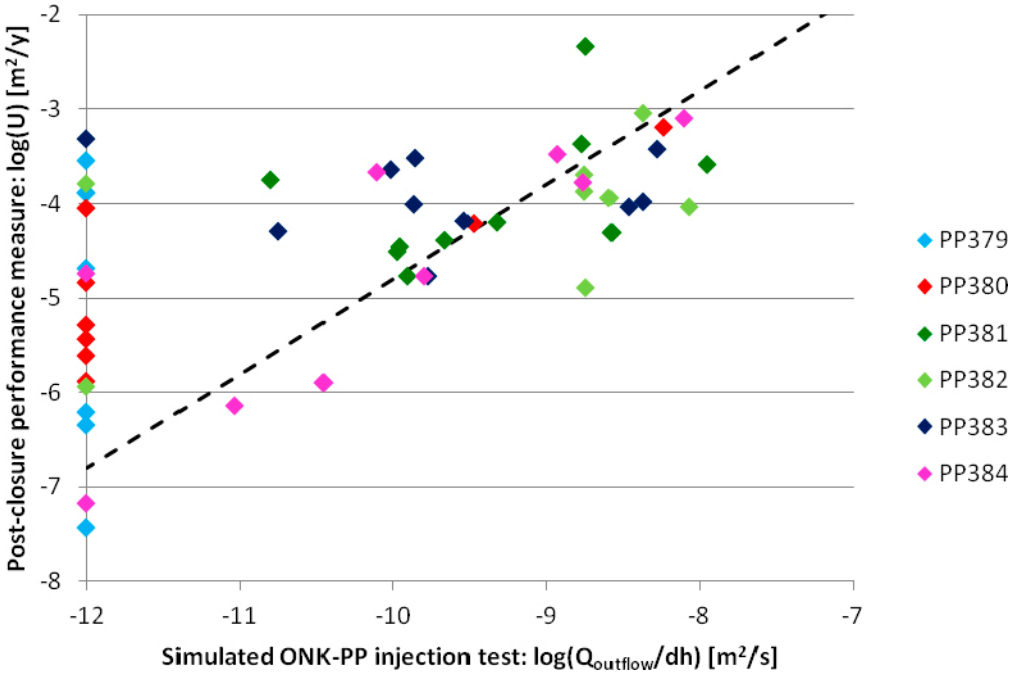

Figure 6-10. *Initial flow rates per unit width (U) for saturated post-closure simulations (PHGC-pc) compared to specific capacity simulated from hydraulic injection in pilot holes for deposition holes (PHGC-pi). Ten realisations of the conditional DFN are considered, based on geometric data including data for pilot holes of deposition holes. An equivalence line, based on the (pilot hole specific capacity multiplied by post-closure head gradient is also shown.*

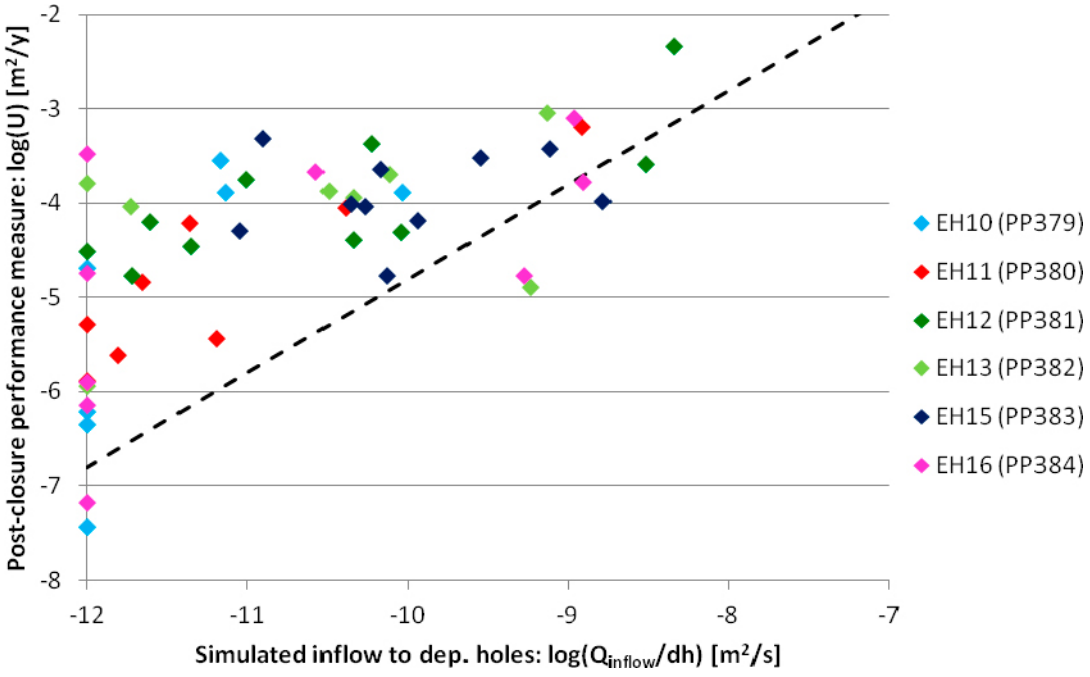

Figure 6-11. *Initial flow rates per unit width (U) for saturated post-closure simulations (PHGC-pc) compared to specific capacity from simulation of open deposition holes (PHGC-do). Ten realisations of the conditional DFN are considered, based on geometric data for pilot holes for deposition holes. An equivalence line, based on the (deposition hole specific capacity multiplied by post-closure head gradient is also shown.*

6.2 Hydraulic conditioned DFN on injection tests in pilot holes (PHHC)

The conditioned simulation of DT2 based on injection tests performed within the pilot holes for experimental deposition holes (PHHC) is detailed in this section. A library of over 26 000 realisations of the unconditioned DFN model is generated, creating a total of more than 40 million distinct fractures creating over 65 million unique fracture traces (note each fracture may intersect more than one tunnel). Similar to the geometric conditioning of pilot hole for deposition holes performed in Section 6.1, the library generation can be defined such that a number of realisations only generate the larger fractures – corresponding to those fractures which are hardest to match in the observed data and for which the power-law size model will generate fewest in any given realisation of the library. However, unlike the geometric conditioning, flow simulations are performed for each realisation of the library in order to condition on the specific capacities of the injection tests. The percolation of the underlying stochastic fracture model will typically require all fractures down to a few metres radius to be considered; and as such the 'large' fracture libraries considering only those fractures greater than 25 m radius are not suitable in this case. These have been replaced with additional 'small' and 'medium' libraries, and a breakdown of the library generation by fracture size is given in Table 6-2. As well as adjusting the fracture sizes permitted in the library generation, hydraulic conditioning offers an additional constraint on the fracture area open to flow. Recall from Chapter 2 that fractures are subdivided into sub-fractures of side length 20 m, and whether each of these tessellates is open to flow is sampled probabilistically according to a uniform random deviate. For conditioned models using hydraulic information, the sub-fracture area intersecting the pilot hole can be deterministically set as open for fractures selected to represent flowing observations, whereas for sub-fractures matched to non-flowing observations, the open criteria is sampled stochastically. In both cases, the open proportion of the remainder of the fracture area away from pilot hole intersection is sampled stochastically (as applied in the unconditioned and geometrically conditioned models).

Table 6-2. Sizes of fractures and numbers of realisations in each generated library used for conditioning based on the pilot hole injection tests.

Library	Smallest fracture radius (m)	Largest fracture radius (m)	Number of realisations
All-fractures	0.5	316.0	2010
Small-fractures	1.5	316.0	10050
Medium-fractures	5.0	316.0	14070
Large-fractures	25.0	316.0	0

Ten realisations of the hydraulically conditioned DFN based on the injection tests in pilot holes are generated, with the following three flow metrics evaluated:

- injection tests performed sequentially in each of the six short pilot holes for deposition holes in DT2 (Section 6.2.1),
- inflows to the six experimental deposition holes of DT2 during open repository conditions (Section 6.2.2), and
- the initial flow rate per unit width around the deposition hole positions under saturated post-closure conditions (Section 6.2.3).

In each case predictions are compared to the unconditioned model simulations detailed in Chapter 5, and the geometrically conditioned models in Section 6.1, identifying any reduction in uncertainty associated with the additional hydraulic constraints introduced in the conditioning process.

6.2.1 Injection to pilot holes (PHHC-pi)

In this subsection, simulations consider the sequential injection into the six pilot holes for deposition holes based on conditioned realisations using the injection test data (PHHC-pi). Results are directly comparable to the unconditioned DFN models in Section 5.1 and the geometrically conditioned models in Section 6.1.2.

Figure 6-12 illustrates the specific capacities calculated from the simulated injection tests in each of the pilot holes. For holes ONK-PP379, ONK-PP380 and ONK-PP383 injection tests record no flows above detection limits, and the majority of simulations (all but three) predict no flow in these three holes. In contrast, flows are measured in pilot holes ONK-PP381, ONK-PP382 and ONK-PP384 during the *in situ* injection tests, with 22 simulations predicting inflows to these holes with magnitudes more consistent with measurements than unconditioned simulations. For the latter three holes, the stochastic uncertainty in the predicted specific capacities between realisations of the conditioned DFN is approximately three orders of magnitude. This is a reduction in variability compared to the unconditional DFN models (four orders of magnitude variability) or the geometrically condition models, PHGC-pi (over three orders of magnitude variability). It is noted that although the conditional simulations utilise the injection test data directly, they do not directly predict the measured injection rates in each of the pilot holes. This is as expected, as conditioning the DFN model based on the injection test data matches fractures with the correct (to within some tolerance) specific capacities as simulated within the DFN realisations considered as part of the conditioning library. Therefore, although specific capacities within the library provide an adequate match to the measured injection rates within their host realisation, they will not necessarily produce the same specific capacity when selected as part of the conditioned fracture network (see Section 4.1).

Finally, it is noted that although the ten realisations of the conditioned DFN provide an illustrative study of the stochastic uncertainty of the models; it is unlikely with such few realisations that one particular DFN model will provide adequate prediction of all six injection tests. To further constrain the DFN, an alternative approach would be to generate hundreds of realisations of the conditioned DFN, and then screen those models based on their predictive capability of the injection tests. Applying this methodology, would allow selection of the 'optimal' ten realisations of the conditioned DFN model from the suite of realisations considered. This approach of screened conditional simulation of pilot hole injection tests (PHHC) is considered in Section 6.3.

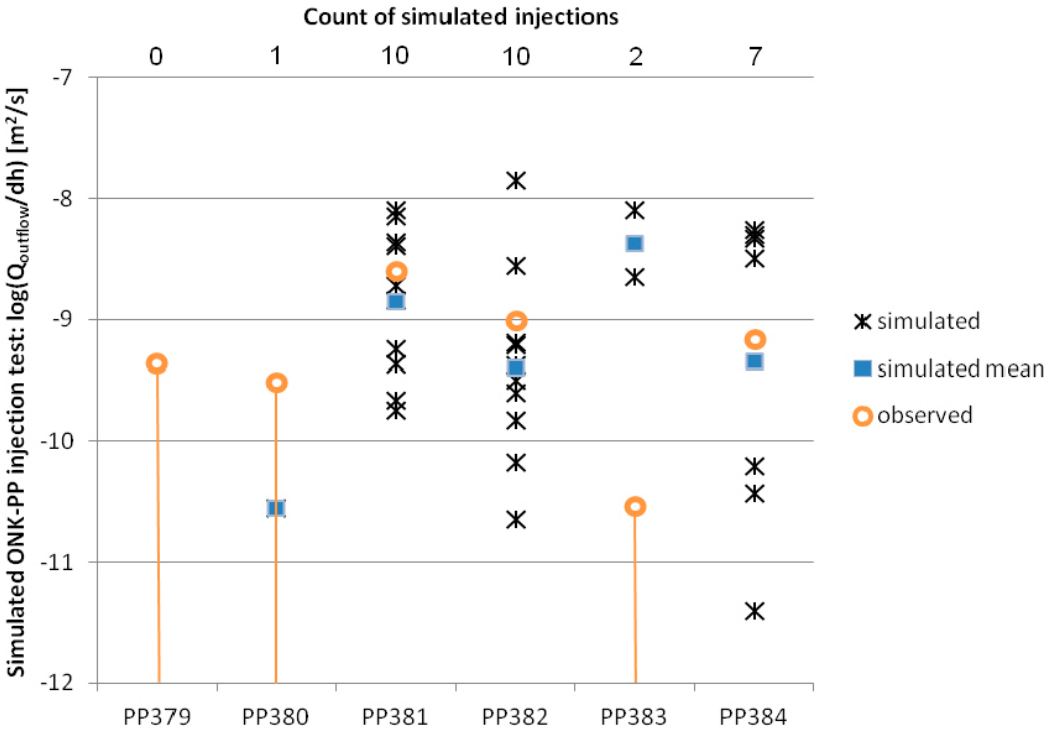

Figure 6-12. *Log specific capacity from simulated injection tests by pilot hole for ten realisations (black markers) of the conditional DFN (PHHC-pi) based on injection test data for pilot holes for deposition holes. Geometric mean (blue squares) from simulation and injection test measurements (orange circles) are shown. Orange lines indicate measurements not being above the detection limit of the tool.*

6.2.2 Inflows to deposition holes (PHHC-do)

In this subsection, simulations consider open repository conditions, evaluating the inflow to each of the six experimental deposition holes (PHHC-do) for comparison with the unconditioned DFN in Section 5.2 and the geometrically conditioned models in Section 6.1.3. Again, the predictions are made without prior knowledge of the measurements as a validation of the model.

Inflows to each of the deposition holes, predicted from the ten realisations of the PHHC conditioned DFN are shown in Figure 6-13, showing only those realisations where the deposition hole is hydraulically connected to the wider network. Note the number of realisations for which an individual hole is hydraulically active can reduce when considering inflows to open deposition holes compared to injection to pilot holes. This is because injection tests can include local injection directly into the open demonstration tunnel. Results show a similar trend to the geometrically conditioned models (compare with Figure 6-7) with only a few realisations predicting inflows to the dry deposition holes ONK-EH10 and ONK-EH11. For the remaining four deposition holes, simulations are consistent with the measured inflows (although simulations slightly over predict measurements in ONK-EH15; where measured inflows are low and somewhat uncertain – see Section 3.4). When considering predictions of inflows to deposition holes from the unconditioned (UC-do) or geometric conditioned (PHGC-do) models, the stochastic uncertainty has been slightly reduced.

The correlation between the simulated specific capacities from inflows to open deposition holes (PHHC-do) against corresponding simulated hydraulic injections in the pilot holes for deposition holes (PHHC-pi) are shown in Figure 6-14. Corresponding figures for the unconditioned and geometrically conditioned models are presented in Figure 5-3 and Figure 6-8, respectively. A detailed description of this type of analysis is presented for the unconditioned simulations in Section 5.2.

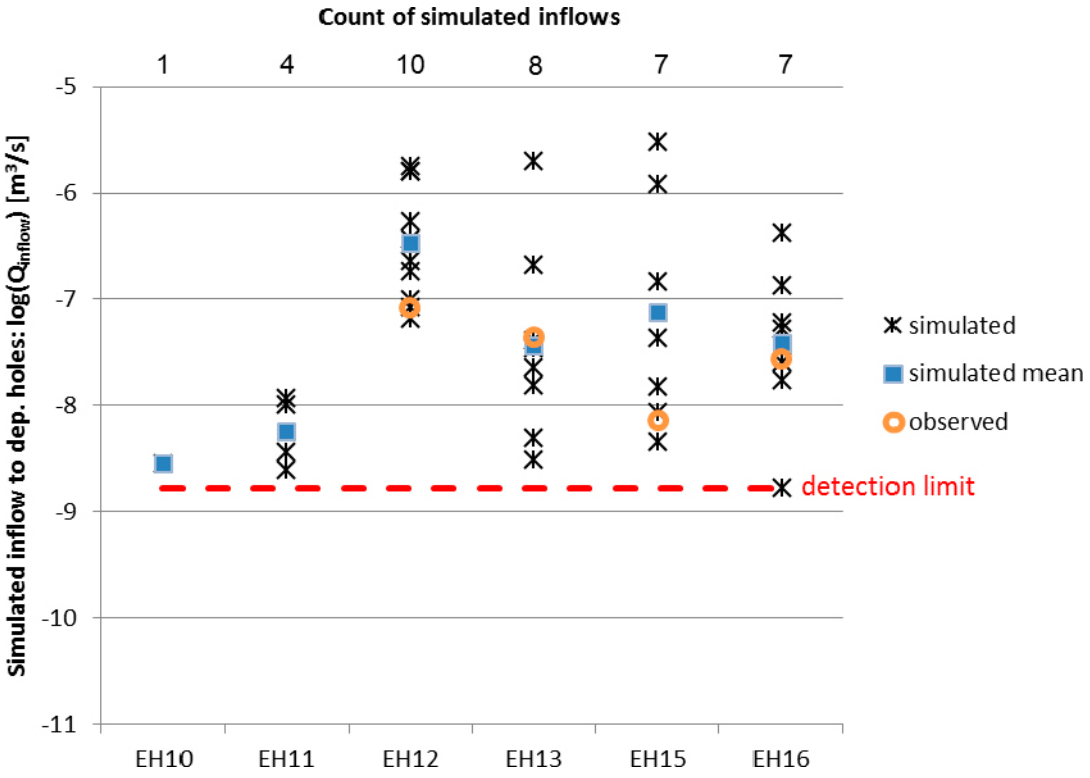

Figure 6-13. *Log inflow simulated for open deposition holes for ten realisations of the conditioned DFN (PHHC-do) on injection tests in pilot holes for deposition holes.*

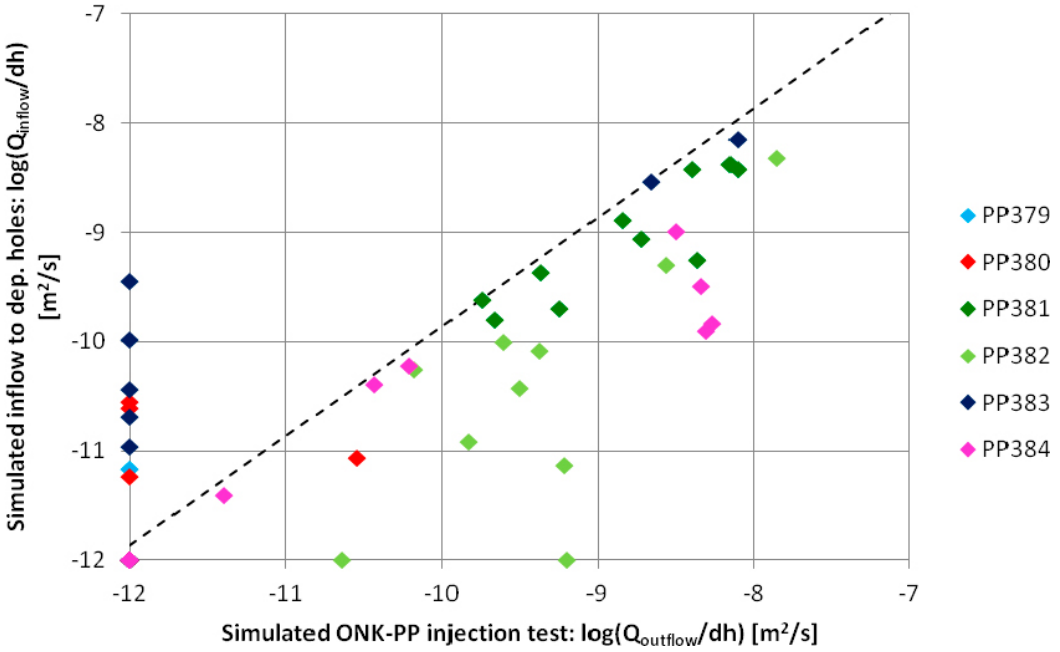

Figure 6-14. *Specific capacity from simulated inflows to open deposition holes (PHHC-do) against corresponding specific capacity simulated from hydraulic injections in the pilot holes for deposition holes (PHHC-pi). Ten realisations of the conditional DFN based on injection tests for pilot holes are shown.*

Here a comparison is made to the unconditioned and geometrically conditioned results, respectively, with the following observed:

1. The majority of simulations correspond to the case where the specific capacities predicted by injection tests overestimate those simulated in open deposition holes. This is consistent with the unconditioned or geometrically conditioned models; although the variability is significantly reduced.
2. From the conditioned models using injection tests, the number of simulations predicting no inflows to the open deposition holes despite pilot hole injection tests identifying non-zero specific capacity is substantially reduced. This scenario is typical of hydraulic "short-circuits", where the pilot holes / deposition holes connect to the tunnels or neighbouring holes. They are filtered out in the case of conditioning on injection tests to pilot holes because the simulated specific capacities in these instances are relatively high, as there is limited resistance to the injection from the fracture network to the nearby underground openings (typically connected by no more than a handful of fractures). However, measurements do not indicate exceptionally large specific capacities, and as such library fractures with such large specific capacities are excluded from the list of potential matches during conditioning.
3. Consistency of specific capacities from simulated injection tests and simulated inflows is much improved after conditioning.

6.2.3 Post-closure flow and transport (PHHC-pc)

In this subsection, simulations of flow rates per unit width (U) around the deposition holes at saturated post-closure conditions are considered (PHHC-pc). Results are comparable to the unconditioned DFN models in Section 5.3 and the geometrically conditioned models in Section 6.1.4.

The variability in predicted flow rates per unit width for the six experimental deposition holes is shown in Figure 6-15 corresponding to ten realisations of the conditioned DFN. The stochastic uncertainty in model predictions is similar to the unconditioned and geometrically conditioned DFN models for holes EH11, EH13 and EH 15, but much reduced for others.

A possible criterion for the acceptance of deposition holes infers the performance of the hole from the specific capacity of the pilot holes drilled for deposition holes (PHHC-pi). Cross-plots comparing post-closure flow with injection tests for ten realisations of the conditioned DFN model are shown in

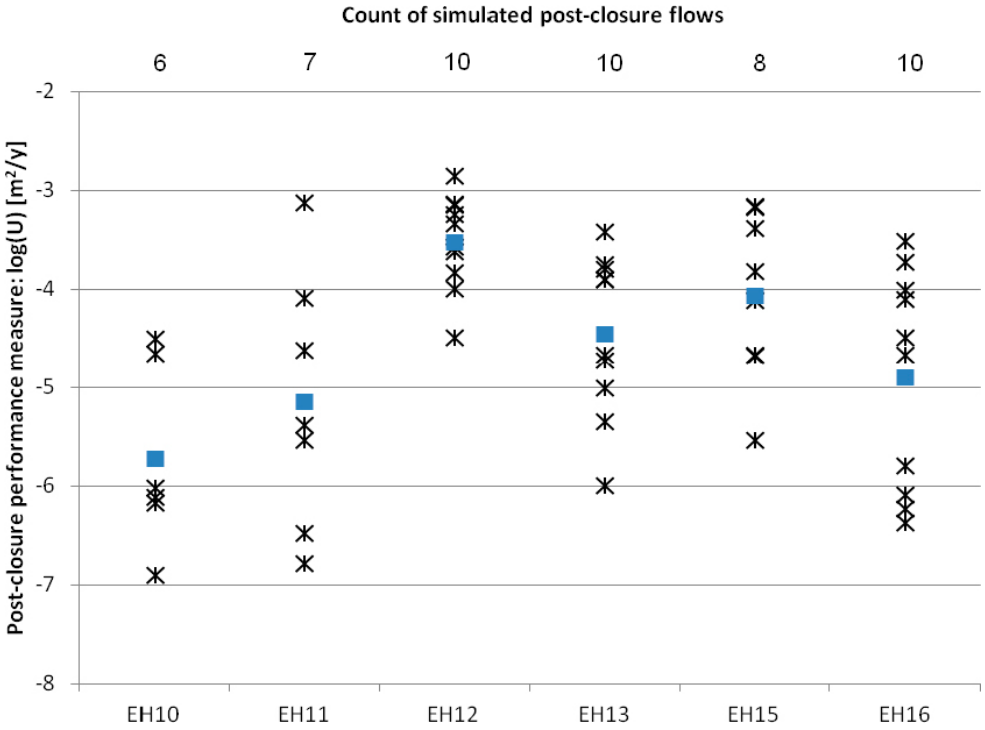

Figure 6-15. *Initial flow rates per unit width (U) simulated for saturated post-closure conditions from ten realisations of the conditional DFN (PHHC-pc) Conditioned DFN are based on injection test data for pilot holes.*

Figure 6-16. The variability in model predictions is reduced when compared with the geometrically conditioned model (Figure 6-10). The match to pilot holes ONK-PP379, ONK-PP380 and ONK-PP383 with flows below detection limit is improved for the majority of realisations, seen as points on the vertical axis of the figure. In contrast, pilot holes ONK-PP381 and ONK-PP382, which record the largest specific capacities during the injection tests, form the bulk of the significant post-closure prediction results.

Cross-plots comparing post-closure flow with inflows to open holes (PHHC-do) for ten realisations of the conditioned DFN model are considered in Figure 6-17. Unlike the unconditioned (Figure 5-8) and geometrically conditioned model (Figure 6-11), when conditioning models based on injection test data is considered, predictions of large post-closure flows ($U > 10^{-4}$ m^2/s) correlating to small simulated inflows (10^{-12} to 10^{-11} m^2/s) to the deposition holes are substantially reduced. Small inflows to deposition holes can be a consequence of either:

1. hydraulic restrictions (bottle-necks) in the fracture network, constraining inflows to the deposition hole, or
2. the open tunnel network significantly disturbing the pressure field local to the deposition hole.

Typically, in the case of point 1 above, the inflows are dominated by the connectivity and hydraulic properties of the wider fracture network; and as such, low inflows caused by poor hydraulic connectivity of the fractures will also yield low initial flow rates at post-closure conditions. In contrast, for point 2, inflows are dominated by the presence of the tunnel at open repository conditions. Hydraulic "short-circuits" in the fracture system connecting the deposition holes and the tunnels result in substantially reduced inflows, although post-closure flows are not necessarily small as backfilled tunnels may still support groundwater flow across the Demonstration Area.[1] However, when conditioning on injection tests to pilot holes, instances of these localised connections between the pilot holes

[1] Identification of these "short-circuits" would require the deposition holes to be packed-off, with reduced build-up of pressures indicating connectivity with the open tunnel system. However, this can only be realised in pilot holes for depostion holes and observed as steady state pressures being much lower than the full hydrostatic pressure

and tunnels are reduced, as subsequent injection test simulations would produce specific capacities significantly greater than those measured during the tests. This is consistent with observations in Section 6.2.2 for comparison of predictions of inflows to deposition holes with simulated injections in the preceding pilot holes.

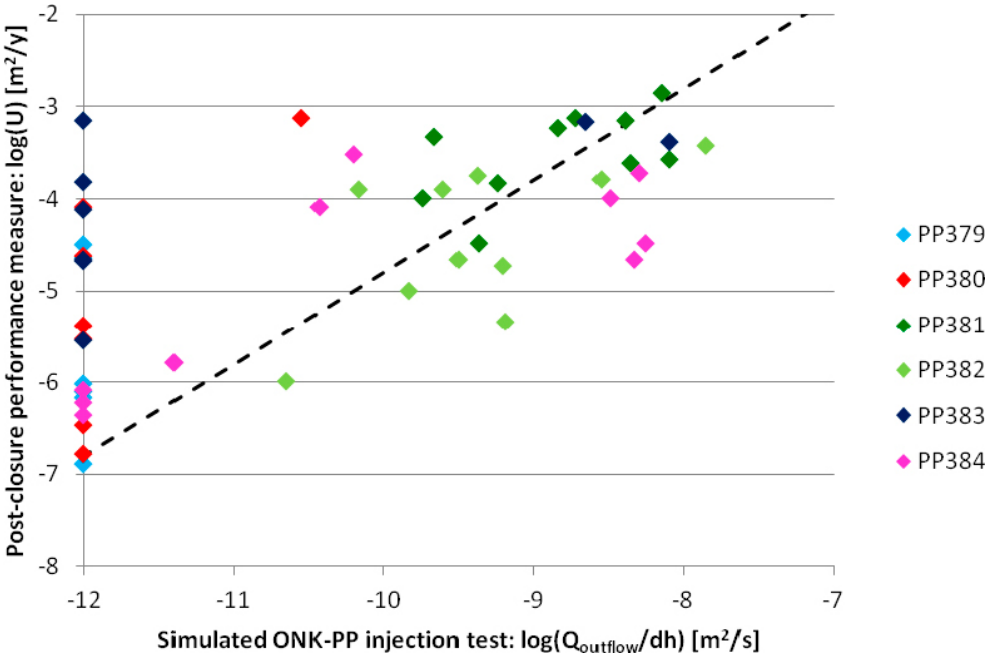

Figure 6-16. *Initial flow rates per unit width (U) at post-closure (PHHC-pc) compared to specific capacity simulated from injection to the pilot holes (PHHC-pi). Ten realisations of the conditional DFN are considered, based on pilot hole injection tests. An equivalence line, based on the pilot hole specific capacity multiplied by post-closure head gradient is also shown.*

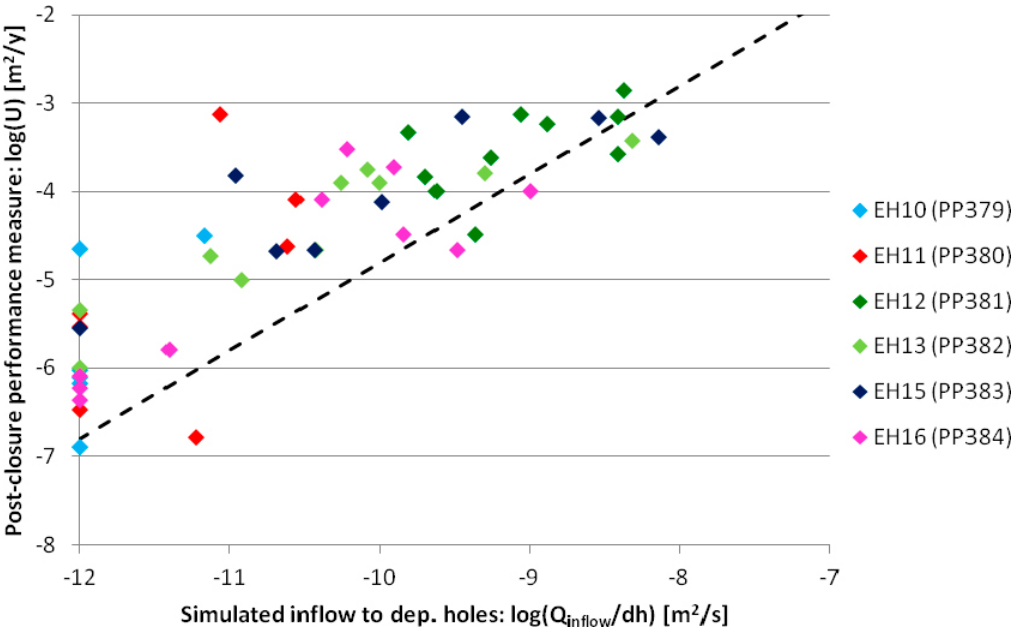

Figure 6-17. *Initial flow rates per unit width (U) for saturated post-closure simulations (PHHC-pc) compared to inflows from simulation of open deposition holes (PHHC-do). Ten realisations of the conditional DFN are considered, based on injection test data for pilot holes.*

Cross-plots of the reciprocal flow-related transport resistances (1/*F)* up to a model domain boundary against injection tests in pilot holes for deposition holes (PHHC-pi); and inflows to open deposition holes (PHHC-do) are shown in Figure 6-18 and Figure 6-19, respectively. A simulated 1/*F* value is mostly below that estimated from both types of the simulated specific capacity. In both cases, a limited correlation between the transport resistance and predicted specific capacity of the hole is observed, offering a slight improvement in correlation when compared to the unconditioned DFN considered in Chapter 5.

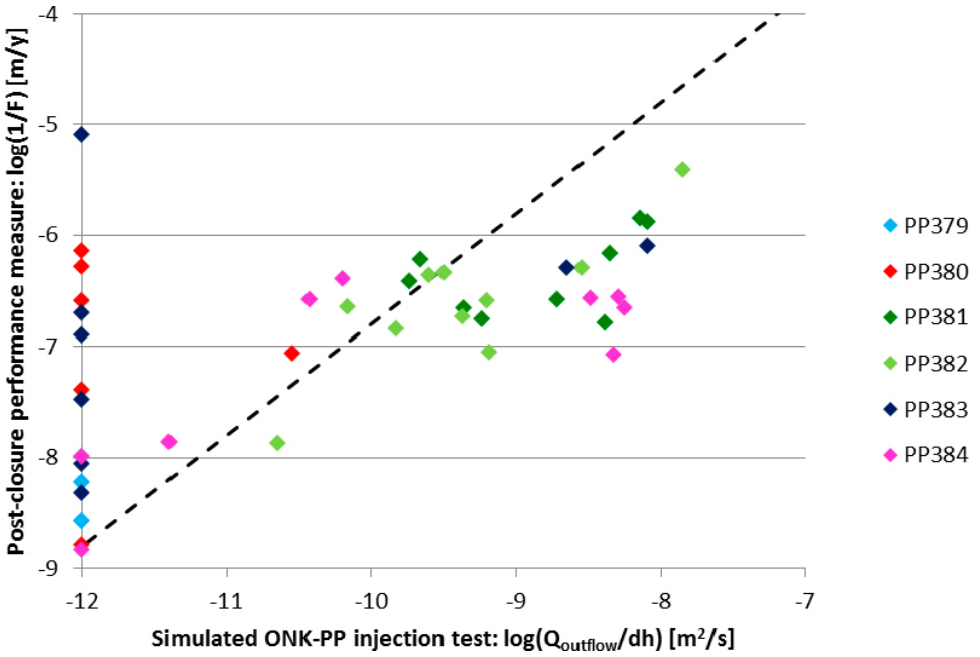

Figure 6-18. *Comparison of reciprocal flow-related transport resistance (1/F) at post-closure (PHHC-pc) with specific capacity simulated from injection to pilot holes (PHHC-pi). Ten realisations of the conditional DFN are considered, based on the injection tests. The dashed line is a simple analytical estimate of 1/F.*

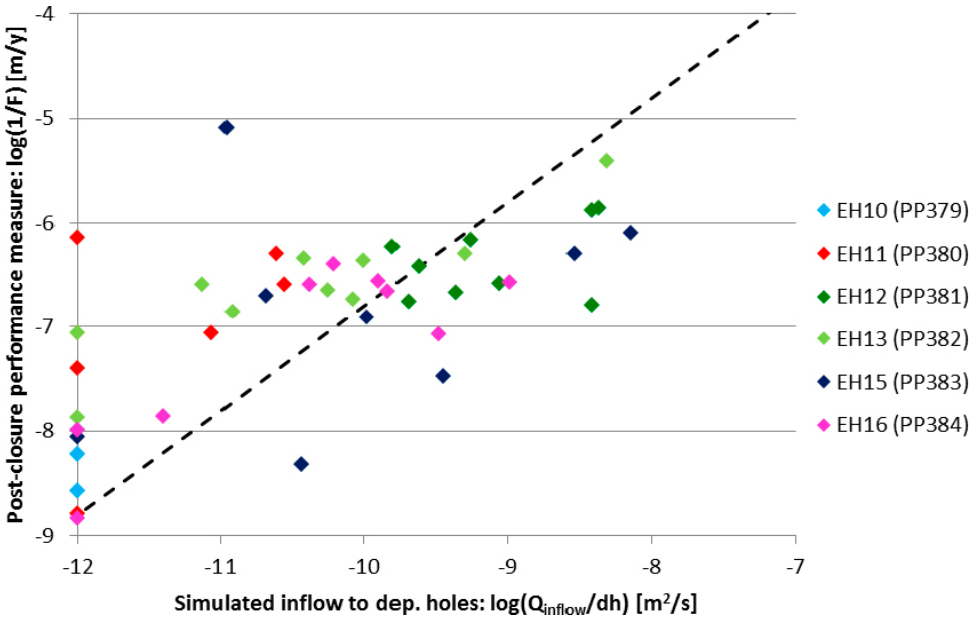

Figure 6-19. *Reciprocal flow-related transport resistance (1/F) for saturated post-closure simulations (PHHC-pc) compared to specific capacity from simulation of open deposition holes (PHHC-do). Ten realisations of the conditional DFN are considered, based on injection test data for pilot holes. The dashed line is a simple analytical estimate of 1/F.*

6.3 Screened hydraulic conditioned DFN on injection tests in pilot holes

To further constrain the DFN, a two-stage approach is considered, generating hundreds of realisations of the PHHC conditioned DFN, and then screening those models based on their predictive capability of the flow tests performed. Applying this methodology, the 'optimal' ten realisations of the conditioned DFN model are selected from the suite of realisations generated, and used to simulate post-closure conditions.

The library of unconditioned DFN realisations generated for injection test conditioning (see Section 6.2) is used here to generate 150 realisations of the hydraulically conditioned DFN based on the injection test in pilot holes. For each of these realisations, injection tests performed sequentially in each of the six short pilot holes for deposition holes in DT2 are simulated (Section 6.3.1). From these 150 realisations, the ten 'optimal' realisations, identified by their consistency with the injection tests, are selected and taken forward for the simulation of the following

- inflows to the six experimental deposition holes of DT2 during open repository conditions (Section 6.3.2), and
- the initial flow rate per unit width at saturated post-closure conditions at deposition hole positions (Section 6.3.3).

In addition, as the largest overhead with regard to simulation time is a consequence of the conditioned library generation; although this screening approach requires the generation of hundreds of realisations of the conditioned DFN, the conditioning process still remains tractable.

6.3.1 Screened injection to pilot holes (PHHC-pi)

In this subsection, simulations consider the sequential injection into the six pilot holes for deposition holes based on conditioned realisations using this injection test data (PHHC-pi). Results are directly comparable to the unconditioned DFN models in Section 5.1 and the geometrically conditioned models in Section 6.1.2. In total, 150 conditioned realisations are used to simulate the pilot hole injections, with the ten 'optimal' realisations selected based on the following criteria for the error E between simulation and measurements:

$$E^2 = \sum_{dep.holes} \left(Log\left(\frac{Q_{outflow}^{measured}}{dh}\right) - Log\left(\frac{Q_{outflow}^{simulated}}{dh}\right) \right)^2 \qquad (6\text{-}1)$$

where

- for the three pilot hole where injection tests failed to measure any outflow, the flow rate, $Q_{outflow}^{measured}$ is set at the detection limit; and
- simulated injections, $Q_{outflow}^{simulated}$ that fall below the detection limit are set to the measurement detection limit.

Based on the error metric defined in Equation (6-1), the ten realisations which minimise E are identified from the suite of 150 conditioned DFN models simulated. These ten realisations correspond to an error $E^2 < 0.5$.

Figure 6-20 illustrates the specific capacities calculated from the simulated injection tests in each of the pilot holes for these ten optimal realisations. For holes ONK-PP379, ONK-PP380 and ONK-PP383 injection tests record no flows above detection limits, and all simulations accurately predict this lack of flow. In contrast, flows are measured in pilot holes ONK-PP381, ONK-PP382 and ONK-PP384 during the *in situ* injection tests; with all simulations predicting outflows to these holes with magnitudes consistent with measurements. For the latter three holes, the stochastic uncertainty of the predicted specific capacities between realisations of the conditioned DFN is around one-order of magnitude, much smaller than the standard PHHC conditional simulations. This reduction in uncertainty is consistent with that expected from the screening process adopted.

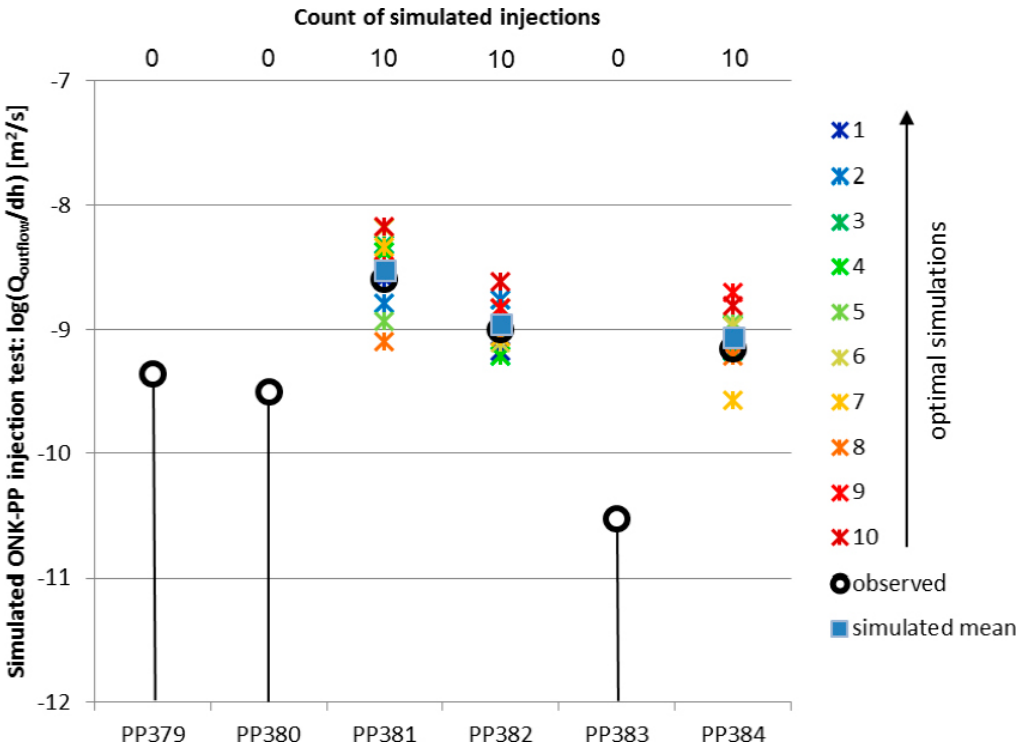

Figure 6-20. *Log specific capacity from simulated injection tests by pilot hole for the ten screened realisations (coloured asterisks) of the conditional DFN (screened PHHC-pi) based on injection test data for pilot holes for deposition holes Geometric mean (blue squares) from simulation and injection test measurements (black circles) are shown. Black lines indicate measurements not being above the detection limit of the tool.*

6.3.2 Inflows to deposition holes (screened PHHC-do)

Simulations of open repository conditions are considered in this subsection, evaluating the inflow to each of the six experimental deposition holes for ten realisations of the conditioned DFN model also screened against sequential injection to the six pilot holes (screened PHHC-do). Inflows to each of the deposition holes (including those simulated below the detection limit), are shown in Figure 6-21, showing only those realisations where the deposition hole is hydraulically connected to the wider network.

When compared to ten realisations of the conditioned DFN model using injection test data (Figure 6-13), the impact of including screening on injection rates to pilot holes reduces the number of simulations predicting inflows to deposition holes for instances where the pilot holes for deposition hole did not record injections. For example simulations predict no inflows to ONK-EH10 and ONK-EH11 where injection tests at pilot hole scale recorded no flow; consistent with the no inflow measurements recorded for these two deposition holes. Likewise, inflows to ONK-EH15 are small and uncertain; and in this instance only two realisations predict inflows to this deposition hole, a consequence of the screening of DFN realisations to injection tests at pilot hole scale (where no flow conditions were measured). For the three remaining holes, screening gives more correct realisations and slightly reduces the uncertainty of inflows to deposition holes compared to the first ten realisations of the conditioned DFN model, as shown in Figure 6-13.

The correlation between the simulated specific capacities from inflows to open deposition holes (screened PHHC-do) against corresponding simulated hydraulic injections in the pilot holes for deposition holes (screened PHHC-pi) are shown in Figure 6-22. Corresponding figures for injection test conditioned DFN models without screening are shown in Figure 6-14. A detailed description of this type of analysis is presented for the unconditioned simulations in Section 5.2. Here, a comparison is made to the unscreened conditional simulations in Section 6.2.2, with the following observed:

1. All but one simulation corresponds to the case where the specific capacities predicted by injection tests over estimate inflows simulated to open deposition holes. This is consistent with the unscreened conditioned simulations.

2. By including screening to the conditioned models using injection tests, the number of simulations predicting no inflows to the open deposition holes despite pilot hole injection tests identifying non-zero specific capacity is substantially reduced. Although conditioning on injection tests to pilot holes provides a mechanism for filtering out some hydraulic "short-circuits" (where the pilot holes / deposition holes connect to the tunnels or neighbouring holes) this process is performed on the simulated specific capacities of the library generated DFN models. By applying a screening phase, additional filtering of hydraulic "short-circuits" is performed by considering the specific capacities simulated on the final conditioned DFN models; therefore taking account of the wider, unconditioned, fracture network.
3. Compared to unscreened models, the consistency of specific capacities from simulated injection tests and simulated inflows is slightly improved.

6.3.3 Post-closure flow and transport (screened PHHC-pc)

In this subsection, simulations of flow rates per unit width (U) around the deposition holes at saturated post-closure conditions are considered for ten realisations of the screened conditional DFN model (PHHC-pc). Results are comparable to the unscreened results presented in Section 6.2.3.

The variability in predicted flow rates per unit width for the six experimental deposition holes is shown in Figure 6-23 corresponding to ten realisations of the conditioned and screened DFN. The stochastic uncertainty in model predictions is similar to the unconditioned and geometrically conditioned DFN models for holes EH12 through EH16, although much reduced for EH10 and EH11. This limited reduction in uncertainty in post-closure flows between realisations of the screened conditional model reflects the residual uncertainty due to changing the flow boundary conditions when considering injection to pilot holes (on which models are screened) compared to fully-saturated post-closure conditions.

A possible criterion for the acceptance of deposition holes infers the performance of the hole from the specific capacity of the pilot holes drilled for deposition holes (PHHC-pi). Cross-plots comparing post-closure flow with injection tests for ten realisations of the screened conditional DFN model are shown in Figure 6-24. The variability in model predictions is reduced when compared to the unscreened models (Figure 6-14). The match to pilot holes ONK-PP381, ONK-PP382 and ONK-PP384 which

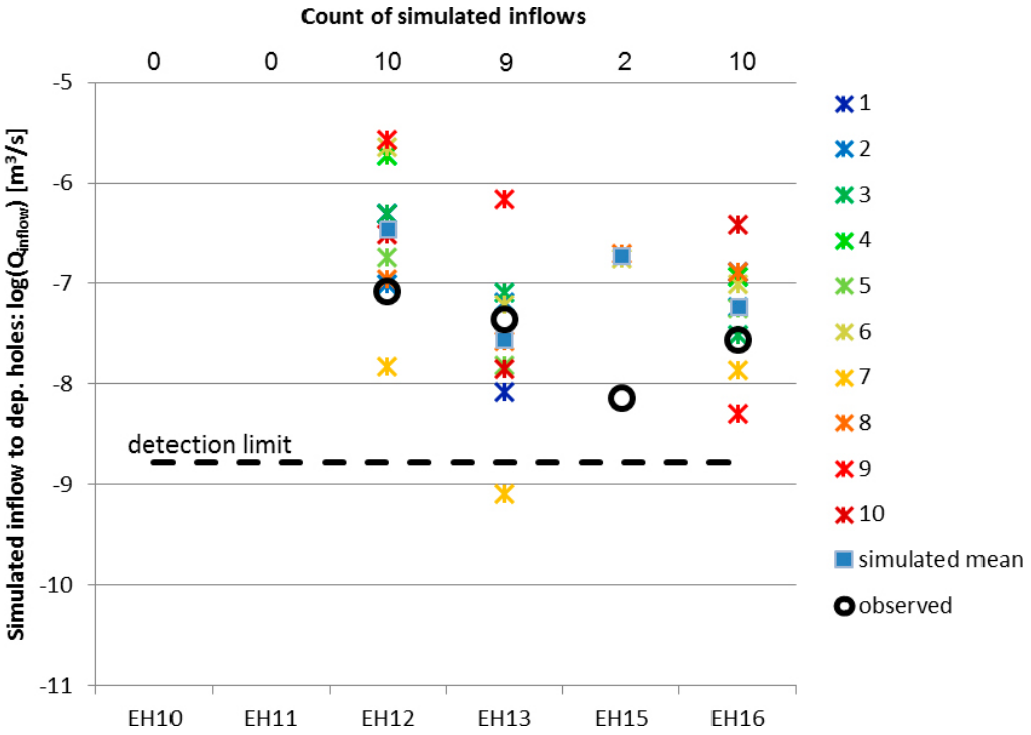

Figure 6-21. *Log inflow simulated for open deposition holes for ten realisations of the screened and conditioned DFN (PHHC-do) on injection tests in pilot holes for deposition holes.*

all record injections at pilot hole scales indicate clustering of post-closure flows. In contrast to the unscreened model, the screened conditioned simulations more accurately reflect the lack of injection to ONK-PP383, although reaming of this hole identifies connectivity to the wider fracture network, seen as points on the vertical axis of the figure.

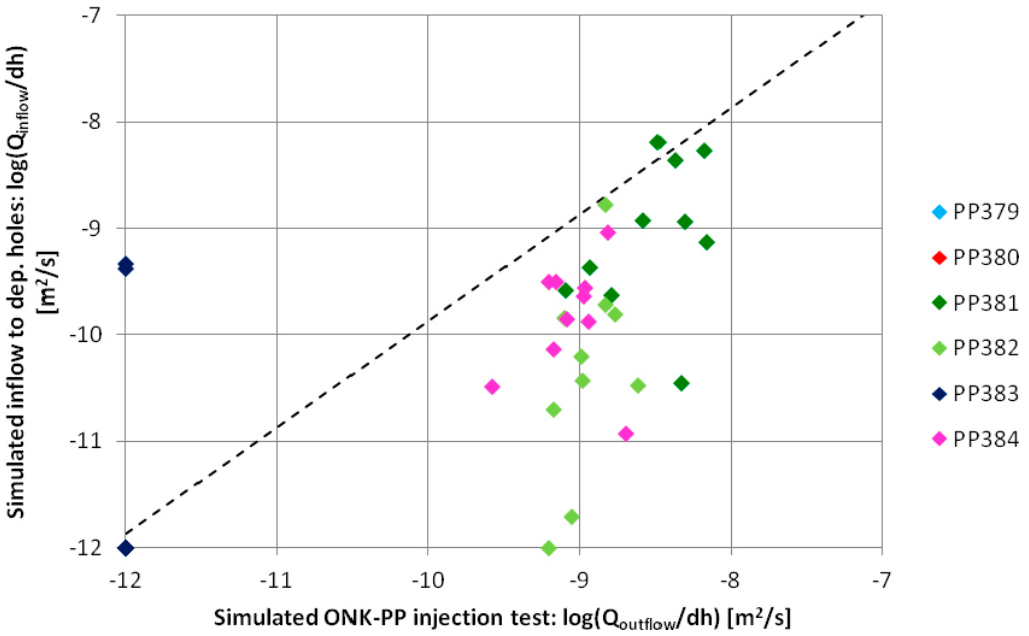

Figure 6-22. *Specific capacity from simulated inflows to open deposition holes (PHHC-do) against corresponding specific capacity simulated from hydraulic injections in the pilot holes for deposition holes (PHHC-pi). Ten realisations of the screened and conditional DFN based on injection tests for pilot holes are shown.*

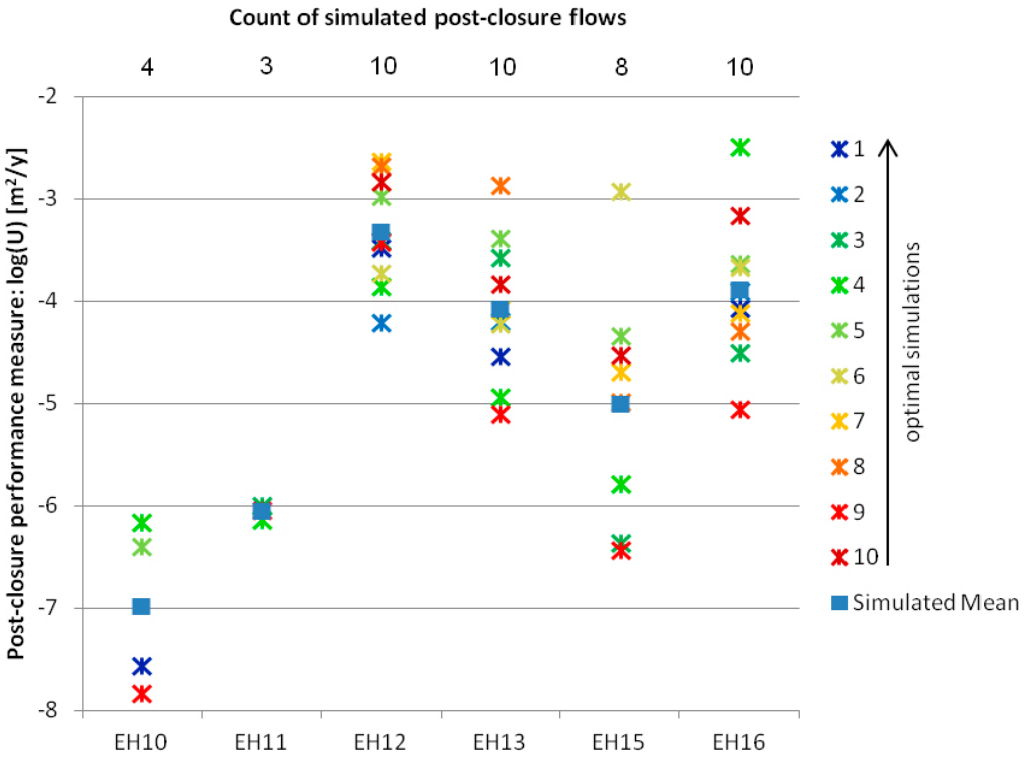

Figure 6-23. *Initial flow rates per unit width (U) simulated for saturated post-closure conditions from ten realisations of the screened and conditioned DFN (PHHC-pc) Conditioned DFN are based on injection test data for pilot holes.*

Cross-plots comparing post-closure flow with inflows to open holes (PHHC-do) for ten realisations of the screened conditional DFN model are considered in Figure 6-25. Similar to the unscreened models (Figure 5-8), when including screening to the conditioned models based on injection test data, predictions of large post-closure flows ($U > 10^{-4}$ m^2/s) occurring for small simulated inflows (i.e. 10^{-12} to 10^{-11} m^2/s) to the deposition holes no longer occur. This is in contrast to the unconditioned simulations (see Figure 5-8).

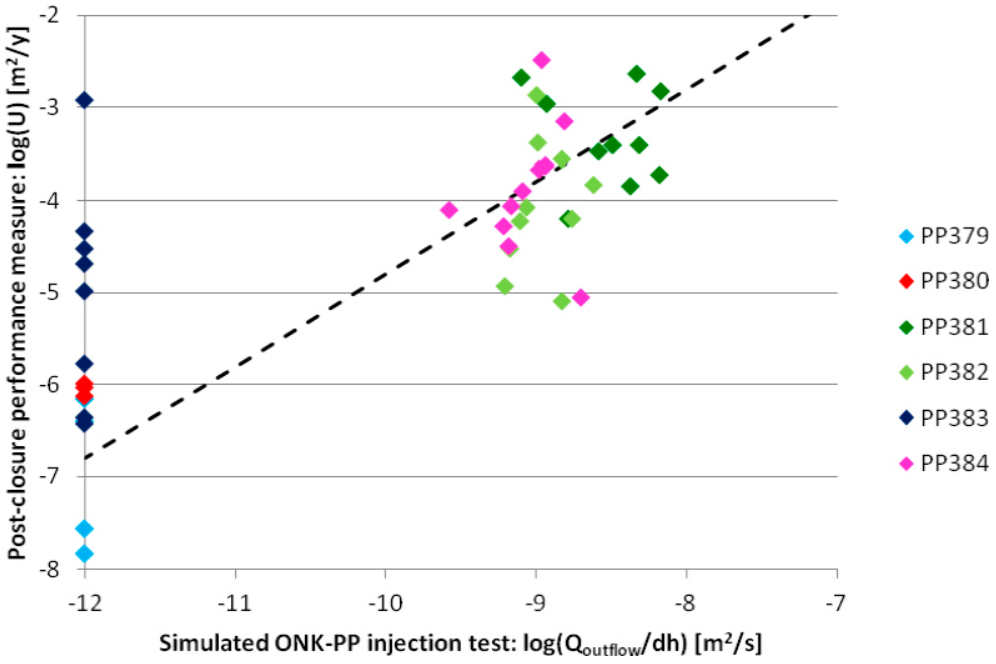

Figure 6-24. *Initial flow rates per unit width (U) at post-closure (PHHC-pc) compared to specific capacity simulated from injection to the pilot holes (PHHC-pi). Ten realisations of the screened and conditioned DFN are considered, based on pilot hole injection tests. An equivalence line, based on the pilot hole specific capacity multiplied by post-closure head gradient is also shown.*

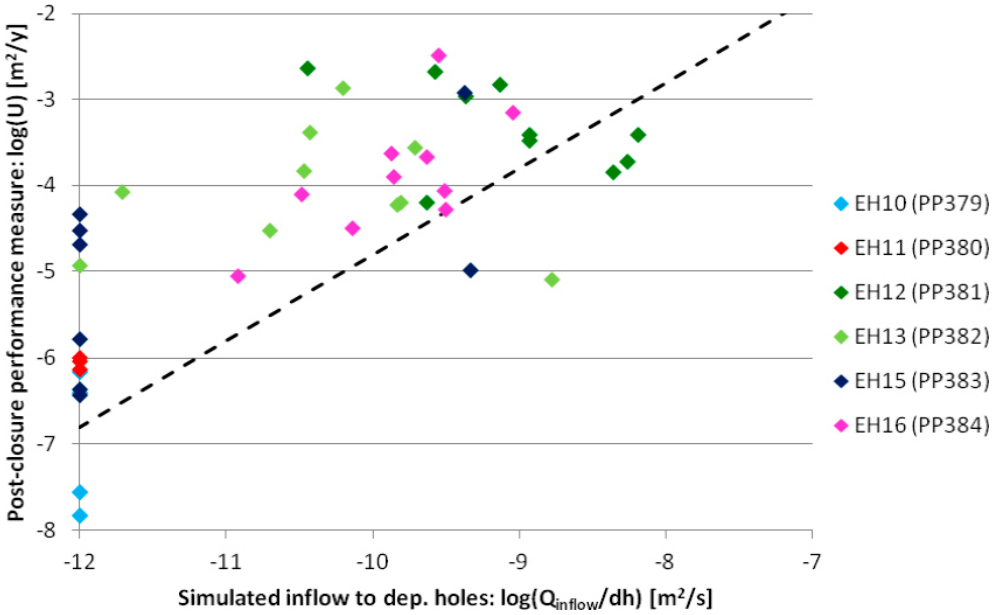

Figure 6-25. *Initial flow rates per unit width (U) for saturated post-closure simulations (PHHC-pc) compared to specific capacity from simulation of open deposition holes (PHHC-do). Ten realisations of the screened and conditioned DFN are considered, based on injection test data for pilot holes. An equivalence line, based on the deposition hole specific capacity multiplied by post-closure head gradient is also shown.*

7 Post-closure flow and transport: conditioned DFN for deposition holes (DH)

In this chapter, suites of ten realisations of DFN conditioned to the following are presented:

- fracture traces mapped along the ONKALO ramp and main access tunnels to the demonstration area,
- fracture traces mapped in the four Demonstration Tunnels (including DT2),
- fracture interpretations within the pilot holes extending beyond DT1 (ONK-PH17) and DT2 (ONK-PH20),
- fracture interpretations within the three pilot holes for deposition holes, drilled in the floor of DT1, and
- fracture traces mapped within the six experimental deposition holes along DT2. Optional also the inflows measured in these holes.

In contrast, the conditioned simulations detailed in Chapter 6 are based on data from pilot holes for deposition holes in DT2 (rather than the deposition hole characterisation used here). For a full review of the available data for conditioning DFN models on the ONKALO Demonstration see Chapter 3. The conditioned models on deposition hole data is denoted 'DH'. Specifically, the consideration of geometric data only is denoted 'DHGC' (see Section 7.1), providing an assessment to the level at which the uncertainty in predictions of inflows to deposition holes can be reduced by conditioning on fracture traces in the hole, and to quantify reduction in uncertainty in post-closure conditions. Conditioning using both geometric and hydraulic data is denoted 'DHHC' (see Section 7.2). A summary of the conditioning data used in this chapter, see Figure 7-1.

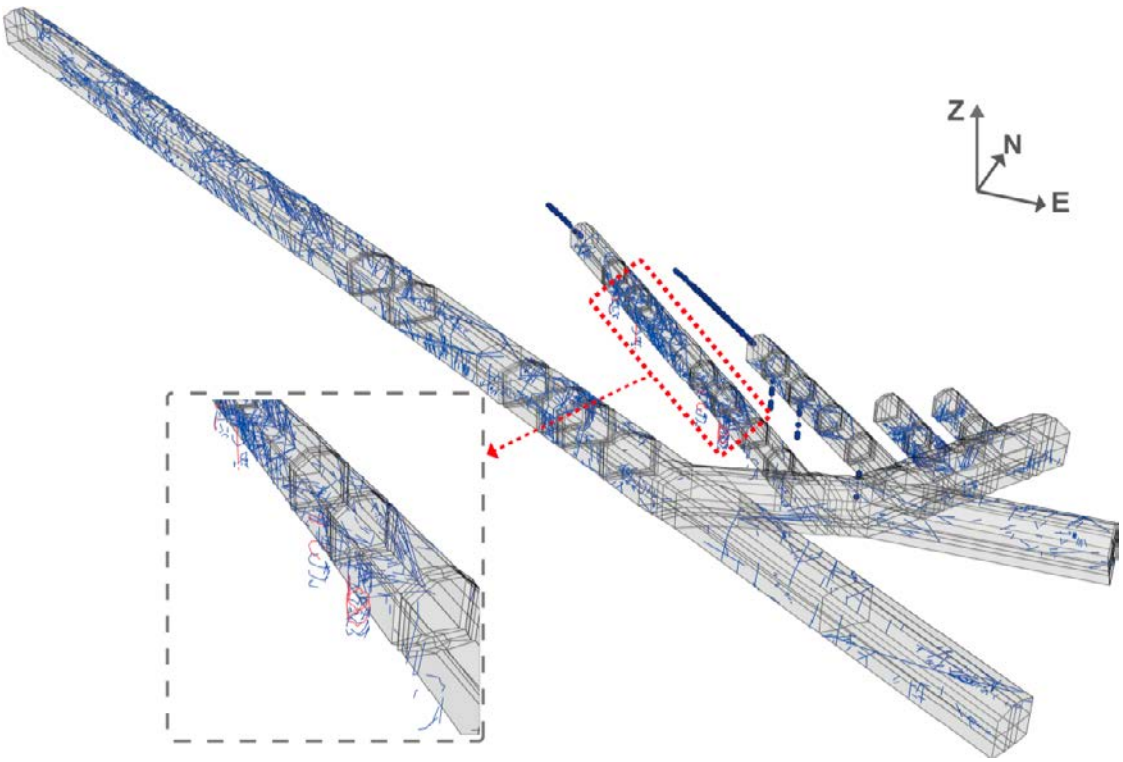

Figure 7-1. *Summary of the data utilised for conditioning of DFN local to the ONKALO Demonstration Area based on deposition holes. Red fracture traces correspond to fracture interpretations assigned flow for conditioning (see Table 3-9).*

7.1 Geometric conditioned DFN of deposition holes (DHGC)

As for geometric conditioning based on data from pilot holes for deposition holes (see Section 6.1), the library generation can be broken down by fracture size, as detailed in Table 6-1, and consists of 33 000 realisations of the unconditioned DFN. The resulting library includes over 31 million distinct fractures corresponding to more than 50 million fracture traces (due to a number of fractures intersecting multiple tunnel structures). Using these libraries, ten realisations of the conditioned DFN are generated, and from them two flow metrics (see Chapter 4) are evaluated, considering:

- inflows to the six experimental deposition holes of DT2 during open repository conditions (Section 7.1.2), and
- the flow rate per unit width local around the deposition hole at saturated post-closure conditions (Section 7.1.3).

In each case, predictions are compared with the unconditioned model simulations (Chapter 5); and the conditioned simulations based on pilot hole for deposition hole data (Chapter 6). Any reduction in modelling uncertainties associated with the conditioned simulations is identified.

7.1.1 Calibration targets

In addition to the flow metrics mentioned above, calibration targets, detailed in Section 4.2, are considered to provide checks that the conditional simulations are working effectively. One of these calibration targets considers the fracture intensity (P_{21}) on the conditioned tunnel surfaces with geological mappings; requiring the conditioned model to accurately reflect the P_{21} of the observed fracture traces mapped on the tunnels of the ONKALO. Note for the geological mappings, the intensity is calculated from the idealised fracture traces corresponding to synthetic tunnel surfaces.

Recall that the acceptance test for the P_{21} calibration target is that the conditioned fracture intensity should be within 5 % of the equivalent value from mapping, and vary by no more than 20 % of the variation of P_{21} between unconditioned realisations (Appleyard et al. 2018). Only the conditioned fractures are considered for the calculation of P_{21}; and as such the variable censoring of the mappings (see Table 3-3) is accounted for. Figure 7-2 illustrates the intensity for all ten realisations of the conditioned DFN, calculated from the intersection of fractures above censoring limits with all underground openings in the ONKALO Demonstration Area.

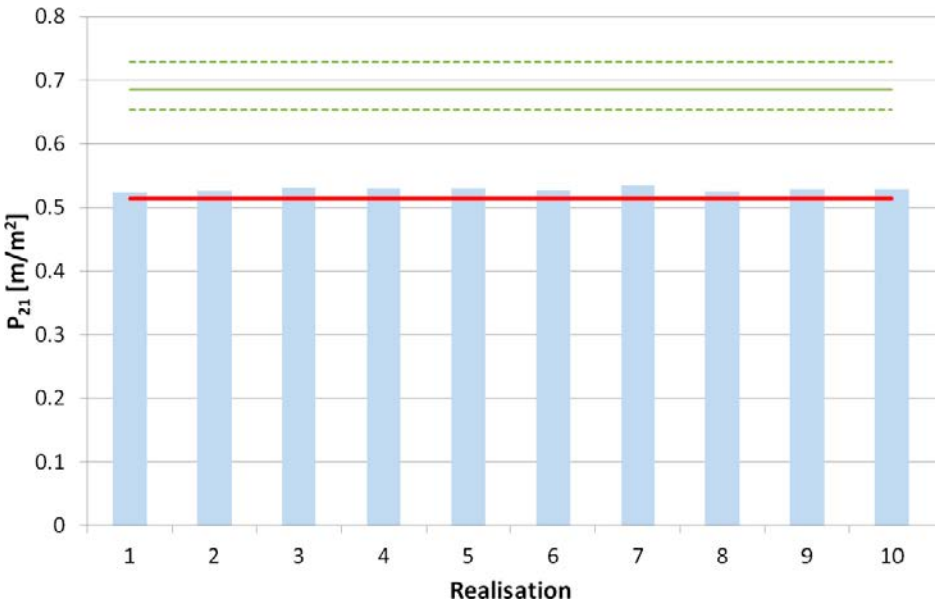

Figure 7-2. *Intensity (P_{21}) for all fracture intersections with underground openings in the ONKALO Demonstration Area. Ten realisations of a conditioned simulation of the tunnels and deposition holes are shown, with the conditioning algorithm only considering geometric properties. Data from the idealised geological mapping are shown in red, with maximum, minimum and mean values from ten realisations of the unconditioned simulations shown in green.*

The fracture intensity, P_{21}, calculated by experimental deposition hole is presented in Figure 7-3 for ten realisations of the conditioned DFN model. Predictions in ONK-EH10 through ONK-EH16 are consistent with the mapping, and the observed relationships between deposition holes are predicted. Specifically, the variability between realisations is substantially reduced when compared with the predictive modelling based on geometric conditional simulations using data from the pilot holes for deposition holes (Figure 6-3).

7.1.2 Inflows to deposition holes (DHGC-do)

The flow metrics for inflow to each of the six experimental deposition holes in DT2 at open repository conditions are reported in this section. Models are geometrically conditioned to deposition holes (DHGC-do) and used to make inflow predictions as shown in Figure 7-4 for ten realisations of the DFN. The following key points are noted:

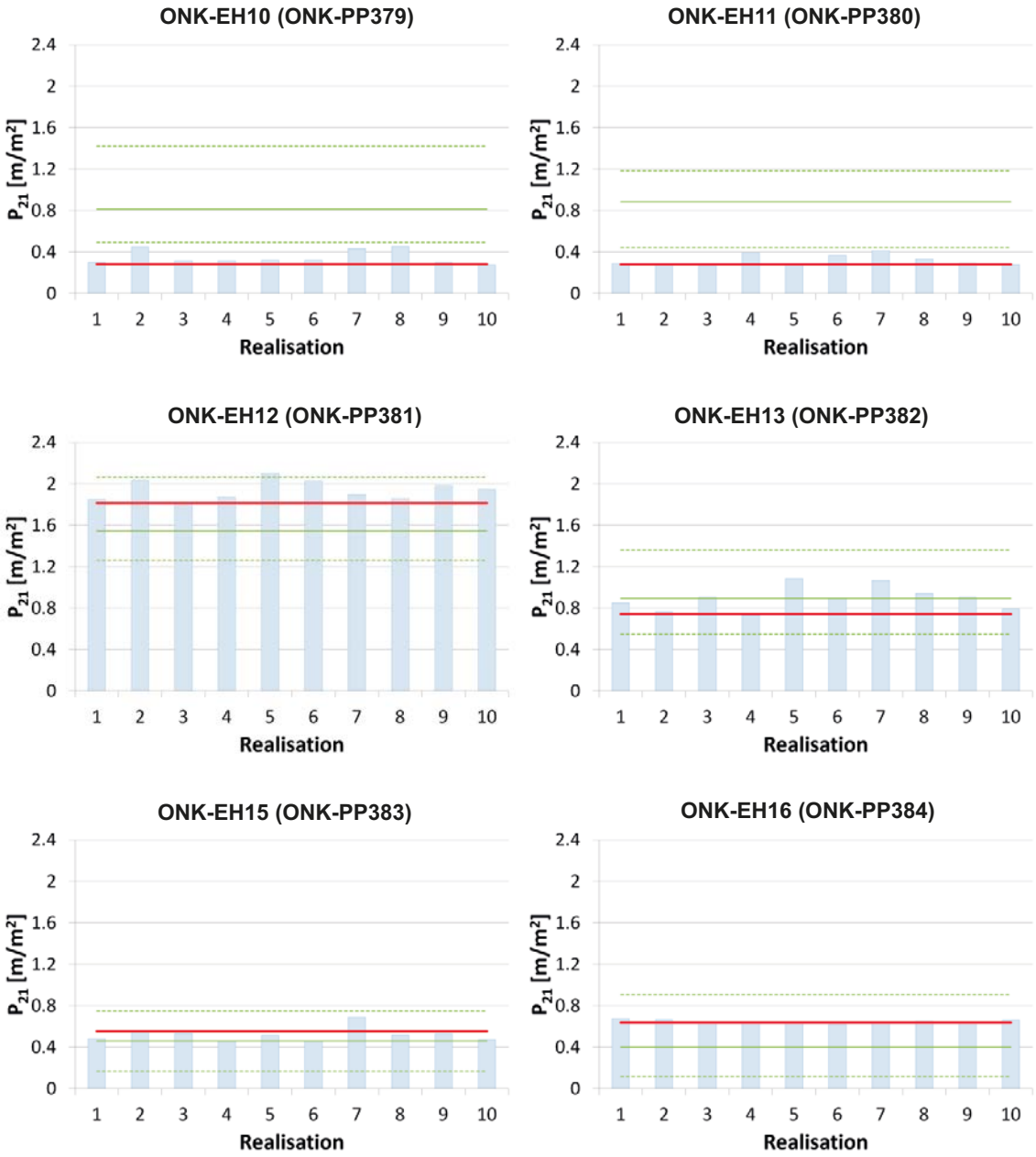

Figure 7-3. *Intensity (P_{21}) for fracture intersections with the six deposition holes of DT2. Ten realisations of a conditioned simulation of the tunnels and deposition holes are shown, with the conditioning algorithm only considering geometric properties. Data from the idealised geological mapping are shown in red, with maximum, minimum and mean values from ten realisations of the unconditioned simulations shown in green.*

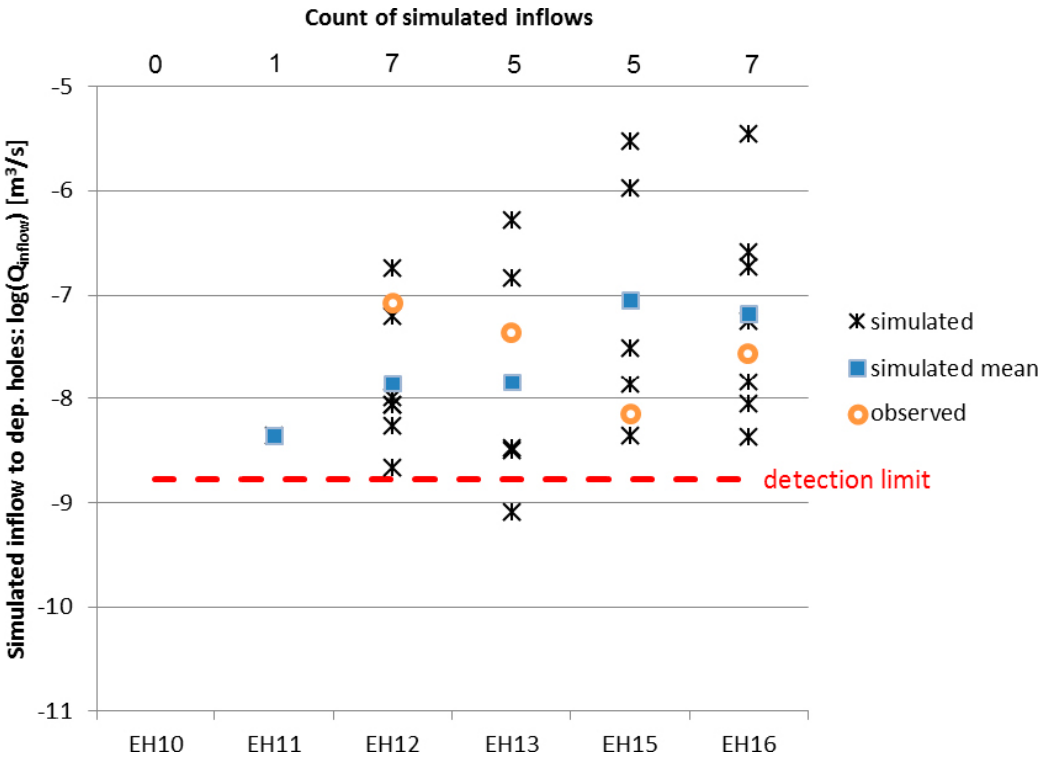

Figure 7-4. *Log inflow simulated for open deposition holes for ten realisations of the conditioned DFN (DHGC-do) based on geometric data for deposition holes. The geometric mean of the simulations (blue squares) are shown, with measured flows (orange circles).*

- Holes ONK-EH10 and ONK-EH11 in DT2 show no inflows above the detection limit. Simulations reflect this lack of flow, with none of the ten realisations predicting flow to ONK-EH10 and only one realisation predicting flow above than the detection limit to ONK-EH11. Conditioning reflects the reduced fracture intensity observed in these two holes, limiting their hydraulic connections to the wider fracture network.
- Inflows are measured in each of the innermost four deposition holes drilled in DT2, with model predictions spanning these measurements.
- The variability in model predictions of inflows to deposition holes between the ten realisations of the conditioned DFN is 2 to 3 orders of magnitude (depending on hole). This uncertainty is slightly reduced compared to those identified for the unconditioned DFN models (Figure 5-2); and the geometrically conditioned model based on pilot holes for deposition holes (Figure 6-7). DFN conditioned to injection in pilot holes (Figure 6-13) indicate similar uncertainty to these models geometrically conditioned to deposition holes; a consequence of the additional hydraulic data (albeit at pilot hole scale) used to condition the models.

7.1.3 Post-closure flow (DHGC-pc)

The metric for the flow rates per unit width (U) around the deposition holes simulated for saturated post-closure conditions are detailed in this subsection. Conditioned DFN models are based on the geometric data for six experimental deposition holes in the floor of DT2 (DHGC-pc), with results comparable to the unconditioned DFN models in Section 5.3 and the conditioned DFN based on pilot holes in Sections 6.1.4 and 6.2.3.

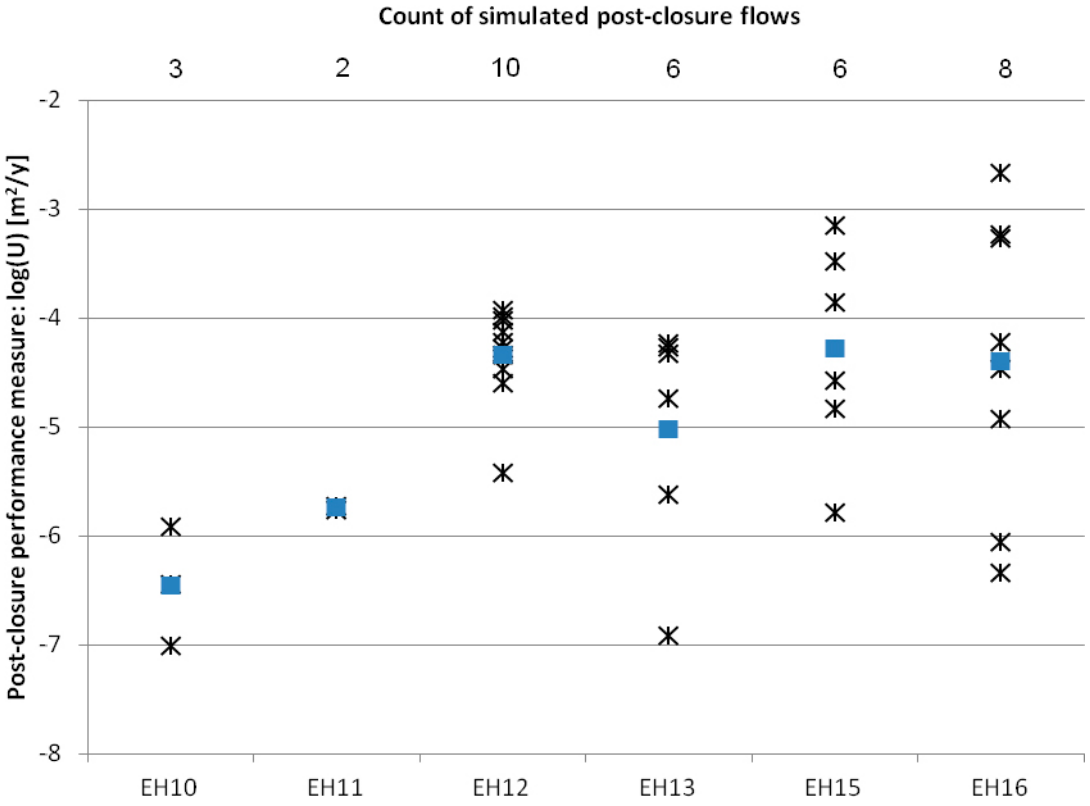

Figure 7-5. *Initial flow rates per unit width (U) simulated for saturated post-closure conditions from ten realisations of the conditioned DFN (DHGC-pc). Conditioned DFN are based on geometry data for deposition holes.*

The variability in predicted flow rates per unit width for the six experimental deposition holes is shown in Figure 7-5 corresponding to ten realisations of the DHGC conditioned DFN. Uncertainty between realisations for a deposition hole ranges from 0 to 4 orders of magnitude; similar to the variability observed in pilot hole conditioned (Figure 6-9) models and slightly reduced when compared to the unconditioned (Figure 5-6) models.

Inflows under open deposition hole conditions provide one possible predictor of post-closure conditions. The simulated post-closure initial flows for ten realisations of the conditioned DFN model (DHGC-pc) are compared to corresponding simulations of inflows to open deposition holes (DHGC-do) as a cross-plot, see Figure 7-6. The key conclusions from these forms of cross-plots are detailed in Chapter 5 for the unconditioned DFN simulations, and the same notes are relevant here. Comparisons to the unconditioned simulations (Figure 5-8) indicate:

- a positive correlation between inflows and the post-closure flows is observed, and
- the number of cases where a deposition hole records zero inflow, but non-zero flow post-closure (i.e. the vertical axis of Figure 7-6) is significantly reduced.

A similar trend is seen as for geometrically conditioned models based on pilot holes for deposition holes (Figure 6-11). The correlation between inflows to open deposition holes and post-closure flows shown in Figure 7-6 is slightly weaker than those observed for conditioned simulations based on the pilot hole injection tests (Figure 6-17).

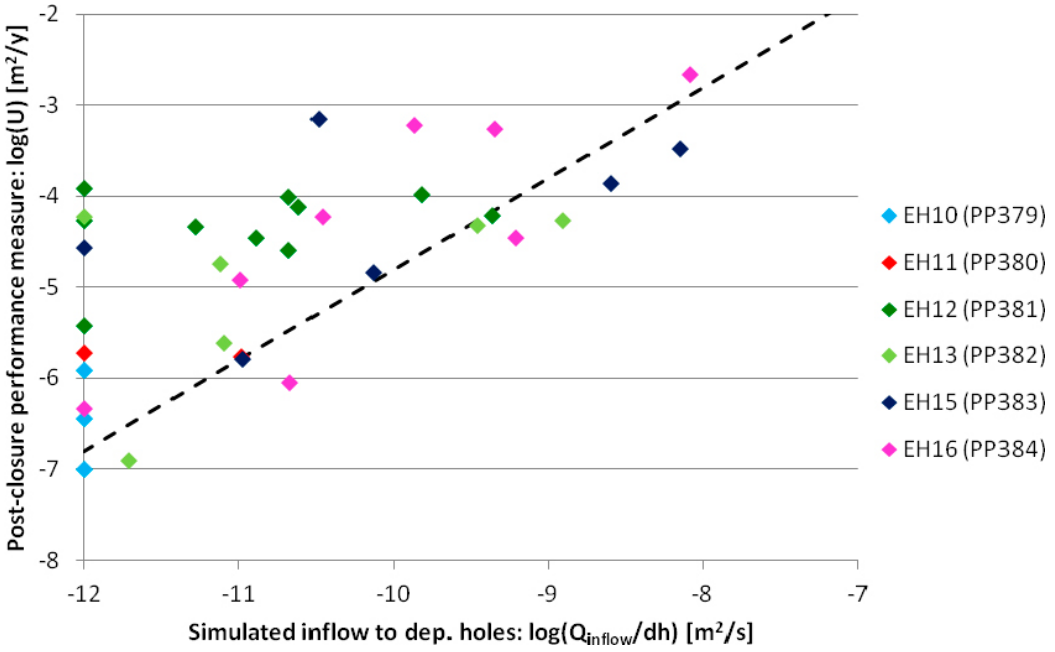

Figure 7-6. *Flow rates per unit width (U) for post-closure conditions (DHGC-pc) compared to specific capacity from simulation of open deposition holes (DHGC-do). Ten realisations of the conditioned DFN based on geometric data for deposition holes.*

7.2 Hydraulic conditioned DFN on inflows to deposition holes (DHHC)

The hydraulic conditioned simulation based on data from deposition hole mapping and associated inflows under open repository conditions (DHHC) is detailed in this section. As for conditioning based on injection tests performed in the pilot hole for deposition holes data (see Section 6.2), the library generation can be broken down by fracture size, as detailed in Table 6-2, and consists of 26 000 realisations of the unconditioned DFN. The resulting library includes over 68 million fracture traces (corresponding to more than 41 million distinct fractures). Using these libraries, ten realisations of the DHHC conditioned DFN are generated, and using these conditioned models, flow metrics for the repository system evaluated, including:

- inflows to the six experimental deposition holes of DT2 during open repository conditions (Section 7.2.1), and
- the initial flow rate per unit width local to the deposition hole at saturated post-closure conditions (Section 7.2.2).

In each case, predictions are compared with the unconditioned model simulations (Chapter 5), the conditioned simulations based on pilot hole for deposition hole data (Chapter 6), and the conditioned simulations based on mapping in deposition holes (Section 7.1). Any reduction in modelling uncertainties associated with the conditioned simulations, as observed across the ten realisations considered, is identified.

7.2.1 Inflows to deposition holes (DHHC-do)

Hydraulic conditioned simulation of inflows to the six open deposition holes, based on inflow measurements (DHHC-do) are detailed in this Section. Model predictions are shown in Figure 7-7 and the following key points noted:

- Inflows are measured in experimental deposition holes ONK-EH12, -EH13, -EH15, and -EH16, with model predictions typically spanning these measurements (the exception being ONK-EH15, where realisations of the conditioned DFN over predict inflow). Experimental deposition holes ONK-EH10 and ONK-EH11 show no measured inflows above the detection limit, and only 2 and 5 of the ten realisations predict inflows to the deposition holes EH10 and EH11, respectively.

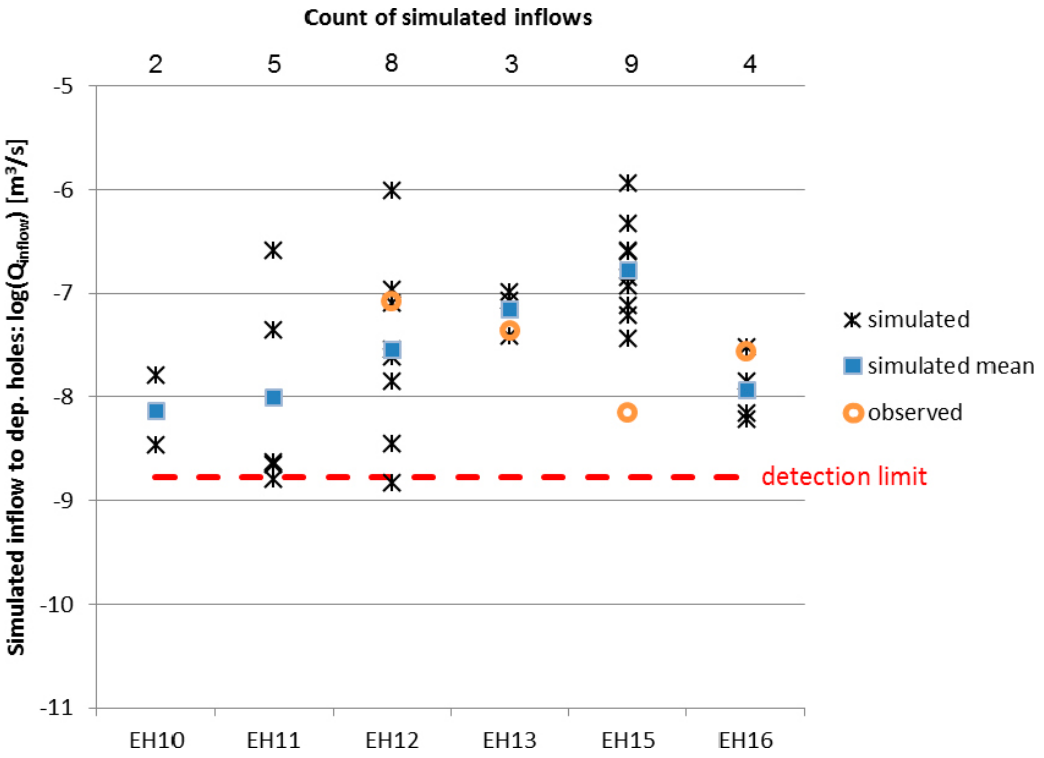

Figure 7-7. *Log inflow simulated for open deposition holes for ten realisations of the conditional DFN (DHHC-do) based on geometric data and inflow measurements for deposition holes. The geometric mean of the simulations (blue squares) are shown, with measured flows (orange circles).*

- The variability in model predictions of inflows to deposition holes between the ten realisations of the conditioned DFN is 2 to 4 orders of magnitude (depending on hole), comparable with the values seen for the unconditioned DFN models (Figure 5-2) and the geometrically conditioned model based on pilot holes for deposition holes (Figure 6-7). The variability is greater than the uncertainties associated with conditioned models of pilot holes for deposition holes based on injection test data (Figure 6-13). This is possibly due to the opposite effects of intersecting underground openings when performing injection and inflow tests: injection tests identifying the maximum flow capacity of the fracture providing the "short-circuit" to the tunnel, whereas inflows are reduced because of fracture connections to other underground openings.
- The variability in model predictions of inflows to deposition holes for the hydraulically conditioned model is similar in magnitude to the geometrically conditioned models (Figure 7-4). However,
  - the prediction of dry experimental deposition holes ONK-EH10 and ONK-EH11 is slightly worse for the DHHC conditioned simulations compared to DHGC models, and
  - the mean inflows predicted for the wet experimental deposition holes (ONK-EH12 – ONK-EH16) are improved in the case of conditioning using the deposition hole inflows information.

7.2.2 Post-closure flow and transport (DHHC-pc)

Simulations of post-closure conditions are detailed in this subsection, with models conditioned on the inflows to the six experimental deposition holes in the floor of DT2 (DHHC-pc). Predictions are directly comparable to simulations based on the unconditioned DFN models (Section 5.3), the geometrically conditioned DFN models based on pilot holes for deposition holes (Section 6.1.4), and the hydraulically conditioned DFN models based on pilot holes for deposition holes (Section 6.2.3). Geometric DFN results can be also compared to simulations using the geometrically conditioned DFN models based on the geometric data for six experimental deposition holes in the floor of DT2, Section 7.1.3.

The variability in predicted flow rates per unit width around the six experimental deposition holes corresponding to ten realisations of the DHHC conditioned DFN is shown in Figure 7-8. Uncertainty between realisations for a given deposition hole is not substantially reduced when compared to other unconditioned and conditioned models.

A cross-plot of the simulated post-closure initial flows for ten realisations of the conditioned DFN model (DHHC-pc) are compared to corresponding simulations of inflows to open deposition holes (DHHC-do), is shown in Figure 7-9.

Similar to the conditioned models based on injection to pilot holes (Figure 6-17), a correlation is observed between the inflows to open deposition holes and the post-closure flows. In contrast, unconditioned DFN models (Figure 5-8) do not indicate such a correlation, a consequence of a number of holes and realisations predicting relatively large post-closure flows ($U \sim 10^{-4}$ m^2/s) despite small inflows (i.e. 10^{-12} to 10^{-11} m^2/s) to the open deposition holes. Recall that small inflows at open repository conditions can be a consequence of either:

1. localised restrictions in the fracture networks capacity (i.e. bottlenecks) to deliver groundwater to the deposition hole; or
2. the open tunnel network significantly disturbing the pressure field local to the deposition hole, affecting the drawdown at the deposition hole and the resulting inflows.

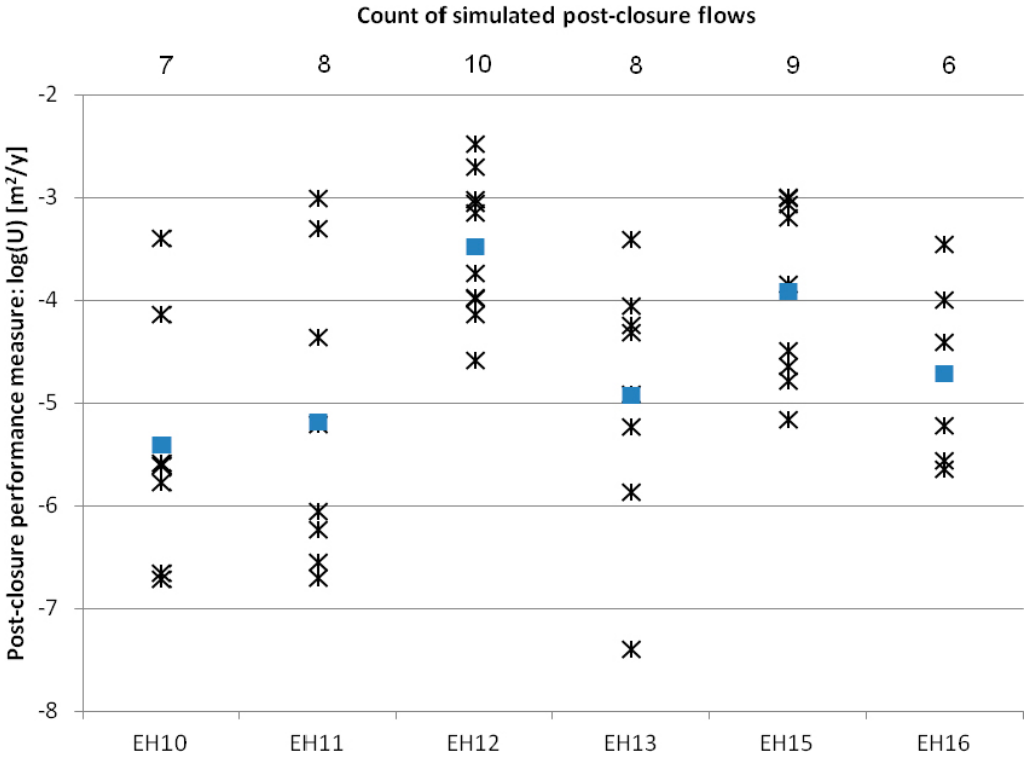

Figure 7-8. *Initial flow rates per unit width (U) simulated for saturated post-closure conditions from ten realisations of the conditional DFN (DHHC-pc). Conditioned DFN are based on geometry and inflow data for deposition holes.*

However, when hydraulic conditioned simulations based on measured inflows to deposition holes are considered, the conditioning process will only select suitable candidate fractures within the library which sufficiently represent the observed flows. For experimental deposition holes ONK-EH12 through ONK-EH16, significant inflows were recorded and assigned to individual fracture traces mapped on the surfaces of each hole (see Section 3.4). In these cases, the conditioning algorithm selects fractures that sufficiently reflect these inflows, which will typically be associated with case 1 above (i.e. flow rates governed by the connectivity and hydraulic properties of the local fracture network). In contrast, holes ONK-EH10 and ONK-EH11 (where flow rates are below detection) are more likely to be associated with case 2 above, and connectivity with other underground openings significantly restricts the potential groundwater ingress to the hole. This also explains the simulations which predict no inflows at open conditions, but non-zero post-closure flow, located on the vertical axis of Figure 7-9. In this instance, predictions could potentially be improved by conditioning DFN models on a data set that also includes fracture specific inflows to the tunnels.

Figure 7-10 illustrates a cross-plot of the reciprocal of flow-related transport resistance ($1/F$) up to the model domain boundary against inflows to open deposition holes (DHHC-do). Similar to hydraulic conditioned simulations based on injection tests to pilot holes (see Section 6.2.3), a correlation between the $1/F$ and predicted specific capacity of the hole is observed. This correlation is particularly evident at high inflows where significant connectivity between the deposition hole and model boundaries exist, corresponding to a lower flow-related transport resistance at post-closure conditions. For more limited inflows (possibly a consequence of shielding due to connectivity with the open tunnels) the background head gradient of the site under post-closure conditions can create flows between connected deposition holes and the tunnel system, with the flow related transport resistance limited by typical properties of the fracture network rather than the effects of local conditioning. In addition, for each deposition hole, the variability of predictions between realisations of the DFN is substantially reduced when compared to both unconditioned (Figure 5-10) and hydraulic conditioned simulations based on injection to pilot holes (Figure 6-18). The effect is similar (although not as strong) to that for the correlation between $1/F$ and the predicted specific capacity for hydraulically conditioned DFN models based in injection tests shown in Figure 6-19.

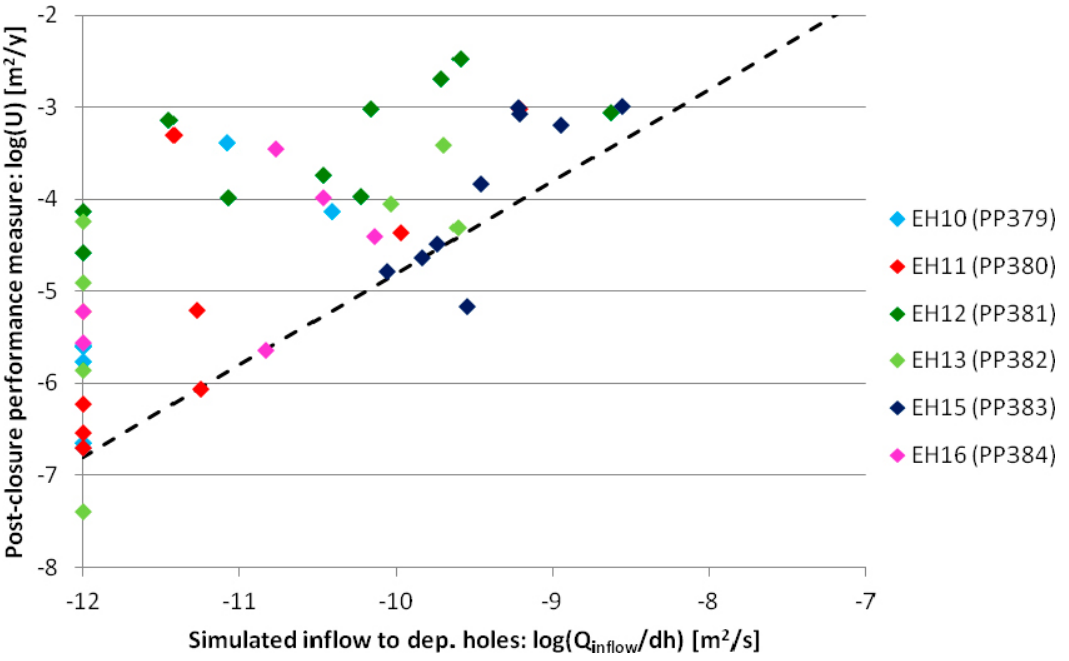

Figure 7-9. *Initial flow rates per unit width (U) at post-closure (DHHC-pc) compared to the specific capacity of open deposition holes. Ten realisations of the conditional DFN are shown, based on fracture trace mappings and inflows to the deposition holes.*

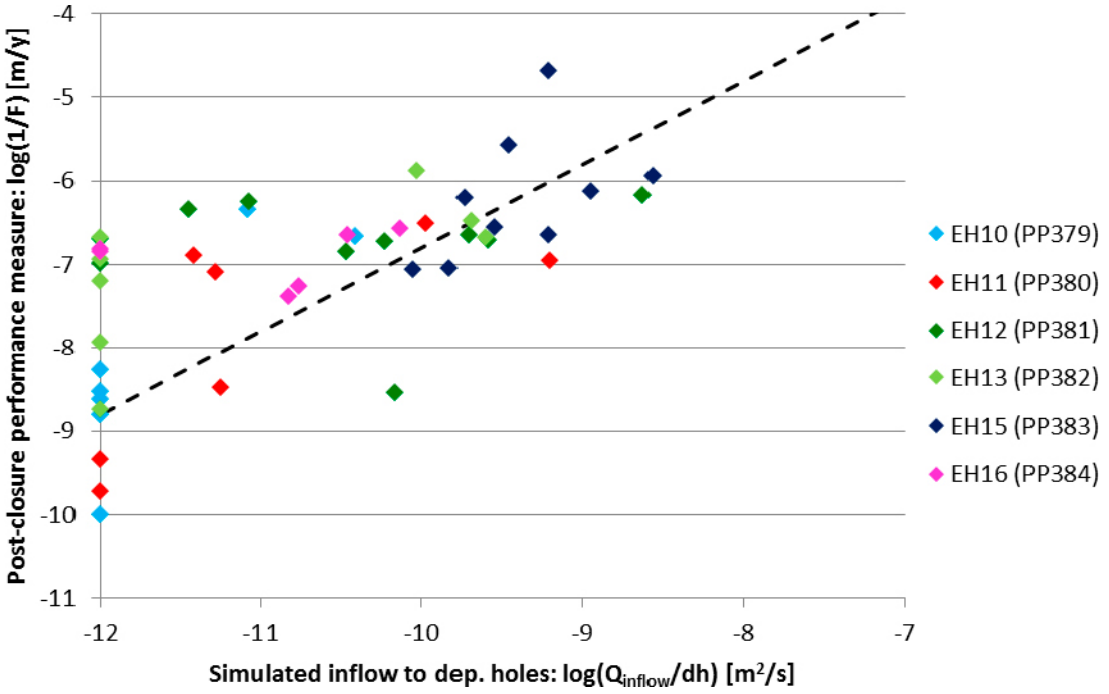

Figure 7-10. *Reciprocal flow-related transport resistance (1/F) for saturated post-closure simulations (DHHC-pc) compared to specific capacity from simulation of open deposition holes (DHHC-do). Ten realisations of the conditional DFN are considered, based on geometric data and inflow measurements for deposition holes. The dashed line is a simple analytical estimate of 1/F.*

8 Conclusions

This study is tasked with exploring how well DFN models of the ONKALO Demonstration Area can predict important flow and transport properties at six experimental deposition holes beneath DT2 under different boundary conditions. These predictions are of importance in developing practical rock suitability and deposition hole acceptance criteria, and also as a validation of the reliability of the current DFN (DADFN) model for predicting measurable geometric and hydraulic fracture properties on the scale of individual deposition hole locations.

In addition, how the uncertainties in these predictions can be reduced by conditioning probabilistic simulations on different types of structural mapping data and hydraulic measurements are considered. Conditioning on data gathered at different times during the construction of the Demonstration Area and deposition holes provides a means for extrapolation of fractures and their properties away from observation points in tunnels, deposition hole pilot holes and deposition holes whilst honouring the underlying conceptual and statistical models for fracture properties. In total, five DFN models are considered: one without local conditioning; and four forms of conditioned DFN using local data (both structural and hydraulic conditioning based on data from pilot holes for deposition holes or the reamed deposition holes themselves). Through this suite of models various comparisons are performed to assess several key questions toward defining effective acceptance criteria for deposition holes:

- With what certainty do the probabilistic unconditioned realisations predict the measured distributions of injection rates in pilot holes and inflows to deposition holes?
- To what extent and how reliable are simulated predictions of the hydraulic measurements at open repository conditions constrained by local conditioning of different types of structural and hydraulic information?
- By how much are predictions of the post-closure flows and transport resistance constrained by local conditioning of different types of structural and hydraulic information?
- To what degree are different types of flow measurements (injection tests vs. inflows) correlated with simulated future post-closure flows and flow-related transport resistance, and how are these correlations affected by conditioning?

The predictive capabilities of the model are summarised in Table 1-1, comparing the effects of each of the four stages of conditioning based on pilot holes for deposition holes and deposition holes themselves. Six of these model simulations involve predicting measurements without prior knowledge being used in the model conceptualisation or parameterisation, and therefore represent an assessment of model reliability in answer to the first two bulleted questions above, i.e. model validation.

8.1 Validation of fracture statistical model using unconditioned DFN

The unconditioned DFN provides a basis for baseline validation of the developed DADFN model (Hartley et al. 2017) in making predictions of injection tests in pilot holes and inflows to open deposition holes with comparisons with measured *in situ* data. It also provides a basis for examining correlations between different measured and post-closure flow properties.

From simulation of ten realisations of the unconditioned DFN model the following is observed:

- Simulations make predictions (without prior knowledge of the measured outcomes) of the P_{21} on the demonstration area tunnel surfaces and in the deposition holes that display many of the trends seen in the mapping data, i.e. areas of low intensity some domains/lithologies and high close to BFZ. For the unconditioned DFN, this provides a baseline validation of the spatial variability of fracture intensity incorporated into the DADFN model description.

- The magnitudes of specific capacities as measured in situ by single hole injection tests are correctly predicted, and the predicted geometric means for individual pilot holes are surprisingly consistent with differences seen in the measurements. This is considered to be a demonstration that systematic trends in interpreted statistics according to ductile domain lithology and proximity to deterministically modelled BFZs included within the DADFN model are producing resulting biases in the predicted statistics consistent with those prevailing in the measured pilot hole tests.
- The pilot holes with specific capacities below the detection limit are correctly predicted due to the spatial constraints on fracture intensity mentioned above.
- For those pilot holes with measurable specific capacity, predictions span the in situ measurements, have mean within half an order of magnitude of that of the measured data and vary typically within about 2 orders of magnitude.
- Similar conclusions can be made regarding the predictions of the measured inflows to the deposition holes. The respective predictions of the geometric mean inflow are close to those of the measurements, and again span the measurements varying by two orders of magnitude.
- Correlation of injection rates predicted at the pilot hole scale with inflows to the experimental deposition holes identifies that:
  - Virtually all simulated specific capacities for pilot hole injection tests exceed those simulated from inflows to the corresponding open deposition hole. This is a consequence of the nature of the respective flow measurement, with injection tests identifying the maximum flow capacity of the fracture network local to the hole, whereas inflows to the open hole can be reduced by other underground openings providing easier outlets for fracture flow at lower resistance.
  - Some deposition holes record no inflow above the detection limit, whereas injectivity into fractures from pilot holes is predicted to be achieved when simulating such tests. This is a consequence of local differences in connections between pilot hole / deposition hole and neighbouring underground openings, respectively. At open repository conditions, no flow will occur between these openings, whereas injection to the pilot hole is feasible (the injected water will flow to the neighbouring tunnel / hole).
  - Some deposition hole specific capacities calculated from inflows to the open hole are in excess of those predicted from injection tests. This is a consequence of the deposition holes, reamed from preceding pilot holes, intersecting additional open fractures, hence providing new hydraulic connections to the hole.
- Predicted post-closure flows for each deposition hole vary by three to four orders of magnitude. There are only weak correlations between post-closure flow conditions and the predicted open repository flow measures (injection or inflows). Simulated post-closure flows nearly all fall below estimates based on specific capacity from injection tests, as this indicates a maximum potential value if there are no hydraulic choke effects resulting from the sparse and heterogeneous fracture network (i.e. a conservative predictor). In contrast, estimates of post-closure flow based on specific capacity derived from inflow measurement span the simulated values.
- For the ten realisations considered, similar interpretations hold for the reciprocal of flow-related transport resistance. The predictions of F using measured specific capacities from injection tests tend to under predict the simulated value, while inflows based estimates tend to span the simulated transport resistance.

In summary, the conceptual model for the Demonstration Area as implemented in the DADFN model offers acceptable predictions for both geometric and hydraulic properties, although the degree of reliability of predictions on the scale of deposition hole in proximity to BFZs is strongly dependent on the modelling of the geometry and damage zone of those structures. Figure 6-3 illustrates a number of the issues. P_{21} is well predicted by unconditioned and conditioned models for experimental deposition holes EH12, EH13 and EH16 despite being close to BFZs, implying the damage zones around those BFZs are well described in the DFN input data. P_{21} in deposition holes EH10 and EH11

is over-predicted by unconditioned models, suggesting these holes are located in an atypical unfractured volume, which is improved by conditioning on the DT2 tunnel trace data above. Deposition hole EH15 is well predicted by unconditioned simulation, despite being close to two BFZs, but the conditioning results in over-prediction, implying that the associated damage zone, as seen in the DT2 tunnel, is perhaps atypical of the general description of these zones and the rock beneath the tunnel. For inflows, the predictions based on the unconditioned realisations (see Figure 5-2) are considered acceptable as they predict geometric means within half an order of magnitude of the measurements; deposition holes EH13 and EH15 stands out though, as they are producing very uncertain predictions, being on the fringe of BFZs. With conditioning (e.g. Figure 6-21) the extra data provide more certainty in the prediction of EH13 and EH15, although EH15 has two outlying realisations predicting flows an order of magnitude above the measurement.

8.2 Conditioning on pilot hole mapping and injection tests

The conditioned simulations based on fracture logs of the pilot holes for deposition holes (PHGC) provide verification that the uncertainly in predictions of flows around individual pilot holes and subsequent deposition holes are reduced when compared to the unconditioned (UC) models. When including the information from simulated injection tests in the pilot holes, simulations also quantify how well local conditioning constrains prediction of these injection tests. In addition, comparison between geometric conditioning alone and conditioning including additional hydraulic injection test data, provides further understanding on the effects of the provided conditioning constraints on flow metrics and post-closure conditions. From simulation of ten realisations of each type of conditioned DFN it is found that:

- Geometrical conditioning (PHGC) reduced the uncertainty in predicted specific capacities of injection tests for each of the pilot holes for deposition holes by an order of magnitude compared with the unconditioned model, with a noted maximum variability of three orders of magnitude in any given hole. Inclusion of injection test data (PHHC) in constraining local fracture properties was shown to constrain predictions of network injection flow rates to just two orders of magnitude variability in any given pilot hole. In the case of PHHC conditioned models, despite selecting fractures from the conditioning library that adequately represent the injection tests, once these fractures are included in the conditioned DFN realisation, differences in their connectivity to the wider fracture network results in a range of predicted injection rates spanning the measurements.
- When simulating inflows to open deposition holes, the geometrically conditioned pilot hole model (PHGC) was not found to reduce the uncertainty in model predictions. In contrast, conditioning also on the injection tests (PHHC) reduced the variability in predicted inflows by around one order of magnitude. The predicted injection test specific capacities at the pilot hole scale was shown to often correlate with the inflows to the experimental deposition holes, with this correlation being stronger for the hydraulically conditioned models. For both PHGC and PHHC conditioned simulations, the correlation was more significant than for the unconditioned simulations.
- Predictions of post-closure flow rates around the deposition holes for DFN models conditioned on the pilot hole injection tests provide a reduction in the uncertainty when compared with unconditioned models. This includes correctly predicting those holes likely to have low or zero post-closure flow. In addition, correlations between simulated post-closure flows and specific capacities from either pilot hole injection tests or deposition hole inflows were found to be more significant for the hydraulically conditioned DFN models than the geometrically conditioned DFN models.
- For the limited number of realisations considered, better correlations between the reciprocal of flow-related transport resistance, 1/F, and specific capacities were also found for conditioned than for unconditioned DFN models.

It is noted that although the ten realisations of the given conditioned DFN provide an illustrative study of the stochastic uncertainty of the models; it is unlikely with such few realisations that one particular DFN model will provide adequate prediction of any given flow measurement (injection to pilot holes or inflows to open deposition holes). To further constrain the DFN, a two-stage approach was considered for the conditional models based on injection to pilot holes for deposition holes. This considered 150 realisations of the conditioned DFN, and then screened those models based on their predictive capability of the injection tests performed as a means to screen realisations of the unknown background network. Applying this methodology, allows selection of the 'optimal' ten realisations of the conditioned DFN model from the suite of realisations generated, which could then be used to simulate post-closure conditions. Because the largest overhead with regard to simulation time is a consequence of the conditioned library generation, this screening approach remains tractable even though it involves the generation of hundreds of realisations of the conditioned DFN. Applying the model to the hydraulically conditioned pilot hole simulations (PHHC) showed significant improvement in constraining the specific capacities simulated for injection as well as moderately reducing uncertainty in the predictions of inflows. However, the screened PHHC simulations did not indicate significant improvement in their predictive capability flow and transport at post-closure conditions. This would suggest there is a residual uncertainty arising from a lack of knowledge about how the fractures seen measured in the deposition hole connect with nearby openings or the wider network. This uncertainty might be reduced by consideration of additional information that has the potential to discern such effects, i.e. applying more constraints on the models. This could involve the use of the following in the conditioning process

- pressures prior to injection to determine if fractures have been dewatered by excavations,
- transient pressure evolution during injection to detect fixed pressure boundaries or finite flow compartments,
- PFL-based specific capacities under pumping eliminate fractures connections to the tunnel above and finite flow compartments, and
- tunnel inflow data to condition fractures providing easier outlets, and thereby improve the simulation of inflows to deposition holes.

8.3 Conditioning on deposition hole mapping and inflows

The conditioned simulations based on fracture trace mapping within the deposition holes (DHGC) provide verification that the uncertainly in predictions of inflows to deposition holes are reduced when compared to the unconditioned (UC) models. When including the inflow measurements in the conditioned simulations (DHHC), models quantify the capability of local conditioning to constrain prediction of these open hole flows. In addition, both suites of conditioned DFNs provide an added understanding of the nature of reduction in uncertainty and improvement in correlations between the measurable inflows at open repository conditions and post-closure flow conditions. From simulation of ten realisations each of the DFN models conditioned on deposition hole information the following was observed:

- Conditioning on deposition hole traces and inflows generally only increases the number of realisations that predict inflows of broadly the correct order of magnitude, and correctly predicts those holes with no or very low flows.
- Only minor reduction in the variability in predicted post-closure flows between realisations of the conditional DFN (DHGC & DHHC) are observed when compared with the unconditioned models. However, predictions of inflows to open deposition holes were found to correlate well to simulated post-closure flow conditions, with a stronger correlation observed when conditioning to hydraulic and geometric data than to geometric data alone. This is consistent with observations made in conjunction with pilot hole conditioning and stands in contrast to the unconditioned simulations where little correlation was found.

In general, the unconditioned simulations as specified by DADFN are non-Poissonian, with fracture occurrences correlated spatially to properties such as locality of BFZs, lithology and ductile domain. As such, they have reasonable predictive capacity of local variations in fracture occurrence as observed from drillhole and tunnel mappings. Since the conditioning performed only constrained the properties of the immediate intersecting fractures rather than the network as a whole, local conditioning only provides a subtle reduction in uncertainty of predicted post-closure flow and transport properties at individual deposition holes. However, conditioning has shown a significant improvement in the correlation between measurable flow metrics (e.g. injection and inflows) and post-closure performance measures of flow rate around deposition holes and the flow-related transport resistance. These correlations were further improved when considering models conditioned to both structural and hydraulic data (rather than structural data alone). When comparing the hydraulic conditioned simulations based on injection to pilot holes with those based on inflows to the open deposition holes, the ability to infer post-closure flow and transport from predicted inflows to the open repository are similar, with little additional value added to the predictive capability of models for post-closure conditions by using data from the deposition hole characterisation.

The large stochastic variability in the simulated flow metrics for individual pilot holes / deposition holes between realisations of the DFN is likely amplified by the particular interpretation of stochastic DFN description from DADFN, where the patchwork of fracture openings produces significantly channelised pathways for groundwater flow within individual fractures and thereby heterogeneity in the simulated flow field. This study implements the base DADFN model, with individual openings within larger fractures sampled at a 20 m length scale along each fracture. It is anticipated that the uncertainty in predictions of the simulated flow metrics between realisations of the DFN model would be further reduced if the length scale of individual openings in the fracture (i.e. the area open to flow) was increased - reducing the heterogeneity of the flow within individual fractures).

A visual summary of the reliability of predictions under different conditions is presented in Table 8-1.

Table 8-1. Summary of conclusions from conditioning – five types of model by three hydraulic situations. Cell colouring highlights the predictive capability of the simulations (green – orange – yellow – red equates to high – low predictive capability).

	Tunnels open, injection tests in pilot holes for deposition holes, calculating injection rates (-pi)	Tunnels and deposition holes open, calculating inflows to deposition holes (-do)	Tunnels and deposition holes backfilled and saturated, calculating post-closure flow and transport (-pc)
Unconditioned (UC)	UC-pi – baseline validation indicates injection rates are correct order of magnitude, with expected spatial variability	UC-do – baseline indicates inflow rates are correct order of magnitude, with expected spatial variability	UC-pc – very weak correlations observed between post closure measures and simulated injection to pilot holes (-pi) and inflow to deposition holes (-do)
Pilot hole geometric conditioned (PHGC)	PHGC-pi – uncertainty in predictions of injection rates reduced by conditioning on fracture mapping	PHGC-do – limited reduction in uncertainty of predictions of inflows when conditioning on fracture traces	PHGC-pc – some correlation between post-closure conditions and injection to pilot holes (-pi). Limited correlation with deposition hole inflows (-do)
Pilot hole hydraulic conditioned (PHHC)	PHHC-pi – uncertainty in predictions of injection rates reduced by conditioning on injection tests	PHHC-do – reduction in uncertainty of predictions of inflows when conditioning on pilot hole injections	PHHC-pc – correlation between post-closure conditions and injection to pilot holes (-pi). Some correlation with deposition hole inflows (-do)
Deposition hole geometric conditioned (DHGC)	DHGC-pi – simulating injection to preceding pilot holes not of practical relevance once deposition holes are reamed	DHGC-do – reduction in uncertainty of predictions of inflows when conditioning on deposition hole trace mappings	DHGC-pc – correlation between post-closure conditions and deposition hole inflows (-do)
Deposition hole hydraulic conditioned (DHHC)	DHHC-pi – simulating injection to preceding pilot holes not of practical relevance once deposition holes are reamed	DHHC-do – some reduction in uncertainty of predictions of inflows when conditioning on deposition hole inflows	DHHC-pc – some correlation between post-closure conditions and deposition hole inflows (-do)

8.4 Notes on data management and modelling methods

The success of the conditioning methodology is dependent on the reliability of upstream interpretations of the continuity of the fractures between drillholes and tunnels and the large scale deterministic structural framework of the BFZ model. The use of data in conditioning could potentially be improved by additional data interpretation and integration:

- Examining if any of the fractures characterised in the pilot holes in the floor of DT2 and/or the deposition holes can be linked to fractures mapped on the floor or walls of DT2.
- Examining steady state pressure in the packed-off pilot holes before the start of injection to indicate the ratio of the connectivities of a hole to a fracture system being capable to deliver a full hydrostatic pressure versus to the open tunnel system.
- Assignment of fracture specific inflows to DT2 (noting the influence of the tunnel engineering on the inflow measurements, e.g. through installing rock bolts in the ceiling and/or the effects of grouting).
- Assignment of fracture specific inflows in the deposition holes beneath DT2 (e.g. by installing collectors / separators in the hole).
- More accuracy of fracture orientations of fractures in pilot holes from image rather than core measurements currently available for pilot holes for deposition holes.
- Consider injection tests in pilot holes performed twice at two different injection pressures to improve hydraulic information, or alternatively include abstraction from open pilot holes using PFL to augment injection data. In particular, these PFL measurements are likely to have higher resolution in identifying specific flowing fractures intersecting the pilot holes when compared to the injection test measurements, although the injection tests do have higher resolution of flow due to the larger drawdowns possible. Other possible improvements are:
  - Augmenting two data sources for flow would potentially provide additional information of local connections to other underground openings.
  - Injection tests of longer duration and analysis of transient changes in pressure could discern fixed pressure boundaries (e.g. conductivity zones or openings) of finite flow compartment.

As mentioned above, it should be emphasised that the current study makes use of a single model interpreted and calibrated in the DADFN prototype study (Hartley et al. 2017). However, the model is non-unique, and it is certainly possible that alternative models could be calibrated by varying ω (the proportion of fracture surface area containing openings/voids) and L_h (the length scale of such openings), or more substantial variants considering uncertainties in fracture intensity and size. The results presented here should therefore be considered as illustrative, and the robustness of conclusions drawn may need to be subjected to alternative viable DFN models as well as additional realisations. In order to discern amongst alternative DFN models, a series of measures should be defined to identify the DFN models. Such measures could include (but not limited to)

- predictions of hydraulic responses between neighbouring pilot holes or deposition tunnels to constrain the connectivity of the system on the 10–30 m scale,
- predictions of specific capacities in the pilot hole that precedes the deposition tunnel to constrain the specific local frequency and magnitudes of flow over a ca. 300 m volume, and
- simulation of transient evolution of injection rate to compare statistics of the numbers of types of transient responses (e.g. times to reach steady-state, eventual closed compartment, nearby fixed boundary).

In addition, the conditioned simulations could potentially be improved by:

- Conditioning on both constraints from pilot hole injections rates and inflows to subsequent deposition holes, providing fractures can be linked between the two.
- Conditioning on both deposition hole hydraulics (or preceding pilot holes) and inflows to demonstration tunnels, provided fractures can be linked between the hole and tunnels. This would provide indication of hydraulic "short-circuits" where injection to the pilot holes are distorted by their connections to the open tunnel.

- Conditioning on both deposition hole hydraulics (or preceding pilot holes) and transmissivities measured in all pilot holes for demonstration and access tunnels, providing detailed flow measurements for conditioning covering a wider range of fracture orientations.
- Adjusting the spatial patterns of area open to flow on the conditioned fractures, such that fractures identified as hydraulically active are indeed open at the position of intersection with the underground openings in which the flow was observed, otherwise closed. Note this is only applied on the fracture area directly intersecting the hole, and the openness of the remainder of the conditioned fracture area will be sampled stochastically (using the existing methodology). This has been implemented for hydraulic conditioning based on injection in pilot holes, but is not currently applied when conditioning on inflows to deposition holes, and
- considering a number of alternative DFN models, to address uncertainties in the underlying DADFN description. These could consider the fraction of open area and scale of heterogeneity within each fracture as the main matching parameters determining hydraulic connectivity in the DADFN model (see previous bulleted list).

8.5 Outlook on application of methodology to disposal criteria

In this section a concluding outlook on the application of the employed characterisation and modelling methods is presented in light of the results obtained from this study.

From this study:

- Six experimental deposition holes have been considered for conditional simulations within the Demonstration Area of the ONKALO, and form the basis for identifying possible correlations/ relationships in support of deposition hole acceptance (rejection).
  - As an attempt to compensate for the limited number of holes considered compared with the real repository situation, multiple realisations of the DFN model have been considered.
- A correlation has been established between post-closure conditions and potential flow-based criteria for deposition holes such as the integrated specific capacity of the fractures intersecting the pilot hole for the deposition hole or inflows to open deposition holes. In Appendix A, the current performance limits for deposition hole post-closure flow *(U)* and transport *(F)* are compared with one possible hydraulic acceptance criteria of deposition holes. Two of the DFN simulations are considered, unconditioned models (Appendix A1), and conditioned simulations based on injection to pilot holes for deposition holes (Appendix A2). The following is concluded:
  - The comparisons of post-closure limits with hydraulic acceptance criteria first compares the simulated post-closure flow (U) with injection to pilot holes to identify the specific capacity of the pilot hole, corresponding to the post-closure flow limit. An equivalent analysis is used to identify the specific capacity of the pilot hole corresponding to the post-closure transport (F) limit. The limit on U provides the more stringent criterion, requiring a specific capacity that does not exceed about 2×10^{-8} m^2/s. In contrast, the limit on F requires specific capacity not to exceed 2×10^{-7} m^2/s. However, the correlations between specific capacity of the pilot hole to post-closure flow and transport are significantly influenced by the following features of the modelled system:
    - When considering injection to pilot holes, the influence of neighbouring underground openings (e.g. the deposition tunnels) is significant, especially when local hydraulic connections to these openings occur.
    - Post-closure transport resistance is dependent on the spatial distribution of flow. Typically most flow resistance is accumulated in the first few fractures traversed after a release from a deposition hole, with a lesser contribution downstream as flow is focussed towards channels of less resistance. For the performance limits of U and F to be consistent would imply the flow field remain below the U limit over the first $L=F_{lim} \times U_{lim} = 10^4 \times 10^{-3} = 10$ m of the path. If U were then to increase downstream as flow is channelled into fractures of increasing T, then F for the whole path might still be dominated by this first 10 m. For the fracture system derived in DADFN it would however appear that U remains small for several tens of metres for many release paths, and so the limit on F provides a less stringent requirement on transmissivity than the limit on U.

  - Based on these limits for specific capacity of the pilot hole for deposition hole, the simulated injection to pilot holes can be compared with inflows to open deposition holes to identify the corresponding inflow limits. The improved correlation between inflows and injection derived specific capacities with conditioning DFNs implies an inflow criterion of about 0.3 l/min, while a more scattered unconditioned model implies a limit of 0.01 l/min.
    - It is noted that the proposed limits on inflow are somewhat uncertain due to the large scatter that occurs when considering the correlation of specific capacities from injection to pilot holes to the inflows to open deposition holes. One of the most significant sources of this scatter is the effect of connections to neighbouring underground openings, which act to enhance the specific capacity of the hole whilst lowering the predicted inflows.

Application to disposal:

- This study has demonstrated the potential of using location specific characterisation methods combined with probabilistic conditional DFN simulation (along with the required understanding of the local flow situation) to support the assessment of the suitability of each position for disposal.
- Characterisation of pilot holes by mapping and hydraulic testing seems to offer sufficient information to screen locations unsuitable for reaming of full deposition holes, thereby avoiding the need to backfill unsuitable deposition holes. However, despite this characterisation, a number of uncertainties do persist (e.g. limited understanding of the local hydraulic connectivity of the pilot hole to underground openings).
- However, it remains to be seen if the measurement and integration of additional characterisation data, either between the tunnel and hole or use of more pressure and flow test data from within the hole, would lead to more certain predictions of post-closure flow conditions. Hence, the characterisation and modelling methods need to be further refined and proven, for them to be considered reliable operational tools. Such data could include:
  - PFL tests of the pilot holes for deposition tunnels.
  - Inflows to the deposition tunnels.
  - Pressures in and abstractions from the pilot holes for deposition holes.

As a more straightforward application, DFN modelling provides a basis for justifying criteria to apply to proxy flow measurements, as discussed above. If criteria are to be quantified in this way, it is recommended that a more comprehensive modelling study be performed so as to consider a wider range of geological situations as expected over the full repository footprint, beyond the Demonstration Area considered here.

References

SKB's (Svensk Kärnbränslehantering AB) publications can be found at www.skb.com/publications. Posiva's publications can be found at http://posiva.fi/en/databank.

Amec Foster Wheeler, 2016. NAPSAC Technical Summary, Release 11.3. AMEC/ENV/CONNECTFLOW/12, Amec Foster Wheeler, UK.

Appleyard P, Jackson P, Joyce S, Hartley L, 2018. Conditioning discrete fracture network models on intersection, connectivity and flow data. SKB R-17-11, Svensk Kärnbränslehantering AB.

Barton C A, Zoback M D, Moos D, 1995. Fluid flow along potentially active faults in crystalline rock. Geology 23, 683–686.

Baxter S, Hartley L, Witterick W, Fox A, 2016. Database design and prototyping for Olkiluoto Discrete Fracture Network (DFN) in support of site descriptive modelling 2016. Posiva Working Report 2016-13, Posiva Oy, Finland.

Bym T, Hermanson J, 2018. Methods and workflow for geometric and hydraulic conditioning. DFN-R – status report 2013–2015 SKB R-17-12, Svensk Kärnbränslehantering AB.

Cordes C, Kinzelbach W, 1992. Continuous groundwater velocity fields and path lines in linear, bilinear, and trilinear finite elements. Water Resources Research 28, 2903–2911.

Engström J, Kemppainen K, 2008. Evaluation of the geological and geotechnical mapping procedures in use in ONKALO access tunnel. Posiva Working Report 2008-77, Posiva Oy, Finland.

Fox A, Forchhammer K, Pettersson A, La Pointe P, Lim D-H, 2012. Geological discrete fracture network model for the Olkiluoto site, Eurajoki, Finland, Version 2.0. Posiva 2012-27, Posiva Oy, Finland.

Joyce S, Swan D, Hartley L, 2013. Calculation of open repository inflows for Forsmark. SKB R-13-21, Svensk Kärnbränslehantering AB.

Hartley L, Appleyard P, Baxter S, Hoek J, Roberts D, Swan D, 2013a. Development of a hydrogeological discrete fracture network model for the Olkiluoto site descriptive model 2011 Volume I. Posiva Working Report 2012-32, Posiva Oy, Finland.

Hartley L, Hoek J, Swan D, Appleyard P, Baxter S, Roberts D, Simpson T, 2013b. Hydrogeological modelling for assessment of radionuclide release scenarios for the repository system 2012. Posiva Working Report 2012-42, Posiva Oy, Finland.

Hartley L, Hoek J, Swan D, Baxter S, Woollard H, 2013c. Hydrogeological discrete fracture modelling to support rock suitability classification. Posiva Working Report 2012-48, Posiva Oy, Finland.

Hartley L, Baxter S, Williams T, 2016. Geomechanical coupled flow in fractures during temperate and glacial conditions. Posiva Working Report 2016-8, Posiva Oy, Finland.

Hartley L, Appleyard P, Baxter S, Mosley K, Williams T, Fox A, 2017. Demonstration area discrete fracture network modelling at Olkiluoto. Posiva Working Report 2017-3, Posiva Oy, Finland.

Hjerne C, Komulainen J, Aro S, Winberg A, 2016. Development of hydraulic test strategies in support of acceptance criteria for deposition hole positions – Results of hydraulic injection tests in ONKALO DT2 pilot holes for experimental deposition holes. Posiva Working Report 2016-06, Posiva Oy, Finland.

Mattila J, Viola G, 2014. New constraints on 1.7 Gyr of brittle tectonic evolution in southwestern Finland derived from a structural study at the site of a potential nuclear waste repository (Olkiluoto Island). Journal of Structural Geology 67, 50–74.

McEwen T (ed), Aro S, Kosunen P, Mattila J, Pere T, Käpyaho A, Hellä, P, 2012. Rock Suitability Classification, RSC 2012. Posiva 2012-24, Posiva Oy, Finland.

Norokallio J, 2015. Geological and geotechnical mapping procedures in use in the ONKALO. Posiva 2015-1, Posiva Oy, Finland.

Posiva, 2012. Safety case for the disposal of spent nuclear fuel at Olkiluoto – Design basis 2012. Posiva 2012-03, Posiva Oy, Finland.

Valli J, Kuula H, Hakala M, 2011. Stress modeling of the in situ stress state at the Olkiluoto site, western Finland. Posiva Working Report 2011-34, Posiva Oy, Finland.

Appendix A

Post-Closure flow and transport limits

In this appendix, the current performance limits for deposition hole post-closure flow (U) and transport (F) are compared to one possible hydraulic acceptance criteria of deposition holes. Two of the DFN simulations are considered, unconditioned models (described in Chapter 5 and detailed here in Appendix A1), and conditioned simulations based on injection to pilot holes for deposition holes (described in Section 6.2 and detailed here in Appendix A2). The comparisons of post-closure limits with hydraulic acceptance criteria takes the following approach:

1. Compare the simulated post-closure flow rate per unit width around the deposition hole (U) with injection to pilot holes to identify the specific capacity of the pilot hole, $(Q_{outflow}/dh)_{lim,U}$ corresponding to the post-closure flow limit, $U_{lim} = 1\ l/y \cdot m$.
2. Compare the simulated post-closure transport (F) with injection to pilot holes to identify the specific capacity of the pilot hole, $(Q_{outflow}/dh)_{lim,F}$ corresponding to the post-closure flow limit, $F_{lim} = 10^4\ y/m$.
3. Compare the simulated injection to pilot holes with inflows to open deposition holes to identify the inflows corresponding to the specific capacity limits identified in Steps 1 and 2.

   Using the above approach, inflows to open deposition holes equivalent to the post-closure limits of flow and transport can be inferred from the simulations considered. These values can then be compared to the possible hydraulic acceptance criteria of a maximum inflow of 0.1 l/min to the open deposition hole.

A1 Unconditioned (UC) DFN

In this section, the above process for comparing post-closure limits with hydraulic acceptance criteria are considered for ten realisations of the unconditioned DFN models. As summarised in Table A-1:

- In Figure A-1 the initial flow rates per unit width (U) for saturated post-closure simulations (UC-pc) are compared to specific capacity simulated from hydraulic injection in pilot holes for deposition holes (UC-pi). Ten realisations of the unconditioned DFN are considered with dashed line indicating a best fit for non-zero injection rates. The corresponding limit in $(Q_{outflow}/dh)_{lim,U}$ is 1.5×10^{-8} m^2/s.
- In Figure A-2 the flow-related transport resistance (F) for saturated post-closure simulations (UC-pc) are compared to specific capacity simulated from hydraulic injection in pilot holes for deposition holes (UC-pi). Ten realisations of the unconditioned DFN are considered with dashed line indicating a best fit for non-zero injection rates (although it is noted that the correlation in this case is relatively weak). The corresponding limit in $(Q_{outflow}/dh)_{lim,F}$ is 2.5×10^{-7} m^2/s, a factor 6 larger than the corresponding value calculated from U. Although the performance limits for U and F are defined to be approximately consistent, their equivalence is a function of the length of the transport path. With a simple system of one fracture, F is the integral of $1/U$ along a transport path of length, L (assuming a constant flow and no branching). Therefore a F limit equivalent to the U limit can be evaluated from $F=L/U$. Here a typical transport length is approximately 200 m; and therefore an F limit equivalent to the 1 l/(y·m) performance limit for U is ~ 2×10^5 y/m. Applying this limit for F in Figure A-2 would yield a corresponding limit in $(Q_{outflow}/dh)_{lim,F}$ of 1.8×10^{-8} m^2/s, consistent with the estimate from U.
- In Figure A-3 the specific capacity from simulated inflows to open deposition holes calculated as the inflow divided by hydrostatic pressure at the deposition hole (UC-do) are compared to the specific capacity simulated from hydraulic injections in the whole pilot holes for deposition holes (UC-pi). Ten realisations of the unconditioned DFN are shown along with post-closure flow limits inferred above from Figure A-1 and Figure A-2. The corresponding inflow limits are 0.025 l/min and 18.4 l/min, respectively. Note the first of these limits is below the proposed hydraulic acceptance criteria of 0.1 l/min

Table A-1. Post-closure limits for the initial flow per unit width *(U)* and flow-related transport resistance *(F)* and associated specific capacities simulated from hydraulic injection in pilot holes for deposition holes as shown in Figure A-1 through Figure A-3. Analysis is based on ten realisations of the unconditioned DFN.

Post-closure measure	Post-closure limit	Associated limit in specific capacities from injection to pilot holes $(Q_{outflow}/dh)_{lim}$	Associated inflow limit (at −420 m) to open deposition holes $Q_{inflow\,lim}$
Flow (*U*)	1 l/(y·m)	1.5×10^{-8} m²/s	0.013 l/min
Transport (*F*)	10^4 y/m	2.5×10^{-7} m²/s	0.2 l/min

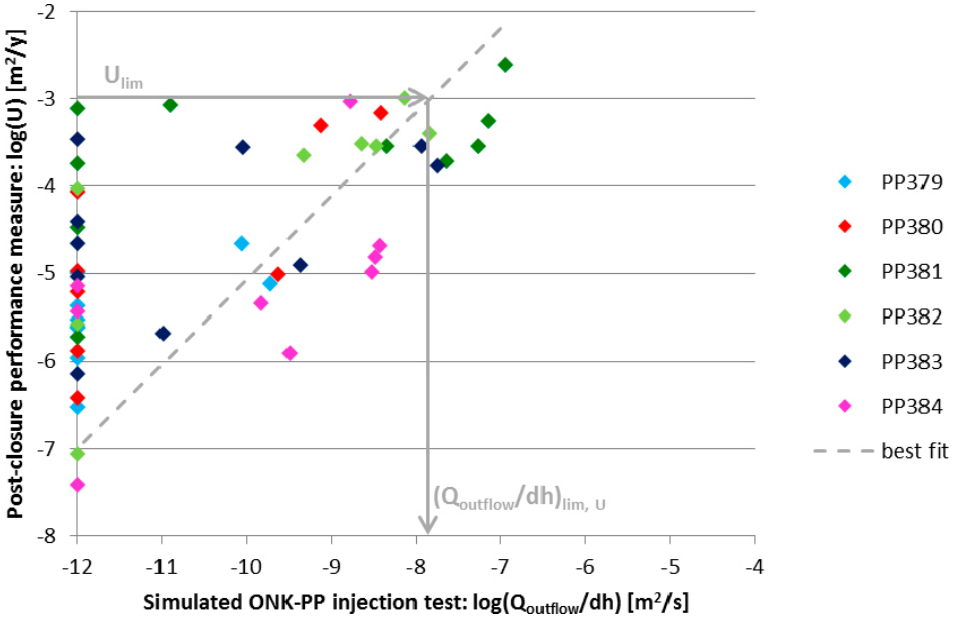

Figure A-1. *Initial flow rates per unit width (U) for saturated post-closure simulations (UC-pc) compared to specific capacity simulated from hydraulic injection in pilot holes for deposition holes (UC-pi). Ten realisations of the unconditioned DFN are considered with dashed line indicating a best fit for non-zero injection rates.*

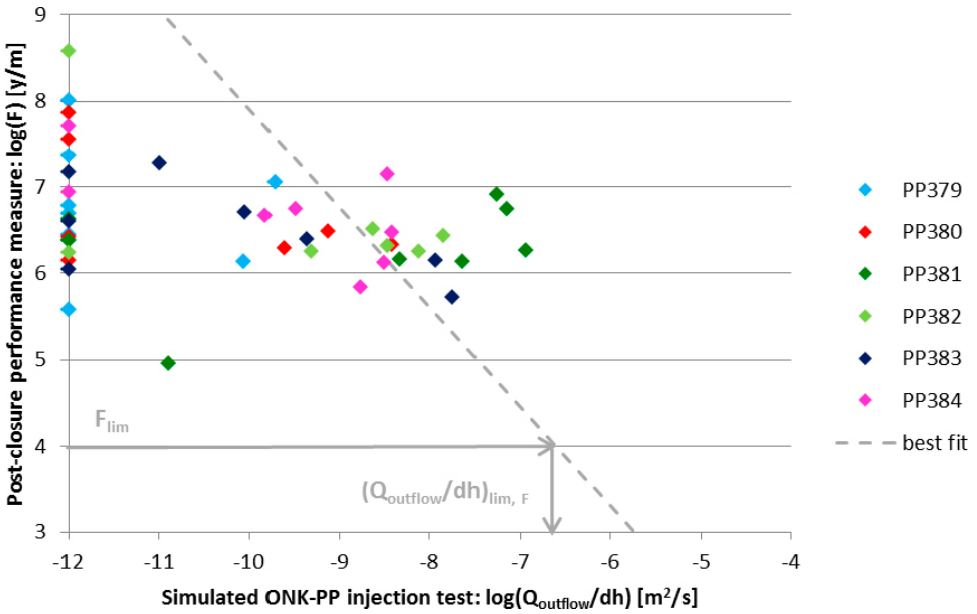

Figure A-2. *Flow-related transport resistance (F) for saturated post-closure simulations (UC-pc) are compared to specific capacity simulated from hydraulic injection in pilot holes for deposition holes (UC-pi). Ten realisations of the unconditioned DFN are considered with best fit for non-zero injection rates indicated.*

A2 Conditioned simulation of pilot hole injection tests (PHHC)

In this section, the above process for comparing post-closure limits with hydraulic acceptance criteria are considered for ten realisations of the DFN models conditioned to injection in pilot holes. As summarised in Table A-2:

- In Figure A-4 the initial flow rates per unit width *(U)* for saturated post-closure simulations (PHHC-pc) are compared to specific capacity simulated from hydraulic injection in pilot holes for deposition holes (PHHC-pi). Ten realisations of the DFN conditioned to injection measurements in pilot holes are considered with dashed line indicating a best fit for non-zero injection rates. The corresponding limit in $(Q_{outflow}/dh)_{lim,U}$ is 1.8×10^{-8} m^2/s.
- In Figure A-5 the flow-related transport resistance *(F)* for saturated post-closure simulations (PHHC-pc) are compared to specific capacity simulated from hydraulic injection in pilot holes for deposition holes (PHHC-pi). Ten realisations of the DFN conditioned to injection measurements in pilot holes are considered with dashed line indicating a best fit for non-zero injection rates. The corresponding limit in $(Q_{outflow}/dh)_{lim,F}$ is 2.0×10^{-7} m^2/s, about an order of magnitude greater than that observed for U. Similar to the unconditioned case, a performance limit for F based on the limit of U can be estimated from $F=L/U$; and for a transport path length of 200 m this would provide an equivalent F limit of 1.1×10^{-8} m^2/s, consistent with the value identified from Figure A-4.
- In Figure A-3 the specific capacity from simulated inflows to open deposition holes calculated as the inflow divided by hydrostatic pressure at the deposition hole (PHHC-do) are compared to the specific capacity simulated from hydraulic injections in the whole pilot holes for deposition holes (PHHC-pi). Ten realisations of the DFN conditioned to injection measurements are shown along with post-closure flow limits inferred above from Figure A-4 and Figure A-5. The corresponding inflow limits are 0.16 l/min and 93.5 l/min, respectively. Note that compared to unconditioned simulations (see Section A.1) both of these limits meet the proposed hydraulic acceptance criteria of 0.1 l/min.

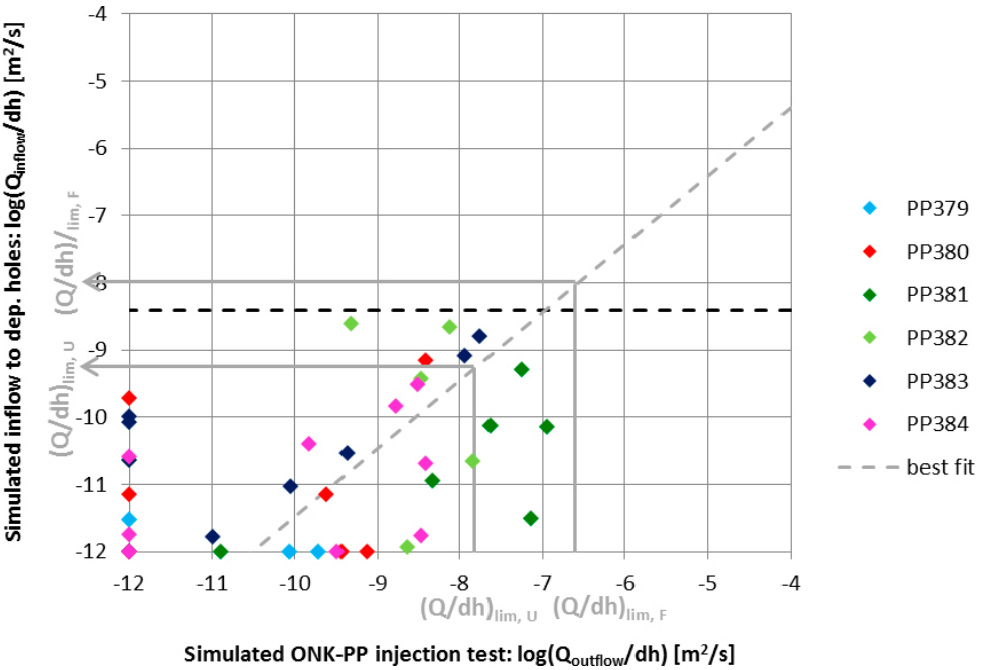

Figure A-3. *Specific capacity from simulated inflows to open deposition holes (UC-do) are compared to the specific capacity simulated from hydraulic injections in the whole pilot holes for deposition holes (UC-pi). Ten realisations of the unconditioned DFN are shown along with post-closure flow limits inferred from Figure A-1 and Figure A-2. Q_{lim} corresponds to the proposed hydraulic acceptance criteria of 0.1 l/min divided by the drawdown of c. 420 m.*

Table A-2. Post-closure limits for the initial flow per unit width *(U)* and flow-related transport resistance *(F)* and associated specific capacities simulated from hydraulic injection in pilot holes for deposition holes as shown in Figure A-4 through Figure A-6. Analysis is based on ten realisations of the DFN conditioned to injection in pilot holes.

Post-closure measure	Post-closure limit	Associated limit in specific capacities from injection to pilot holes $(Q_{outflow}/dh)_{lim}$	Associated inflow limit (at −420 m) to open deposition holes $Q_{inflow\,lim}$
Flow (*U*)	1 l/ym	1.8×10^{-8} m²/s	0.29 l/min
Transport (*F*)	10^4 y/m	2.0×10^{-7} m²/s	3.2 l/min

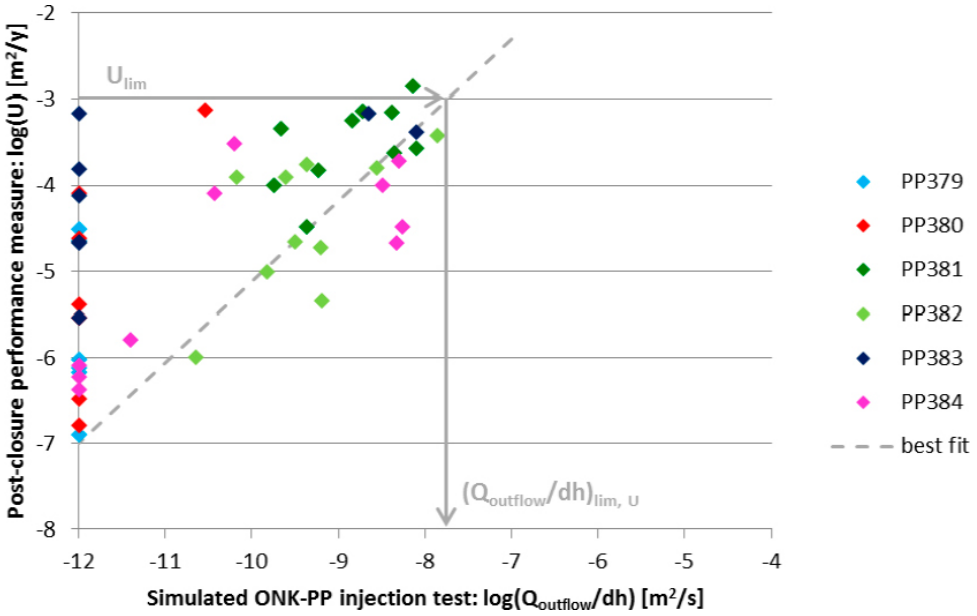

Figure A-4. *Initial flow rates per unit width (U) for saturated post-closure simulations (PHHC-pc) compared to specific capacity simulated from hydraulic injection in pilot holes for deposition holes (PHHC-pi). Ten realisations of the injection to pilot hole conditioned DFN are considered with dashed line indicating a best fit for non-zero injection rates.*

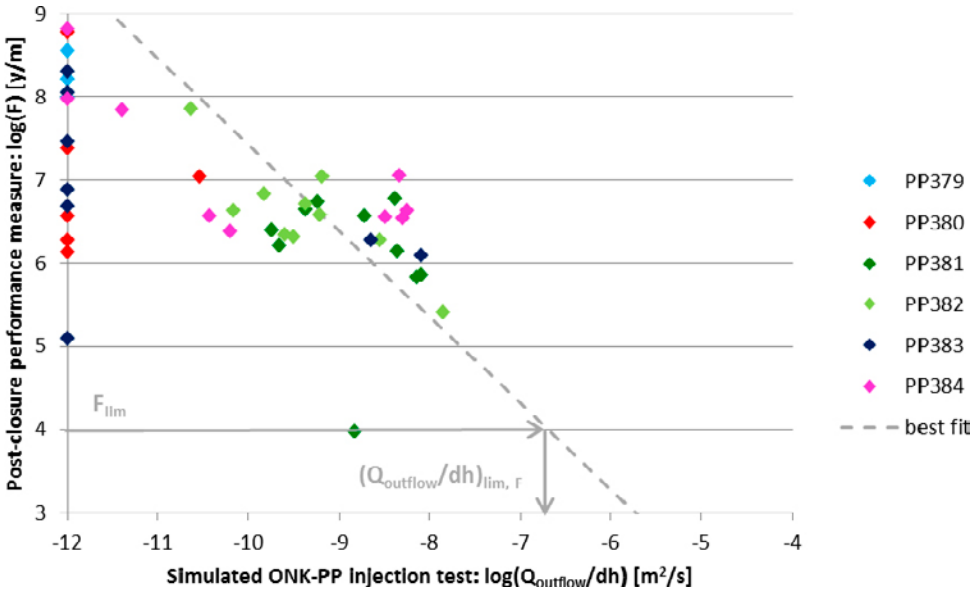

Figure A-5. *Flow-related transport resistance (F) for saturated post-closure simulations (PHHC-pc) are compared to specific capacity simulated from injection in pilot holes for deposition holes (PHHC-pi). Ten realisations of the injection to pilot hole conditioned DFN are considered with best fit for non-zero injection rates shown.*

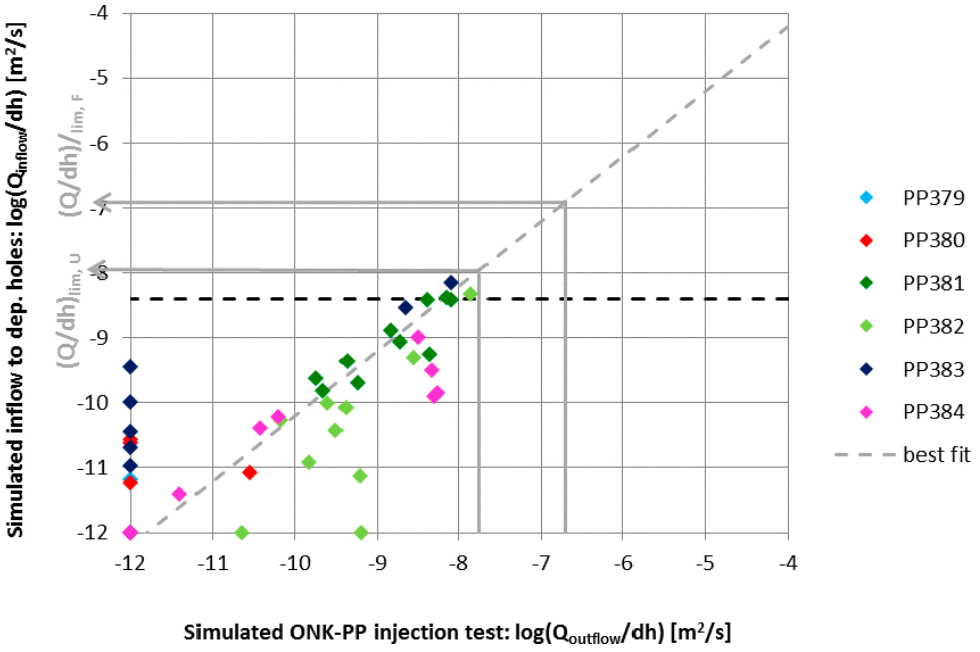

Figure A-6. *Specific capacity from simulated inflows to open deposition holes (PHHC-do) are compared to the specific capacity simulated from hydraulic injections in the whole pilot holes for deposition holes (PHHC-pi). Ten realisations of the DFN conditioned to injection in pilot holes are shown along with post-closure flow limits inferred from Figure A-4 and Figure A-5. Q_{lim} corresponds to the proposed hydraulic acceptance criteria of 0.1 l/min divided by the drawdown of c. 420 m.*

Arkitektkopia AB, Bromma, 2018

A CO-OPERATION REPORT BETWEEN SVENSK KÄRNBRÄNSLEHANTERING AB AND POSIVA OY

SKB's and Posiva's programmes both aim at the disposal of spent nuclear fuel based on the KBS-3 concept. Formal cooperation between the companies has been in effect since 2001. In 2014 the companies agreed on extended cooperation where SKB and Posiva share the vision "Operating optimised facilities in 2030". To further enhance the cooperation, Posiva and SKB started a series of joint reports in 2016, which includes this report.